



Universiteit
Leiden
The Netherlands

Uncovering vulnerabilities in triple-negative breast cancer

He, J.

Citation

He, J. (2019, October 31). *Uncovering vulnerabilities in triple-negative breast cancer*. Retrieved from <https://hdl.handle.net/1887/79947>

Version: Publisher's Version

License: [Licence agreement concerning inclusion of doctoral thesis in the Institutional Repository of the University of Leiden](#)

Downloaded from: <https://hdl.handle.net/1887/79947>

Note: To cite this publication please use the final published version (if applicable).

Cover Page



Universiteit Leiden



The following handle holds various files of this Leiden University dissertation:
<http://hdl.handle.net/1887/79947>

Author: He, J.

Title: Uncovering vulnerabilities in triple-negative breast cancer

Issue Date: 2019-10-31

Uncovering vulnerabilities in triple-negative breast cancer

Jichao He

赫记超

PhD thesis with summary in Dutch

Uncovering vulnerabilities in triple-negative breast cancer

Jichao He @October 2019

The research described in this thesis was performed at the division Drug Discovery and Safety of Leiden Academic Centre for Drug Research (LACDR), Leiden University (Leiden, The Netherlands).

The research was financially supported by China Scholarship Council (no. 201407060007) and the European Research Council Advanced grant Triple-BC (grant no. 322737).

Cover by: Adapted from www.besthdwallpaper.com/hua-hui/yi-zhu-pu-gong-ying-hua-dt_zh-CN-11102 (under CC0 license) by Jichao He with no intention of infringing copyright

Thesis lay-out by Jichao He

Printed by Ridderprint | www.ridderprint.nl

©2019 Jichao He. All rights reserved. No part of this thesis may be reproduced or transmitted in any form or by any means without written permission of the author.

Uncovering vulnerabilities in triple-negative breast cancer

Proefschrift

Ter verkrijging van de graad van Doctor aan de Universiteit Leiden,

op gezag van Rector Magnificus prof. mr. C.J.J.M. Stolker,

volgens besluit van het College voor Promoties

te verdedigen op donderdag 31 oktober 2019

klokke 10:00 uur

door

Jichao He

geboren te Henan, China

In 1988

Promotor

Prof. Dr. B. van de Water

Co-promotor

Dr. Y. Zhang

Promotiecommissie

Prof. Dr. H. Irth (Chair)

Prof. Dr. J.A. Bouwstra (Secretary)

Prof. Dr. J.V.M.G. Bovée (LUMC, The Netherlands)

Prof. Dr. J.W.M. Martens (Erasmus MC, The Netherlands)

Dr. L.H. Heitman

Table of Contents

Chapter 1	1
General introduction and scope of the thesis	
Chapter 2	19
FRET biosensor-based kinase inhibitor screen for ERK and AKT activity reveals differential kinase dependencies for proliferation in TNBC cells	
Chapter 3	39
A kinome screen for lapatinib drug resistance identifies FYN as a suppressor of EGFR/PI3K/AKT signaling axis dependency in triple-negative breast cancer	
Chapter 4	57
Multi-targeted kinase inhibition alleviates mTOR inhibitor resistance in triple-negative breast cancer	
Chapter 5	79
Integrative analysis of genomic amplification-dependent expression and loss-of-function screen identifies ASAP1 as a driver gene in triple-negative breast cancer progression	
Chapter 6	105
Discussion and future perspectives	
Appendix	
References	113
Summary	124
Samenvatting	127
List of publications	130
Curriculum vitae	131
Acknowledgements	132

Chapter 1

General introduction and scope of the thesis

1. Breast cancer

Worldwide, breast cancer is the most frequently diagnosed cancer and the leading cause of cancer mortality among women. In 2018, about 2.1 million people were diagnosed, accounting for almost 1 in 4 cancer cases in females, and over half a million people died from this disease ¹. Early transcriptomic profiling studies have categorized breast cancer into at least four clinically relevant intrinsic subtypes: luminal-A, luminal-B, HER2-enriched and basal-like ². Breast cancer can also be classified into three major receptor subtypes, based on the presence of molecular markers estrogen (ER), progesterone (PR) receptors and human epidermal growth factor 2 (HER2), i.e. HR+/HER2- (70% of patients), HER2+ (15%-20%) and triple-negative (15%) ³. While overlapping among the classifications, these subtypes have been characterized for distinct prevalence, prognoses and therapeutic strategies (Figure 1). HR+ tumors are more prevalent in older women, whereas triple-negative tumors are more likely to occur in women who are younger, African-American or Hispanic ⁴. The prognoses of triple-negative tumors are worse than that of HR+ or HER2+, with approximately 1 year and 5 years median overall survival, respectively ⁵⁻⁷.

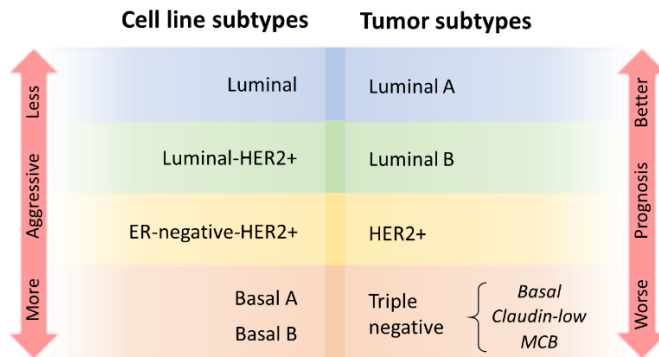


Figure 1. Breast cancer subtypes and prognosis. According to the status of ER, PR, HER2, breast cancer is classified as luminal A, luminal B, HER2 positive, and triple negative, where triple negative tumors can be further differentiated into at least basal, claudin-low, MCB (metaplastic breast cancer). The morphological features of the subtypes in tumors and cell lines accord well, with luminal tumors having better prognosis and luminal cell lines less aggressive than that in triple negative tumors and cell lines. (Adapted from Dai et al, 2017)

2. Triple-negative breast cancer

2.1 Molecular stratification

Triple-negative breast cancer (TNBC) represents about 15% of all breast cancers, but proves to be a highly malignant subtype, with earlier age of onset, high risk of metastasis and unfavorable clinical prognosis. Given the nature of heterogeneity, a collection of studies has profiled the distinct genetic landscape and therapeutic response of TNBC. By

analyzing transcriptomic profiles of 587 TNBC cases, Lehmann et al demonstrated that TNBC consists of seven subtypes (TNBCtype) and displays a heterogeneous biology with differential response to various therapies ⁸. By the measurement of in total 2188 genes and consensus clustering, they recognized seven molecular subtypes, namely basal-like 1 (BL1), basal-like 2 (BL2), mesenchymal (M), mesenchymal stem-like (MSL), immunomodulatory (IM), luminal androgen receptor (LAR) and unstable (UNS). Each subtype represents a unique genetic background and driver signaling pathways. For example, BL1 subtype depicts increased cell cycle and DNA damage response gene signature, while BL2 involves high growth factor signaling. M illustrates gene enrichment in cell motility, growth and differentiation, which is partially resembled by MSL, but with low expression of proliferative genes. IM is associated with immune cell processes, whereas LAR characterized for elevated androgen signaling. To address the molecular heterogeneity of TNBC and the associated therapeutic responses, **Chapter 4** exploited a broad kinase inhibitor library screen across ~20 TNBC cell lines representative for the six main TNBC subtypes. Our research demonstrated a poor correlation of TNBC molecular subtypes with their proliferative responses to various kinase inhibitors. Of relevance, a retrospective study found the TNBCtype to be an independent predictor of pathological complete response (pCR) for patients receiving standard chemotherapy regimens ⁹. Research by Ring et al revealed a small gene set algorithm (101 genes) showing the ability to recapitulate TNBCtype and predict therapeutic response, which might be more manageable in the clinic by focusing on the most relevant molecular alterations in the diverse TNBC categories ¹⁰. Yet, limited by their small size of cohorts, these studies pinpoint the clinical precautions for the potential use of molecularly TNBC subtyping. Lehmann and colleagues recently refined their sub-classification into four (TNBCtype-4) tumor-specific subtypes (BL1, BL2, M and LAR), having recognized the influence of infiltrating lymphocytes and tumor-associated stromal cells on IM and MSL subtypes ¹¹. Other attempts to stratify TNBC using mRNA and DNA profiling include the four subtypes by Burstein et al: basal-like immune suppressed (BLIS), basal-like immune activated (BLIA), mesenchymal (MES) and LAR ¹². The diversity in TNBC classifications and their notable intersection not only confirm the great heterogeneity in this disease, but also accentuate a requirement for more comprehensive and optimized designation of TNBC molecular subtypes to eventually translate in the clinical settings.

2.2 Chemotherapy

Notwithstanding the extensive efforts in discerning the molecular landscape and complexity of tumor biology, no targeted therapies have been approved for TNBC. To date, cytotoxic chemotherapy remains the standard of care in the management of TNBC. Commonly used chemotherapeutic agents include alkylating agents, anti-tubulins,

anthracyclines, platinum and antimetabolites. Typical adjuvant and neoadjuvant therapy consists of an anthracycline (Adriamycin) plus an alkylating agent (Cyclophosphamide). Patients with TNBC have higher neoadjuvant response rate than those with other breast cancer subtypes^{13,14}. The phenomenon of high likelihood of pCR but with worse prognosis is referred to as triple-negative paradox¹⁵, which might be attributed to its highly proliferating property and high risk of recurrence.

Despite progress in optimizing systemic therapy, very few patients with metastatic breast cancer (including TNBC) have benefited from the treatment¹⁶. Efforts in exploring combination chemotherapy have been attempted to improve the clinical outcomes. Although heightening response rates in comparison with single agents, combination therapies have to be compromised with increased adverse effects and no significant survival benefits¹⁷. With the exception of poly ADP-ribose polymerase (PARP) inhibitors for the treatment of germline BRCA-mutated (gBRCA) HER2- disease¹⁸, there are currently no targeted options beyond chemotherapy in the TNBC settings.

Considering that optimal systemic chemotherapy has yet to be established, and that molecular research has been assisting in the discovery of driver mutations in TNBCs, novel alternate therapeutic strategies are underway and more targeted treatments could become accessible.

2.3 Targeted therapy

Triple-negative tumors are likely to relapse after chemotherapy despite initial response. Patients with TNBC who do not respond to neoadjuvant and adjuvant regimens, in a large proportion, represent intrinsic or acquired drug resistance. Large-scale genomic profiling of TNBC tumors has identified major mutations such as TP53 loss (84%), c-MYC amplification (40%), PTEN loss (35%) and PIK3CA mutation (7%)^{19,20}. Yet, these frequent mutations have not been druggable, pressing a necessity for exploring actionable targeted therapeutic options.

2.3.1 Poly ADP-ribose polymerase

PARP is a constitutively expressed nuclear enzyme essential for DNA repair in response to DNA single-strand and double-strand breaks, therefore facilitating genomic stability and cell survival. PARP deactivation leads to DNA double-strand breaks during replication. Tumor cells with wild-type BRCA1/2 rely much on homologous recombination for DNA repair. In BRCA1/2-deficient cells, double-strand breaks are repaired via PARP-mediated DNA metabolic processes, independently of homologous recombination. Thus, genetically or pharmacologically targeting PARP causes severe cell death in tumors representing BRCA1/2 deficiency, a classical example of synthetic lethality²¹.

Critical findings in both preclinical and clinical studies have led to the approval of PARP inhibitor talazoparib by Food and Drug Administration (FDA) of the United States, for the treatment of germline BRCA-mutated HER2- breast cancer^{18,22}. In addition, alternate mechanisms underlying BRCA1/2 dysfunction have been recognized in different cancer types, including somatic mutations and epigenetic alterations, so-called “BRCAness”²³. As such, PARP inhibition has gained much attention as a promising synthetic lethality therapeutic strategy for treating cancer with BRCA deficiency. Importantly, the anti-tumor activity of PARP inhibitors in combination with chemotherapy or targeted therapy has also been investigated in several clinical trials²⁰. Nevertheless, it has to be noted that both gBRCA and “BRCAness” occurs merely in sporadic breast cancers.

2.3.2 Epidermal growth factor receptor and angiogenesis

Epidermal growth factor receptor (EGFR) is a transmembrane protein that, upon ligand binding, transduces extracellular signals (e.g. EGF, transforming growth factor- α , betacellulin) to intracellular signaling molecules, thereby triggering multiple signaling cascades regulating cell growth, migration, proliferation and apoptosis²⁴⁻²⁶. Overexpression of EGFR is commonly observed in several human cancers. EGFR is amplified in 2% of breast tumors, but is more frequently overexpressed in basal-like subtype than non-basal-like ones^{19,27}. Several agents targeting EGFR have been approved for clinical use, including small-molecule kinase inhibitors (KIs) and monoclonal antibodies (mAbs). However, no statistically significant prognostic improvements have been achieved in patients with TNBC in comparison to platinum-based therapy^{28,29}. Two independent studies reported that compensatory feedback loop via AKT and HER3 conferred acquired resistance against EGFR-directed treatments^{26,30}. In line with these findings, kinome-wide siRNA and lapatinib combination screen in **Chapter 3** has demonstrated that, a Src family member FYN, conferred TNBC resistance against EGFR kinase-targeted inhibition via negatively regulating EGFR/PI3K/AKT signaling. A multi-centric neoadjuvant Phase II study of cetuximab plus docetaxel demonstrated modest activity in operable TNBC, despite acceptable toxicity³¹. In another Phase II trial, there was no increased efficacy with the combination of panitumumab over that expected from chemotherapy alone in metastatic TNBC (mTNBC)³².

Angiogenesis plays a central role in breast cancer metastasis and survival. Vascular endothelial growth factor (VEGF) is the most important angiogenic factor with proven significance in metastatic breast cancer. Given the high metastatic potential of TNBC, the development of VEGFR inhibitors is of great interest in combating this incurable disease. Bevacizumab is a mAb targeting angiogenesis by slowing the growth of new blood vessels, and approved for the treatment of a series of diseases, including colon cancer, lung cancer and glioblastoma. Several clinical studies have documented that treatment

with Bevacizumab improved pCR rates of patients with TNBC³³⁻³⁵. However, the survival benefits of Bevacizumab were marginal in most neoadjuvant trials.

2.3.3 PI3K/AKT/mTOR pathway

Activation of PI3K/AKT/mTOR pathway is repeatedly observed in TNBC, which could be attributed to loss of negative regulators such as PTEN (35%) and INPP4B (30%), as well as activating mutation of PIK3CA (7%)¹⁹. Provided the essential role in modulating tumor cell metabolism and proliferation, targeting this signaling axis represents a promising therapeutic avenue.

The anti-tumor activity of PARP inhibitors is limited to a small portion of TNBCs with gBRCA. A preclinical study showed that, in BCRA-proficient TNBC, PI3K blockade resulted in homologous recombination impairment and sensitization to PARP inhibition, and effectively suppressed tumor growth in patient-derived xenografts (PDXs)³⁶. In BELLE-4 Phase II/III study, the addition of a pan-PI3K inhibitor buparlisib failed to show improvement in progression-free survival (PFS) in the full and PI3K pathway-activated populations with HER2- breast cancer³⁷.

Ipatasertib is an oral and highly selective AKT inhibitor and has been evaluated in several clinical trials. Results from a randomized Phase II study, LOTUS, demonstrated improved PFS of patients with advanced TNBC for ipatasertib plus paclitaxel group compared to chemotherapy alone (6.2 versus 4.9 months, respectively)³⁸. Notably, the median PFS was 9.0 months with ipatasertib versus 4.9 months with placebo in the predefined cohorts with PIK3CA/AKT1/PTEN alteration. This has provided a rationale for the ongoing randomized phase III IPATunity130 trial testing the combination in patients with activated PI3K signaling (NCT03337724).

Phosphorylated mTOR, the active form, is present in the majority of TNBC populations³⁹. **Chapter 4** also showed that rapalog-resistant TNBC cells presented a high phosphorylation level of mTOR in response to mTOR inhibition. A Phase II trial showed 36% clinical benefit rate from combination of everolimus and carboplatin in patients with mTNBC⁴⁰. Another Phase I study on 52 females with mTNBC indicated that treatment with liposomal doxorubicin, bevacizumab, and temsirolimus or everolimus achieved improved responses, but the benefits were restricted to patients with aberrations in PIK3CA, AKT or PTEN⁴¹. In neoadjuvant setting, the addition of everolimus increased adverse events without additional benefits in patients with stage II/III TNBC⁴².

Given the high prevalence of activation in TNBC, effectively targeting PI3K pathway warrants the development of more specific inhibitors and a better pathway aberration-based preselection of patients, as well as more clinical investigation.

2.3.4 Androgen receptor

The LAR subtype of TNBC is characteristic of AR signaling and demonstrates sensitivity to anti-androgen agents both in vitro and in vivo ⁴³. In a Phase II trial of 424 patients with HR-metastatic breast cancer, 12% of the cohort were tested to be AR+ ⁴⁴. Treatment with AR antagonist bicalutamide exerted 19% clinical benefit rate (defined as complete response, partial response, or stable disease) for more than 6 months in AR+ patients, with a median PFS of 12 weeks. Another clinical trial reported that AR-driven gene signature was associated with overall survival treated with enzalutamide, a highly potent anti-AR agent ⁴⁵.

2.3.5 Cyclin-dependent kinases (CDKs)

Various cyclin-CDK complexes are responsible for the regulation of cell cycle progression both in normal and malignant cells. CDKs are naturally inhibited by CDK inhibitors. Loss-of-function mutations of these inhibitors or overexpressed cyclins lead to uncontrolled proliferation during tumorigenesis. mTOR inhibition could elevate cyclin D1 expression level in TNBC cells, therefore allowing for continuous proliferation of the rapalog-refractory cells, as shown in **Chapter 4**. Several cyclins are amplified in TNBCs ¹⁹. Three CDK4/6 inhibitors, palbociclib, ribociclib and abemaciclib, have been approved by FDA for the treatment of HR+/HER2- breast cancer. Targeting CDK4 by palbociclib efficiently eliminated chemo-refractory cells and breast cancer stem cells in TNBC ⁴⁶. Amplification of MYC is frequently observed in TNBC (40%) ¹⁹. Selective inhibition of CDK1 and CDK2 resulted in TNBC tumor regression in mouse xenografts harboring MYC amplification, highlighting the potential of targeting CDK1 and CDK2 in MYC-driven TNBC ⁴⁷.

2.4 Emerging novel therapy

2.4.1 Immune checkpoint inhibitors

Among all breast cancer subtypes, TNBC has the highest mutational frequency, with an increased likelihood of generating neoantigens by immunogenic mutations ^{48, 49}. Gene expression profiling analysis has identified the IM subtype of TNBC, characteristic of elevated expression of genes modulating antigen production and T cell function ⁸, providing a strong rationale for testing immunotherapy. High PD-L1 expression was reported in 20% of patients with TNBC, associated with enriched tumor-infiltrating lymphocytes (TILs) ⁵⁰. Consistently, results from other studies indicated that elevated PD-L1 level strongly correlated with high TIL number and improved prognosis in neoadjuvant settings ^{51, 52}. Recently, while the manuscript being written, atezolizumab, a mAb against PD-L1, has received the approval for individuals with mTNBC based on the Phase III trial IMpassion130 ⁵³. Compared to nab-paclitaxel treated group, combination with

atezolizumab prolonged PFS from 5.5 to 7.2 months in the intention-to-treat population, and from 5.0 to 7.5 months in the PD-L1-positive subgroup, respectively. No new adverse effects were identified with the combination. Several other clinical trials evaluating the efficacy of immunotherapy in TNBC are still ongoing.

2.4.2 Antibody-drug conjugate (ADC)

Differential glycoprotein expression between malignant and normal cells has sparked the design and development of ADCs. Trop-2 is a commonly expressed glycoprotein in TNBC, making it an attractive therapeutic target⁵⁴. Sacituzumab govitecan (IMMU-132), an ADC targeting Trop-2 for selective delivery of SN-38, has demonstrated 30% overall response rate with mild toxicity in heavily pretreated patients with mTNBC⁵⁴. These findings have led to the breakthrough therapy designation by FDA and a confirmatory Phase III study is currently recruiting.

3. Drug resistance

Tumor heterogeneity is dominantly responsible for both intrinsic and acquired resistance and represents a major hurdle for established therapy. For the intrinsic resistance, sensitive tumor cells are eliminated, subsequently resulting in an accumulated population of residual tumor cells which are genetically and histologically distinct from the sensitive ones. Contrarily, acquired resistance occurs when initially susceptible tumor cells obtain the ability to resist the activity of the therapy despite continued drug administration.

3.1 Resistance to chemotherapy

TNBC is a highly heterogeneous disease with an unfavorable prognosis. Paradoxically, the initial higher pCR rate to chemotherapy fails to correlate with better overall survival. TNBC is much aggressive with high frequency of developing resistance to chemotherapy. Tumor recurrence and resistance can be due in part to intratumoral heterogeneity of TNBC, which allows selective enrichment for cancer stem cell-like subpopulation. Single-cell sequencing of TNBC patients has also demonstrated that resistance occurred through adaptive selection of pre-existing genotypes by neoadjuvant chemotherapy, with associated transcriptional reprogramming of the resistant signatures⁵⁵. Some chemotherapeutic agents, such as doxorubicin and paclitaxel, are substrates of ATP-binding cassette (ABC) transporters. The efflux of drug by these transporters results in decreased drug concentration in tumor cells, hence weakening the efficacy^{56,57}.

3.2 Resistance to targeted therapy

Advancements in high-throughput next-generation sequencing technologies and massive parallel sequencing studies, as well as integrated bioinformatics-based tumor biology investigation have expanded our knowledge on the genomic complexity and intratumoral heterogeneity of breast cancer. Consequently, several targetable vulnerabilities have been identified in predefined patient subgroups to tailor treatment for improved therapeutic benefits. However, the activity of targeted therapy in the management of TNBC remains modest, due in a large part to drug resistance. Resistance involves reactivation of signaling pathways targeted by the drug and activation of compensatory signaling pathways, which can be resulted from dysregulated feedback loops and pathway crosstalk⁵⁸⁻⁶⁰. Evidences have shown that, in response to PI3K/mTOR inhibition, activated β -catenin served as an alternate survival pathway conferring glioblastoma and colorectal cancer resistance both in vitro and in vivo^{61, 62}. Concordantly, a study employing colorectal cancer patient-derived sphere cultures and mouse tumor xenografts showed that blocking Wnt/ β -catenin pathway by tankyrase inhibition reverted resistance to PI3K and AKT Inhibitors⁶³. In TNBC, MEK-targeted inhibition triggered dynamic reprogramming of the kinome, thereby limiting its anti-cancer effects⁵⁸. **Chapter 2** elucidated that drug resistant TNBC cells remained active ERK activity when treated with EGFR inhibitors. Proteolytic shedding and inactivated negative regulators of receptor tyrosine kinases (RTKs) have been shown to elevate surface RTK levels and enhance mitogenic signaling, resulting in kinase inhibitor resistance⁶⁴⁻⁶⁶. Contrarily, targeting FYN, a negative regulator of EGFR signaling identified in **Chapter 3**, released the activity of downstream PI3K and AKT signaling, rationalizing the co-targeting strategy to subvert resistance against inhibitors targeting EGFR/PI3K/AKT signaling axis. Recently, results from kinome dynamics mapping have concluded that maintenance of AURKA after drug treatment conferred therapy failure in breast cancer treated with inhibitors targeting PI3K/AKT/mTOR pathway⁶⁷. Our research in **Chapter 4** found that elevated cyclin D1 expression contributed in part to mTORi resistance. It has also been reported that FAK/IGF1R dependent PI3K pathway activation drives tumor resistance against mTOR inhibitors in various cancer cell lines and mouse models, including TNBC⁶⁸.

Altogether, drug resistance remains one of the major determinants limiting drug efficacy in TNBC therapy. With the various resistance mechanisms being well studied, the discovery of new therapeutic strategies and novel attainable targets are still of high demand.

4. Novel therapeutic strategies and target identification approaches

4.1 Role of gene expression profiling in patient stratification

TNBC is a highly aggressive disease of a great histological and biological heterogeneity, which has a notorious impact on the primary end points in clinical trials. Gene expression profiling plays a central role in dissecting this complexity and generating clinical benefits. A comparative study on TNBC clinical outcomes has noted that genomic signatures strongly correlate with response and survival after polychemotherapy typically in the basal-like subgroup of triple-negative tumors⁶⁹. These high-risk basal-like tumors with high proliferation scores are very sensitive to chemotherapy, whilst the lower-proliferating ones are less responsive with a worse prognosis. Thus, in the latter scenario, novel therapies are warranted. These findings highlight the importance of using gene expression data in patient stratification to predefine homogenous tumor groups and provide clinically relevant information. Supportively, encouraging results presented at ASCO 2018 showed that the biomarker selected group (i.e. with alterations in PIK3CA, AKT or PTEN genes) greatly contributed to the prolonged PFS by AKT-targeted therapy (AZD5363) plus first-line paclitaxel in the metastatic setting of TNBCs⁶⁹.

4.2 Exploiting combinatorial strategies to subvert resistance

Therapeutic inactivation of an essential protein, in some cases the protein complex, produces selective pressure, allowing tumor cells to evolve mechanisms of resistance. Provided the molecular complexity and interplay between signaling pathways within tumor cells, single agents are insufficient to block driving survival pathways to tackle TNBC, rationalizing multi-targeted remedy to neutralize intrinsic and/or acquired resistance. Multi-targeted therapy can be achieved by either combination of highly selective drugs or multiple-targeting single agents based on polypharmacology.

Inhibitors targeting different protein kinases have been tested in combinations, as well as with other therapy modalities. Activation of PI3K/AKT/mTOR pathway is common in TNBC. A randomized Phase II study has assessed the combination efficacy of AKT inhibitor AZD5363 with paclitaxel as first-line treatment for mTNBC⁷⁰. The patients with alterations in PI3K pathway demonstrated remarkably improved median PFS of 9.3 months in the combination group, whereas the median PFS was 3.7 months for the paclitaxel alone group. Co-inhibition of MEK and BRAF has been attempted to target separate components in the same pathway to restrain downstream signaling reactivation. Indeed, a Phase III trial reported that the combination reduced the risk of disease progression compared to BRAF-targeted monotherapy⁷¹. In **Chapter 2**, FRET imaging-based high throughput kinase activity screen for ERK and AKT revealed that sustained ERK activity conferred EGFRi-targeted inhibition resistance in TNBC cells, presenting an excellent possibility to simultaneously target EGFR and downstream MEK/ERK signaling. Another approach for combination therapy is to targeting compensatory pathways in parallel. MEK inhibition was shown to reactivate ERK via upregulating multiple RTKs. The

combination with multi-RTK targeted inhibitor sorafenib could sensitize TNBC cells to MEK inhibition and greatly suppressed tumor regression⁵⁸. PI3K pathway is known to be activated by MEK inhibition, thus combining MEK-targeting drugs with inhibitors against PI3K/AKT/mTOR has been applicable. Significant tumor shrinkage by MEK inhibition was found in TNBC mouse model when combined with PI3K inhibitor^{72,73}, as well as for the combination with AKT inhibitor in TNBC patients with both MEK and PI3K pathway activation⁷⁴. Co-targeting of MEK and mTOR or upstream EGFR/VEGFR has also been tested in clinical trials (NCT02583542, NCT01586624 and NCT00600496). In our study, **Chapter 3** has identified FYN as a negative regulator of EGFR signaling, and proposed co-targeting FYN to reverse drug resistance in cancer cells with elevated EGFR expression, including TNBC. Recently, the emerging combinations of targeted therapy for the treatment of TNBC have been summarized in a review⁷⁵. Alternatively, polypharmacology with multi-target KIs might be exploited to circumvent drug resistance. Targeting multiple signaling elements by single agents could resist pathway reactivation and reprogramming, thus ultimately delay the onset of resistance. An important example is the utilization of ponatinib, a dual PDGFRA/FGFR1 inhibitor, which overcomes PDGFRA inhibitor resistance by disrupting the driver signaling event (PDGFRA) and the adaptive FGFR1 pathway⁷⁶. By utilizing an integrated systematic screening and cheminformatics approach, **Chapter 4** revealed the synergistic effects of multi-kinase targeted inhibitor AEE788 on rapalogs treatment in TNBCs and its underlying polypharmacology.

The discovery of immune checkpoints and recent clinical success of their blockade have led to a surge in cancer immunotherapy. It has been reported that lymphocytic infiltration correlates improved response to chemotherapy and clinical outcomes in TNBC, pressing the potential of combining immune checkpoint inhibition and chemotherapy for the treatment of this disease^{50-52, 77}. Recently, results from Phase II TONIC trial have been presented at ASCO 2018, indicating that an upregulation of pro-immunogenic signatures and an increase in T-cells and T-cell clonality were observed after cisplatin or doxorubicin treatment, in which their combination with nivolumab (an anti-PD-1 mAb) enhanced the overall response rate in mTNBC⁷⁰. And these higher-responsive cohorts will be expanded in the next phase of the trial owing to the encouraging results. More recently, FDA has approved the combination of PD-L1 inhibitor atezolizumab with nab-paclitaxel for PD-L1-positive, advanced TNBC⁵³. Other clinical trials testing the efficacy of immunotherapy in combination with neoadjuvant or adjuvant chemotherapy in early-stage TNBC are currently on going (NCT03036488, NCT02954874, NCT03197935, NCT03281954 and NCT02926196)⁷⁸. In addition to combination with chemotherapy, immune checkpoint inhibitors are also under clinical investigation along with molecularly targeted agents. The KEYNOTE-162 trial testing the combination of niraparib and pembrolizumab in mTNBC reported remarkably higher objective responses (67%) in

patients with gBRCA⁷⁸. It was reported that Abemaciclib monotherapy increased T cell inflammatory signature in murine cancer model, whereas combination with anti-PD-L1 drugs resulted in complete tumor regression⁷⁹.

Dosing regimens of combined drugs may also have impact on therapeutic potency. For example, studies using TNBC xenografts argued that sequential administration of combined drugs effectively prevented oncogenic pathway rewiring and elevated apoptotic response, as illustrated by the sensitized response to doxorubicin by the pretreatment of EGFR-targeted inhibitor erlotinib⁸⁰. In another preclinical study involving distinct sequential regimens of CDK inhibitor flavopiridol and topoisomerase inhibitor irinotecan, researchers found that the combination effectively induced apoptosis (43%) of colon cancer cells when administrated in a specific order (irinotecan followed by flavopiridol), whereas both the reverse order (15%) and simultaneous therapy (30%) were less effective⁸¹.

4.3 Identification of novel therapeutic targets

High-throughput genetic perturbation drug screens have led to the discovery of gene essentialities, synthetic lethality interactions and drugs with the potential to improve the treatment of cancer, including TNBC⁸²⁻⁸⁴. For example, a genome-wide siRNA screen has identified proteasome addiction in basal-like TNBC cells⁸³. Pharmacologically targeting proteasome inhibited TNBC tumor growth in mice. Another siRNA-based screen across 117 cell lines spanning 10 cancer types revealed cancer driver gene dependencies and enabled the prediction of cancer cell drug responsiveness⁸⁴. Provided the off-target limitation of RNA interference (RNAi), a genome-scale shRNA screen was performed across 501 cancer cell lines, accompanied by DEMETER computational algorithm to remove false positives⁸⁵. Novel kinase dependencies in TNBC have been discovered through a FRET biosensor-based kinase inhibitor screen in **Chapter 2** with a possibility to prioritize therapeutic targets. Comprehensive drug combination screens also reported pivotal findings, resulting in 44 effective combinations evaluated in mouse models⁸⁶. These evaluations have led to the clinical testing of two promising combinations bortezomib + clofarabine and paclitaxel + nilotinib in Phase I trials (NCT02211755 and NCT02379416, respectively).

Gene expression-based approaches have been employed to identify therapeutic targets in TNBC. The integration of genomic and proteomic platform on breast cancer cell lines and tumors revealed five potential candidate genes specifically enriched in TNBC, including STAT5A, POSTN, MYLK, HLA-A and EPHA2⁸⁷. Recently, an integrative analysis of mutations, copy-number changes, mRNA expression, gene fusions and DNA methylation profiles has identified co-occurring actionable alterations, suggesting opportunities for

combination therapies ⁸⁸. Additionally, computational algorithm-based aggregation in recurrently altered genomic regions has also assisted in the identification of novel cancer drivers/therapeutic targets ⁸⁹⁻⁹¹. **Chapter 5** has exploited the robust ADMIRE algorithm to prioritize 148 candidate genes driving TNBC cell growth and proliferation. siRNA-based functional screen further validated, besides known EGFR and MYC oncogenes, novel driver genes including ASAP1 which showed high amplification frequency and gene expression in TNBC cohorts, and associated with poor prognosis in patients. A pooled shRNA breast cancer cell line screen, integrated with siMEM algorithm and omics data, has identified BRD4 as a potential target in luminal breast cancer. In addition to known drivers, this approach also found two potential new amplified drivers ZNF652 and YEATS4, depletion of which significantly inhibited cell proliferation in breast cancer cell lines with corresponding amplification ⁹¹. Another integrative study assessing frequent copy number alterations (CNAs) in TNBCs identified and functionally validated 13 TNBC addiction genes. The role of one potential drug target KIFC1 was mechanistically studied and, accordingly, a selection biomarker was developed to identify patients with tumor exhibiting centrosome amplification ⁸⁹.

5. Recent advances and new opportunities

5.1 Tackling cancer heterogeneity

Cancer cell lines (CCLs) represent easy-to-manipulate systems for high-throughput drug and genetic screens. Equipped with automated liquid handling techniques, large-scale high-throughput screens are now much attainable and less time-consuming. However, faithfully recapitulating cancer heterogeneity requires large panels of available CCLs. With the goal of capturing this diversity, two large projects have been initiated, namely the Cancer Cell Line Factory and the Human Cancer Model Initiative. The former one aims to create over 10,000 CCLs for research use ⁹², while the latter one aims to generate about 1000 new in vitro cancer models ⁹³. Recently, organoids have emerged as novel in vitro 3D cancer models with the capability of self-organizing and phenocopying essential facets of organs where they derive ⁹³. Multiple living organoid biobanks have been established for a collection of cancer types, including breast cancer. Mouse models are highly important in vivo systems in preclinical cancer research, ranging from cell line-derived xenografts (CDXs) to PDXs, to genetically engineered mouse models (GEMMs), and to the recently revisited syngeneic mouse models owing to the breakthrough of immunotherapy.

5.2 Improved gene manipulation

RNA interference (RNAi) allows broad gene inactivation and functional analysis of suppressed genes, which can be achieved transiently by siRNA, or stably by shRNA. Multiple RNAi libraries have been established targeting almost the entire genome or subsets, such as the druggable genome, the adhesome or the kinome. RNAi-based screens have been used to identify addiction genes and drug response-modulating genes. However, this approach is limited by its off-target effects and incomplete gene inactivation. CRISPR/Cas9 is a rapidly developing gene-editing tool with high efficiency and specificity. It has been substantially used in cancer research for generation of cancer models, synergistic gene study and target identification and validation ^{94, 95}. In a comparative study of genome-wide CRISPR/Cas9 dropout screen and shRNA screen, researchers found that CRISPR/Cas9 screen was more capable of detecting cancer essential genes than shRNA screen ⁹⁶. Though, false-positive hits were discovered in highly amplified regions owing to the induction of DNA damage response. It was reported that sgRNA-associated target mismatches caused cell lethality, necessitating the design of more specific sgRNAs. Notably, for both RNAi screen and CRISPR/Cas9 screen, improved algorithms have been developed to examine on- and off- target effects, holding the promise to remove false-positives ^{85, 94}. In context of CRISPR/Cas9 screens, modified sgRNA design algorithms have also been developed to improve screen sensitivity ⁹⁷.

5.3 Advanced high-throughput screening

Nowadays, high-throughput screens have been advanced by exploitation of lentiviral barcoding and mixing genetically labeled cell lines. The novel platform PRISM enables simultaneous detection of a drug's activity on a mixture of CCLs in a single well, resulting in much higher throughput ⁹⁸. In addition, advanced high-throughput imaging allows for tempo-spatial detection of key cancer events in living cells and more complex intravital mouse model with improved fidelity and statistical robustness. Image-based screening approaches can provide high-throughput phenotypic readouts for cancer drug discovery, such as cell morphology, migration, programmed cell death and cell cycle progression ⁹⁹. Our approach described in **Chapter 2**, by leveraging FRET biosensor-based reporter cell systems, has also advanced the live cell high content imaging-based quantification of kinase activity profiles in TNBC cells. Multi-dimensional image analyses of kinase activity dynamics in high temporal resolution revealed differential kinase dependencies in various drug-resistant TNBC cells, as well as possible off-target effect of clinical kinase drugs.

5.4 Genomic sequencing and bioinformatics

Massive next-generation DNA/RNA sequencing studies represent an increasing reservoir of genetic aberration and gene expression information. Coupled with bioinformatics-based pathway analysis approaches, these databases allows for the exploration of

signaling pathway activation and active signaling components. TempO-Seq-based targeted whole genome RNA sequencing analysis performed in **Chapter 5** concluded that, the novel TNBC driver gene ASAP1 regulates various cytokine and apoptosis signaling components that are significantly associated with TNBC prognosis, supporting the potentiality of ASAP1 as a therapeutic target for the dismal disease. In addition, chemoinformatics helps to better understand the drug-target interactions. Chemoinformatics-guided target prediction and validation in **Chapter 4** has pronounced the polypharmacology mechanisms underlying the synergy of multi-kinase targeted inhibition on mTORi treatment in TNBC. An integrated application of these continuously advancing approaches/platforms will eventually lead to potential novel cancer therapy.

6. Aim and scope of this thesis

TNBC represents a highly aggressive disease, and incurable. Cytotoxic chemotherapy is the only option for systemic treatment. Prospective precision medicine in TNBC requires the development of new targeted therapeutic options. The main objectives of the studies described in this thesis are to i) understand the molecular basis of TNBC drug response/resistance to small-molecule KIs, ii) systematically identify vulnerabilities of refractory TNBC cells, and iii) eventually identify novel therapeutic targets and potential combination therapies. **Chapter 2** explored highly dynamic ERK and AKT kinase activity in TNBC cells in response to a well-established KI library. The integrated high-throughput FRET imaging and phenotypic readouts approach has revealed differential kinase dependencies for TNBC cell proliferation. The research also identified TNBC drug resistance against EGFR- and AKT/mTOR-targeted inhibitors, separately. These resistant cell lines were further used for synthetic lethality screens in **Chapter 3** and **Chapter 4**. EGFR inhibitors (EGFRi) have long been explored as targeted therapy for TNBC, but rarely beneficial in the clinic. In **Chapter 3**, a kinome-wide siRNA screen was performed in EGFRi-resistant TNBC cells in combination with lapatinib treatment. The combination screen aimed to identify key modulators of kinase signal transduction, conferring TNBC resistance against EGFR-targeted inhibition. Overactivation of PI3K/AKT/mTOR pathway is common in TNBC. Targeting mTOR, the convergent signaling element of multiple pathways, is of particular interest. A KI library screen was conducted in the absence or presence of rapamycin, as shown in **Chapter 4**. This study aimed to explore effective combined drug treatment to overcome TNBC resistance to mTOR inhibitors (mTORi). The research suggested using polypharmacology to circumvent mTORi resistance by combining multi-targeted kinase inhibition. The targets of the identified KI were predicted by cheminformatics-based survey and functionally validated by siRNA-mediated gene suppression. Over 80% of cases diagnosed with TNBC represent TP53 mutation, resulting

in high likelihood of gene instability. Thus, discovery of recurrent CNAs in the focal regions of TNBC genome provides an excellent possibility to identify therapeutic targets. Using a robust computational algorithm, **Chapter 5** identified not only known oncogenes but also novel putative cancer drivers. Following functional validation via gene inactivation, whole-genome RNA sequencing and pathway analysis were carried out to investigate the functionalities of the most clinically relevant drivers. Last of all, **Chapter 6** summarizes and discusses the findings of the work. Challenges and future perspectives are also provided.

Chapter 2

FRET biosensor-based kinase inhibitor screen for ERK and AKT activity reveals differential kinase dependencies for proliferation in TNBC cells

Jichao He, Steven Wink, Hans de Bont, Sylvia Le Dévédec, Yinghui Zhang, Bob van de Water

Published in *Biochem Pharmacol.* 2019 Sep 16. doi: 10.1016/j.bcp.2019.113640

Abstract

Enhanced expression and activity of protein kinases are critical in tumor cell proliferation and cancer progression. These various cancer-related kinases form intricate interdependent signaling networks. Evaluation of the effect of various kinase inhibitors on these networks is critical to understand kinase inhibitor efficacy in cancer therapy. The dynamic activation of some kinases can be monitored by fluorescence resonance energy transfer (FRET) biosensors with high temporal resolution. Here, we established a FRET biosensor-based high throughput imaging approach to determine ERK and AKT activity in two triple-negative breast cancer (TNBC) cell lines HCC1806 and Hs578T. FRET functionality was systematically evaluated using EGF stimulation and different MEK and AKT inhibitors, respectively. Next, we assessed the effect of a kinase inhibitor library containing >350 different kinase inhibitors (KIs) on ERK and AKT kinase activity using a FRET high-throughput screening setting. Suppression of FRET-ERK activity was generally positively correlated with the proliferation phenotype against inhibitors targeting MAPK signaling in both cell lines containing FRET-ERK reporter. AKT inhibitor (AKTi) resistant HCC1806 showed decreased proliferation associated with downregulated dynamics of FRET-ERK when treated with KIs targeting protein receptor tyrosine kinase (RTK). Yet, MEK inhibitor (MEKi) resistant Hs578T showed positively correlated FRET-AKT and proliferative responses against different PI3K and AKT inhibitors. Altogether, our data demonstrate the feasibility to integrate high throughput imaging-based screening of intracellular kinase activity using FRET-based biosensors in assessing kinase specificity and possible signaling crosstalk in direct relation to therapeutic outcome.

Keywords

FRET; Kinase activity dynamics; TNBC; Drug resistance; Kinase dependencies

1. Introduction

Protein kinases constitute the complexity in signaling networks that orchestrate extracellular and intracellular signals to control cell growth, proliferation and survival¹⁰⁰⁻¹⁰³. Deregulation of kinase signaling cascades underlies the cause of cancer. Triple-negative breast cancer (TNBC) is an aggressive subtype of breast cancer with unfavorable prognosis^{104, 105}. Advanced large-scale gene expression profiling has revealed several frequently altered signaling pathways in TNBC, including high expression of genes in epithelial-mesenchymal transition and growth factor pathways, enriched immune cell processes and androgen signaling, and increased cell cycle and DNA damage responses^{8, 19, 106}. Particularly, overexpression of receptor tyrosine kinases (RTKs) and frequently elevated activation of MAPK/ERK and PI3K/AKT pathways, the two canonical pathways converging RTK signaling, have been observed in a set of TNBCs^{107, 108}. Therefore, kinase targeted therapies with diverse RTK inhibitors, MEK inhibitors (MEKi) and AKT inhibitors (AKTi) to block upregulated RTK, MAPK/ERK and PI3K/AKT signaling in TNBC have been explored under clinical investigation¹⁰⁹⁻¹¹¹. However, TNBC patients do not respond equally well to kinase targeted therapies, often encountering the problem of inhibitor resistance, due to upregulated adaptive signaling pathways or drug induced kinome reprogramming^{58, 112-115}. Hence, dissection of kinase dependency is essential for discovering effective kinase targeted therapeutics for the dismal TNBC.

Fluorescence resonance energy transfer (FRET) imaging has been explored in innovating the discovery of effective therapeutics for cancer therapy^{99, 116-118}. In particular, genetically encoded FRET biosensors that stably express two fluorescent proteins, mostly CFP and YFP (cyan and yellow fluorescent proteins), enable quantitative measurement of kinase dynamic activity and real-time monitoring of inhibitor-target potency in living cells¹¹⁹. FRET biosensors are developed based on phosphorylated peptide substrate of a kinase for its kinase activity¹²⁰ or based on conformational changes of the kinase itself for its activation¹²¹. Substrate-based FRET biosensors have been extensively applied to evaluate the activities of kinase targets in response to kinase inhibitors. For example, a stably expressed FRET biosensor for epidermal growth factor receptor (EGFR) signaling in HeLa cells was reported to predict the efficiency of inhibitors targeting Ras-ERK and PI3K-S6K pathways¹¹⁷. A designed FRET kinase translocation reporter was described to dynamically measure multiple JNK, p38 and ERK activities in live single cells under inhibitor treatment¹²². A panel of optimized FRET biosensors have been established to monitor the kinase activities of PKA, ERK, JNK, EGFR/Abl, Rac1, RSK, S6K, AKT and PKC in response to EGF stimulation and kinase inhibitors^{123, 124}. Therefore, utilization of substrate-based FRET biosensor imaging may allow dissecting the complexity of kinase networks in drug-resistant TNBC cells and predicting effective kinase inhibitors for treating the refractory TNBC.

We have previously profiled the proliferative responses of 19 TNBC cell lines to 378 kinase inhibitors (Selleckchem®). Consistent to the clinical results, our results also demonstrated the differential response phenotype of TNBC cells to MEK and AKT targeted inhibitors, and defined the groups of MEKi-resistant and AKTi-resistant TNBC cell lines (van der Noord et al, submitted). In this study, we described a FRET-ERK and FRET-AKT biosensor based high-throughput imaging approach to quantitatively monitor ERK and AKT dynamic activity in MEKi-resistant and AKTi-resistant TNBC cells in response to the 378 kinase inhibitors. We derived a mathematical model that associates MEK and AKT kinase activity with anti-proliferation effects, by which we revealed unique kinase dependencies on RTK/MAPK and PI3K/AKT pathways that are distinctly targetable in the resistant TNBC cells.

2. Materials and methods

2.1. Reagents and antibodies

A library of 378-kinase inhibitors (the L1200 library), rapamycin, BEZ235, AZD5363, erlotinib, gefitinib, selumetinib, GSK1059615, GSK690693 and TAK733 inhibitors were purchased from Selleckchem (Huissen, the Netherlands). The phospho(Ser473)-AKT (9271), phospho(Thr202/Tyr204)-p44/42 MAPK (ERK1/2, 9101), GFP (D5.1, 2956), AKT (9272) and p44/42 MAPK (ERK1/2, 4695) antibodies were from Cell Signaling (Bioké, Leiden, the Netherlands). The antibody against tubulin (T-9026), blasticidin S (15205) and human epidermal growth factor (EGF, E9644) were from Sigma Aldrich (Zwijndrecht, the Netherlands).

2.2. Cell culture

Human TNBC cell line HCC1806 and Hs578T were provided by Erasmus Medical Center (Rotterdam, the Netherlands). Cells were cultured in RPMI-1640 medium supplemented with 10% fetal bovine serum, 25 U/mL penicillin and 25 µg/mL streptomycin in a humidified incubator at 37°C with 5% CO₂.

2.3. Establishment of stable FRET reporter cell line

Constructs of FRET biosensors for ERK (named pPBbsr-EKAREV-nls) and AKT (named pPBbsr-Eevee-iAKT-nes) have been described previously^{123,124} and kindly provided by Prof. Dr. Michiyuki Matsuda (Laboratory of Bioimaging and Cell Signaling, Kyoto University, Japan). Stable cell lines expressing ERK-FRET and AKT-FRET biosensors using a transposon system were established, as described previously¹¹⁸. pCMV-mPBase (mammalian codon-optimized PBase) encoding a piggyBac transposase was a gift from Allan Bradley (Wellcome Trust Sanger Institute, Cambridge, UK). HCC1806 and Hs578T cells were transfected with pCMV-mPBase and either pPBbsr-EKAREV-nls or pPBbsr-Eevee-iAKT-nes, and selected with blasticidin S at a dose of 2 µg/ml for 10 days to generate cells expressing

EKAREV-nls or Eevee-iAKT. Plasmids were transfected using lipofectamine™ 3000 transfection reagent (Thermo Fisher Scientific, Waltham, USA) according to the manufacturer's instructions. Selected cells were suspended and further FACS (fluorescence activated cell sorting)-sorted at the Leiden University Medical Center flow cytometry core facility (Leiden, the Netherlands).

2.4. *Cell proliferation assay*

A sulforhodamine B (SRB) colorimetric assay was used to measure total amount of proteins indicative of cell proliferation, as previously described¹²⁵.

2.5. *siRNA transfection*

To silence target genes, 50 nM siGENOME Human SMARTpool siRNA mix (GE Dharmacon, Lafayette, CO, USA) was transfected into cells by transfection reagent INTERFERin (Polyplus-Transfection SA, Illkirch-Graffenstaden, France) according to the manufacturer's instructions. The medium was refreshed 24 h post-transfection and transfected cells were used in experiments 48 h post-transfection.

2.6. *Western Blotting*

Cells were seeded in 6-well plates at the appropriate density. For stimulation/starvation assays, medium was refreshed with serum-free medium (SFM) the following day and cells were starved overnight. Thereafter, cells were stimulated with 50 ng/ml EGF (Sigma; E9644) for 5 min in SFM. Cells were lysed with RIPA buffer containing 1% protease/phosphatase inhibitor cocktail (Sigma-Aldrich, P8340). Proteins were resolved by SDS-PAGE and transferred to polyvinylidene difluoride membranes. Membranes were blocked in 5% BSA in Tris-buffered saline with 0.05% Tween-20 (TBS-T), followed by overnight incubation with primary antibodies, washing, and 1 h incubation with HRP-conjugated secondary antibodies. Chemiluminescence was generated in the presence of HRP substrate and detected with an Amersham Imager 600 (GE Healthcare Life Sciences, Eindhoven, the Netherlands). Protein bands were quantified using ImageJ (NIH, US).

2.7. *Time-Lapse imaging*

Cells were imaged using a Nikon Eclipse Ti confocal microscope (Nikon, Amsterdam, The Netherlands) equipped with a PlanApoVC 20x/0.75 objective lens, a cooled CCD camera, a CoolLED pE-100 excitation light source, an automated stage and perfect focus system, and an incubation chamber. The dichroic mirrors and filters used for time-lapse imaging were as follows: a T640LPXR dichroic mirror, and emission filters FF01-482/35 and FF01-525/50 for CFP and FRET, respectively. All images were acquired using NIS software (Nikon). 408 nm LED lamp was used as light source, with 1.4% of lamp power. Acquisition times were 2 s for donor channel and 2 s for FRET at binning 2 × 2. Cells were plated in 96-well,

24

collagen-coated, glass-bottom plate (Greiner, Kremsmünster, Austria). After attachment, cells were imaged in phenol red-free RPMI-1640 medium at 37°C. For EGF exposure study, cells were starved at least 12 h and treated with stimulus, followed by the addition of inhibitors if necessary. 3-5 frames were taken prior to any compound addition to obtain basal CFP and FRET intensity level.

2.8. FRET ratio image analysis

Image analysis was implemented using a combination of ilastik (v1.1.9) and CellProfiler (v2.1.1). Acquired images were split into the original channels. Segmentation was performed based on FRET images using ilastik. Mono-channel images were masked with segmentations using CellProfiler. The FRET and CFP intensities were quantified per pixel and the FRET was divided by the CFP channel. FRET/CFP ratio images were created to represent the FRET efficiency. In the intensity-modulated display mode, eight colors from red to blue are used to represent the FRET/CFP ratio. The FRET/CFP value prior to compounds exposure was averaged and used as the reference. The ratio of raw FRET/CFP value versus the reference value was defined as the normalized FRET/CFP value. FRET dynamics curve for each treatment was modeled using R (v3.2.2) and RStudio (v0.99.887) with an in-house developed “celloscillate” pipeline (Wink et al, manuscript in preparation). Extremes representing maximum FRET effect were extracted from fitted curves and defined as MaxMagnitudeFRET.

2.9. Statistical analysis

Pearson correlation analysis were performed using GraphPad Prism 7 with 95% confidence band. Significance was set at $r > 0.5$. All experiments were performed in at least three independent biological replicates. Data were expressed as mean \pm SEM. The hierarchical clustering in heatmap was performed using CRAN pheatmap package in RStudio (v0.99.887).

3. Results

3.1. Establishment of stably expressed FRET-ERK and FRET-AKT biosensor in TNBC cells resistant to MEK or AKT inhibition

To monitor ERK and AKT dynamic activity in control of TNBC cell proliferation, we firstly ectopically expressed YPet/ECFP pair and substrate-based FRET-ERK biosensor (EKAREV) and FRET-AKT biosensor (Eevee-iAkt)^{123, 124} into an AKTi-resistant TNBC cell line (HCC1806) and a MEKi-resistant TNBC cell line (Hs578T), respectively. Two stable FRET-ERK biosensor lines (HCC1806/ERK, Hs578/ERK) and two FRET-AKT biosensor lines (HCC1806/AKT, Hs578T/AKT) were established, overall achieving > 85% of fluorescent positive cell population (Fig. 1A) and high levels of FRET pair expression (GFP bands) (Fig. 1B, left panel). Ectopic expression of FRET-ERK and FRET-AKT biosensors did not affect the

endogenous ERK and AKT levels, compared to parental cells (Fig. 1B). Moreover, the fluorescent protein was homogeneously expressed in the established FRET biosensor cells, as observed via GFP channel of fluorescent microscopy (Fig. 1C). In response to proliferative inhibition by MEKi selumetinib and AKTi AZD5363, HCC1806 FRET biosensor cells remained MEKi-sensitive and AKTi-resistant, while Hs578T FRET biosensor cells were AKTi-sensitive and MEKi-resistant, phenocopying the drug responses of parental cells (Fig. 1D).

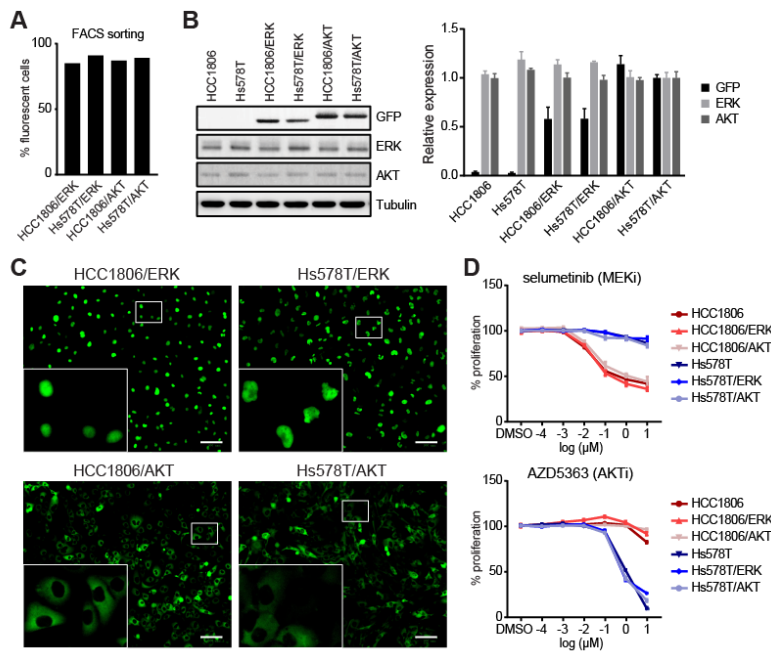


Fig. 1. Establishment of FRET reporter TNBC cell lines. (A) Percentage of FRET biosensor positive cells sorted by FACS. TNBC cells were transfected with DNA plasmids encoding FRET-ERK and -AKT biosensors and selected with blasticidin (20 μg/ml) for one week, followed by trypsinization and suspension prior to FACS. **(B)** Biosensor expression in FRET reporter cells. Antibody against GFP was used to detect fluorescence of expressed biosensors. Quantification of ERK, AKT and total fluorescent protein level in parental and FRET reporter TNBC cell lines. The expression level was normalized to Tubulin and further compared to that in Hs578T/AKT cells. **(C)** Fluorescence imaging of FRET reporter cells. Cells were imaged in GFP channel using ZOE™ fluorescent cell imager. Scale bar = 100 μm. **(D)** Effects of selumetinib and AZD5363 on cell proliferation of parental and FRET biosensors cell lines. Both parental and FRET-ERK (AKT) reporter HCC1806 and Hs578T cells were treated with selumetinib and AZD5363 in concentration range for 4 days, followed by SRB proliferation assay.

3.2. FRET-ERK and FRET-AKT activity in the biosensor TNBC cells are responsive to EGF stimulation and MEK or AKT inhibition

Since ERK and AKT are essential effectors of EGF-triggered signaling cascades, we next evaluated FRET-ERK and FRET-AKT activity dynamics in the presence of EGF at 10, 25, 50 and 100 ng/ml concentrations, respectively. The ratio of fluorescence intensity of the YFP (acceptor) channel (FRET) versus fluorescence intensity of CFP (donor) channel (CFP),

26

FRET/CFP, was used to represent the level of FRET-ERK and FRET-AKT kinase activities [15].

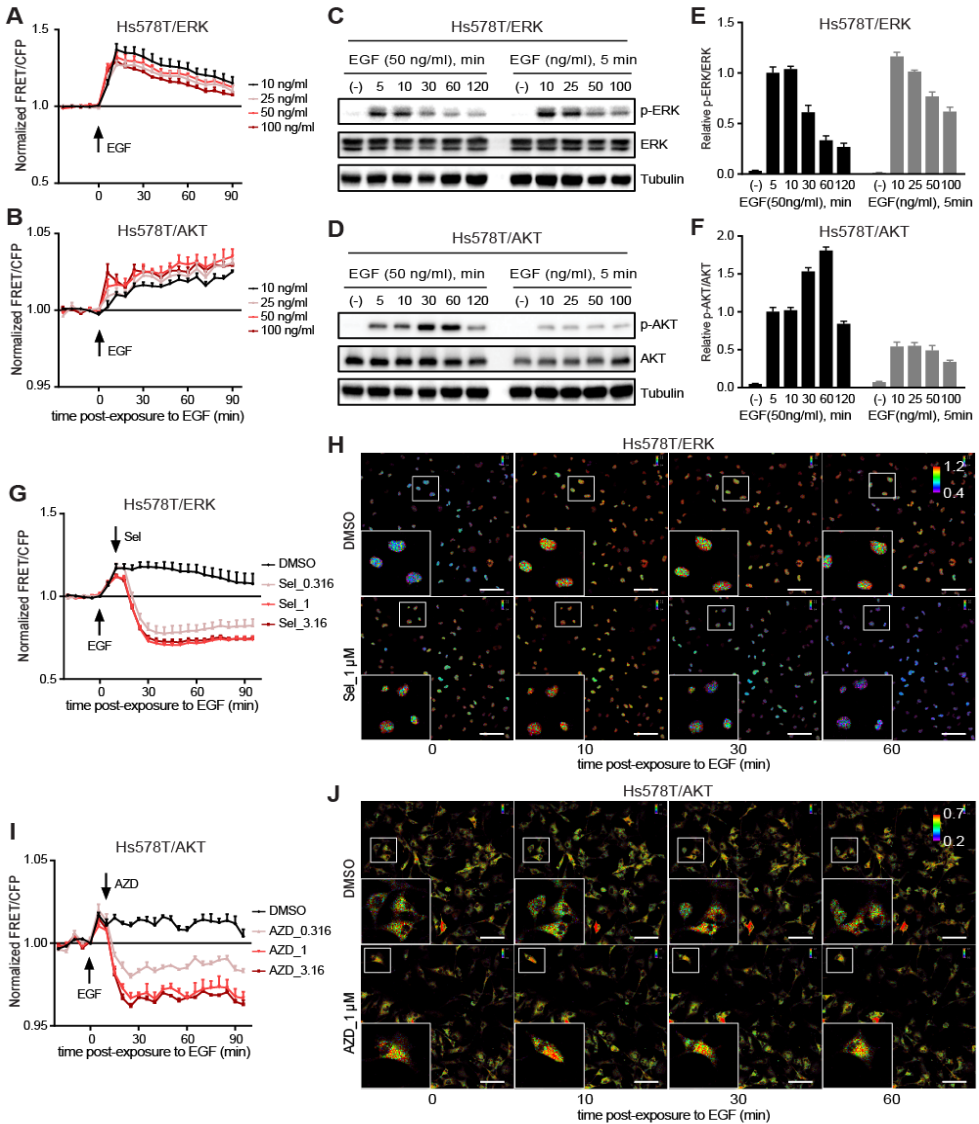


Fig. 2. Effects of MEK and AKT inhibitors on FRET-ERK and FRET-AKT activity. (A-B) Dynamics of FRET-ERK (A) and FRET-AKT (B) activity upon concentration range of EGF exposure. FRET reporter cells were serum-starved overnight and exposed to EGF in at different concentration. Five basal images were taken before EGF (ng/ml) was added. (C-D) Effects of EGF exposure on ERK (C) and AKT (D) phosphorylation. FRET reporter cells were serum-starved overnight and exposed to EGF in time course (left panel, 50 ng/ml) and concentration range (right panel, 5 min). (E-F) Quantification of phosphorylated ERK (E) and AKT (F) level, derived from (C-D). The expression level was normalized to total ERK or AKT and further compared to that in the sample exposed to EGF (50 ng/ml) for 5 min, the second bar. (G-J) Effects of selmetinib (Sel) and AZD5363 (AZD) on FRET-ERK (G-H) and FRET-AKT (I-J) activity dynamics in the presence of EGF. FRET reporter cells were serum-starved overnight and exposed to EGF at 50 ng/ml. Five basal images were taken before EGF was added. Arrow indicates when EGF, Sel or AZD was added; values represent μM . Raw FRET/CFP ratio was color-coded in rainbow scale. Scale bar = 100 μm .

In Hs578T/ERK reporter cells, FRET-ERK activity was effectively induced by EGF even at low concentration of 10 ng/ml, peaking at 10 min post-exposure and declining gradually till 90 min (Fig. 2A; Supplementary videos 1-2). The rapid induction of FRET-ERK activity by EGF was also captured in HCC1806/ERK cells (Fig. 3; Supplementary videos 3-4), but attenuated swiftly, compared to Hs578T/ERK cells. FRET-AKT activity in Hs578T/AKT

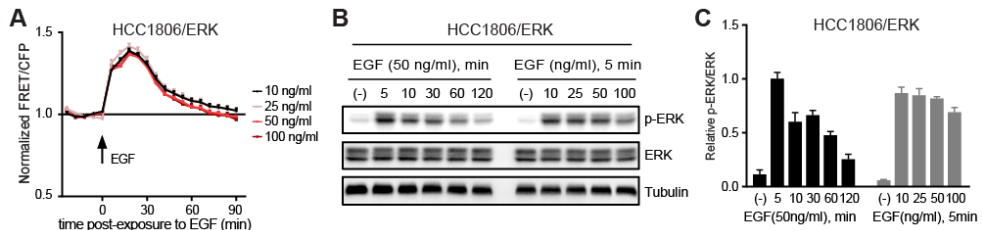


Fig. 3. EGF stimulates FRET-ERK in HCC1806/ERK cells. (A) Dynamics of FRET-ERK activity upon EGF exposure in dose range. FRET reporter cells were serum-starved overnight. Five basal images were taken before EGF was added. **(B)** Effects of EGF exposure on ERK phosphorylation. FRET reporter cells were serum-starved overnight and exposed to EGF in time course (left panel, 50 ng/ml) and dose range (right panel, 5 min). **(C)** Quantification of phosphorylated ERK level, derived from **(B)**. The expression level was normalized to total ERK and further compared to that in the sample exposed to EGF (50 ng/ml) for 5 min, the second bar.

reporter cells was immediately triggered upon EGF stimulation, being enhanced during the 90-min imaging period (Fig. 2B). The FRET-ERK and FRET-AKT activities did not show significant EGF dose dependency. The FRET/CFP detection window in our established FRET-ERK and FRET-AKT biosensor TNBC cells were consistent with that shown in the original publications^{123, 124}. It has been reported that FRET-ERK and AKT signal positively correlates with ERK and AKT phosphorylation^{124, 126-128}. Consistently, our western blot results confirmed the activation of p-ERK in Hs578T/ERK and p-AKT in Hs578T/AKT biosensor cells, when stimulated with EGF in time course (5, 10, 30, 60 and 120 min, at 50 ng/ml) and in concentration range (10, 25, 50 and 100 ng/ml, for 5 min) (Fig. 2C-F). Next, we demonstrated that the EGF-stimulated FRET-ERK activity in Hs578T/ERK cells was dropped down upon 20 min exposure to MEKi selumetinib in dose dependent manner (Fig. 2G), and the ratiometric FRET intensity was declined post 20 min of selumetinib exposure, as captured by time lapse imaging (Fig. 2H; Supplementary video 5). Similarly, the EGF-stimulated FRET-AKT activity in Hs578T/AKT cells was subject to the inhibitory effect of AKTi AZD5363 (Fig. 2I-J; Supplementary videos 6-8). To clarify if the EGF-induced FRET kinase activity is attributed to EGFR signaling transduction upon EGF stimulation, we silenced EGFR and ERK2 in Hs578T/ERK cells by siRNA transfection, with AKT1 silencing as negative control. Knockdown of EGFR or ERK2, not AKT1, markedly blocked EGF-induced FRET-ERK activity in Hs578T/ERK cells (Fig. 4A) and moderately in HCC1806/ERK cells (Fig. 4B).

Taking together, our established FRET-ERK and FRET-AKT biosensor TNBC cell models are applicable for capturing ERK and AKT dynamic activities in response to

28

EGF/EGFR signaling cascades and inhibition of MAPK/ERK and PI3K/AKT upstream signaling pathways.

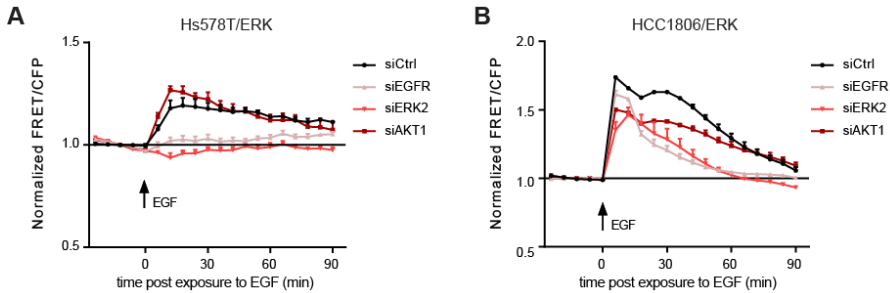


Fig. 4. EGFR and ERK played a role in EGF-stimulated FRET-ERK. (A-B) Effects of EGFR, ERK2 or AKT1 siRNA knockdown on EGF-stimulated FRET-ERK in Hs578T/ERK **(A)** and HCC1806/ERK **(B)** cells. FRET reporter cells were transfected with siRNAs for 48 h and serum-starved overnight prior to exposure to EGF at 50 ng/ml. Five basal images were taken before EGF was added.

3.3. FRET-ERK and FRET-AKT imaging-based kinase inhibitor screening reveals multiple signaling pathways interacting with ERK and AKT kinase activity for TNBC cell proliferation

MAPK/ERK and PI3K/AKT pathways are the major intracellular mechanisms in response to extracellular signaling cues to control cell survival, proliferation, cell cycle and DNA damage¹²⁹⁻¹³³. To characterize ERK and AKT dynamic kinase activities in relation to kinase inhibition and proliferation in TNBC cells, we performed high-throughput FRET screening and proliferation screening with 378 inhibitors (Selleckchem®) targeting 118 kinases in the FRET-ERK and FRET-AKT biosensor TNBC cells above. FRET imaging was automated continuously for 90 min in the presence of kinase inhibitors (1 μ M), and proliferation assay was performed 4 days after treatment. To evaluate FRET kinase activities in response to individual inhibitors, we modeled each temporal FRET dynamics curve based on FRET/CFP ratio and extracted fitted value for maximum FRET effect (MaxMagnitudeFRET). Pearson correlation analysis of the fitted value for each replicate showed high reproducibility of the FRET screening in each FRET biosensor cell line ($r > 0.8$, Fig. 5A-D). Pearson coefficient r for proliferation assays demonstrated high reproducibility of the replicate proliferation screens ($r > 0.9$, Fig. 5E-H). The maximum FRET effect was plotted to relative proliferation for each kinase inhibitor for each FRET biosensor cell line. Given that the positive control for FRET-ERK (i.e. selumetinib) and FRET-AKT (i.e. AZD5363) achieved 0.8 and 0.96, respectively, we considered half maximum inhibitory effect on proliferation (50%) and FRET/CFP ratio 0.9 for FRET-ERK activity and 0.98 for FRET-AKT activity as effective inhibition. Consequently, 44 kinase inhibitors were screened to effectively inhibit both FRET-ERK activity and proliferation in HCC1806/ERK cells, while only 8 in Hs578T/ERK cells (Fig. 5I-J). In HCC1806/AKT and Hs578T/AKT biosensor cells, 14 and 26 inhibitors were selected, respectively (Fig. 5K-L). The FRET-ERK biosensor inhibitors mainly target signaling components in RTK and MAPK pathways, and the FRET-AKT effective inhibitors mostly

suppress the kinases of PI3K/AKT pathway (Fig. 5M). The FRET-ERK and FRET-AKT biosensor inhibitors also block the signaling networks of angiogenesis, cell cycle, epigenetics, NF- κ B, cytoskeletal signaling, JAK/STAT and DNA damage, indicating their interplay with MAPK/ERK and PI3K/AKT pathways.

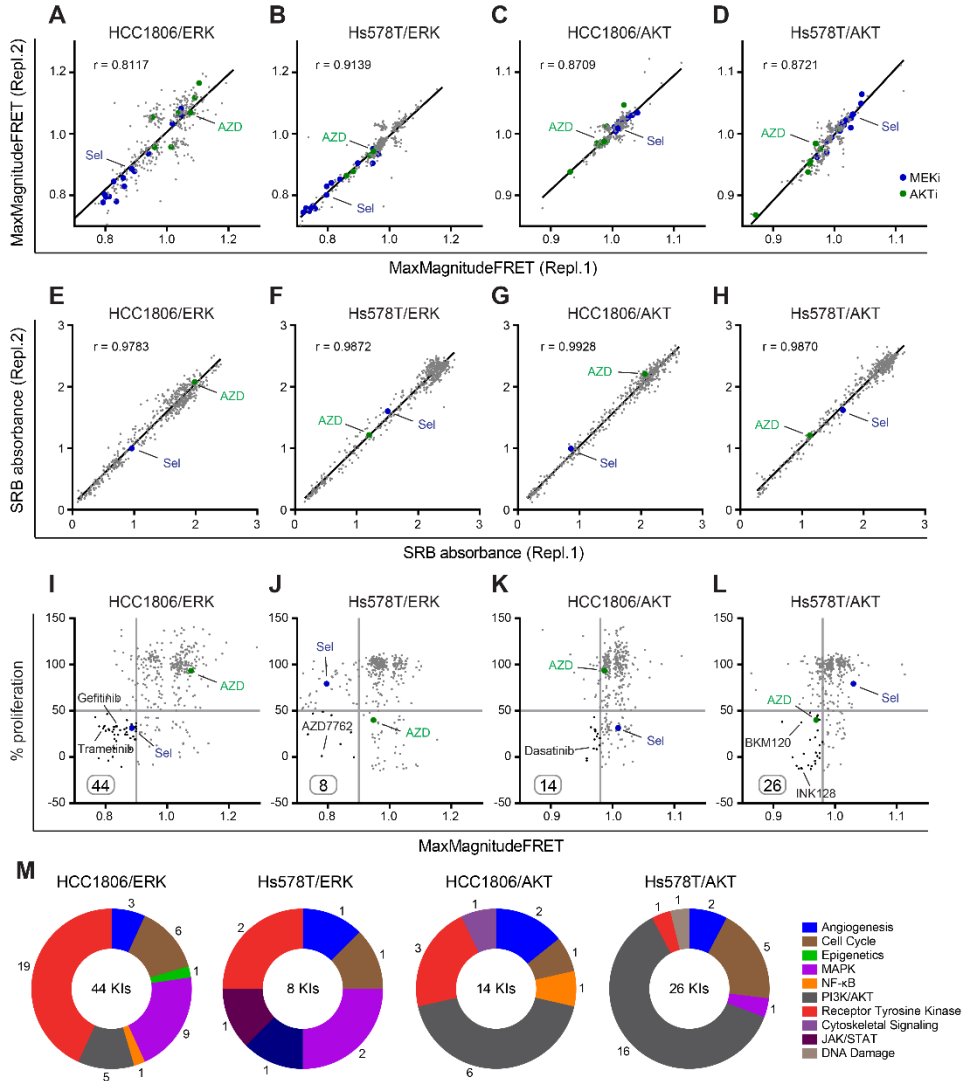


Fig. 5. FRET KI screen identifies differential kinase dependencies in TNBC cells. (A-H) Reproducibility of FRET kinase inhibitor (KI) screen on FRET (A-D) and cell proliferation (E-H). Pearson correlation coefficient r showing reproducibility of replicate screen in FRET reporter cells. Maximum magnitude FRET effect (MaxMagnitudeFRET) was extracted from fitted time-lapse FRET dynamic curve. Blue dots, MEKi. Green dots, AKTi. **(I-L)** Association of relative proliferation of each KI with maximum magnitude effects on FRET in reporter cell lines. KIs showing relative proliferation $\leq 50\%$ and MaxMagnitudeFRET ERK (AKT) ≤ 0.9 (0.98) are numbered and circled. **(M)** Donut plot of KIs selected from (I-L). Numbers of KIs and their targeted signaling pathways are annotated.

3.4. FRET-ERK and FRET-AKT imaging for ERK and AKT activity visualizes RTK/MAPK and PI3K/AKT dependencies for TNBC cell proliferation

The observation above that RTK, MAPK and PI3K/AKT pathways were most frequently targeted by FRET-ERK and FRET-AKT biosensor inhibitors, suggests their essential role in TNBC cell proliferation. Next, we explored the relationship between the FRET effect (MaxMagnitudeFRET) and proliferation in response to inhibitors targeting RTK, MAPK and PI3K/AKT pathways. In response to MAPK inhibitors (MAPKi), both HCC1806 and Hs578T FRET-ERK biosensor cell lines displayed strong positive correlation between cell proliferation and FRET-ERK activity ($r = 0.8318$ and $r = 0.8557$, respectively) (Fig. 6A). While

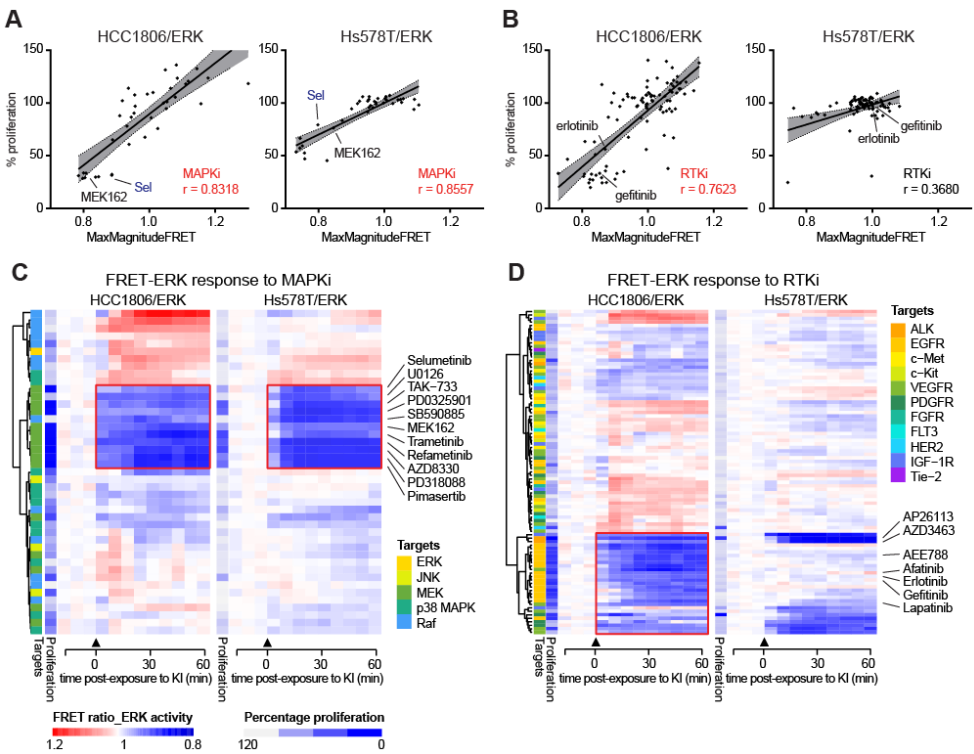


Fig. 6. Correlation between inhibition of FRET-ERK and cell proliferation by selective kinase inhibitors. (A-B) Association of MaxMagnitudeFRET with relative proliferation of KIs targeting MAPK signaling (MAPKi, **A**) and Receptor tyrosine kinase (RTKi, **B**) in FRET-ERK reporter cells. 95% confidence band is shown in grey. Significance is set at Pearson correlation coefficient $r > 0.5$ (red). **(C-D)** Clustering of FRET-ERK activity dynamics against MAPKi (**C**) and RTKi (**D**). Heatmaps were vertically clustered across KIs, annotated with relative proliferation and corresponding targets. FRET/CFP ratio was normalized to DMSO control. Arrow indicates when KIs were added.

the proliferation of HCC1806/ERK cells was highly related to RTK-mediated FRET-ERK activity ($r = 0.7623$), Hs578T/ERK cells were poorly responsive to RTK inhibitors (RTKi) with low correlation ($r = 0.3680$) in proliferation and FRET-ERK activity (Fig. 6B). Furthermore, hierarchical analysis of time-resolved FRET dynamics data clustered the MAPKi effect on FRET-ERK biosensor cells, revealing some MEK inhibitors correlatively inhibiting FRET-ERK

activity and proliferation in both HCC1806/ERK and Hs578T/ERK cells (Fig. 6C). A group of RTKi, including EGFR inhibitors (EGFRi), displayed concurrent inhibitory effect on FRET-ERK activity and proliferation in HCC1806/ERK cells, not in Hs578T/ERK cells (Fig. 6D), indicating the RTKi resistance in Hs578T cells.

In FRET-AKT biosensor cells, positive correlation in FRET-AKT activity and proliferation was monitored in Hs578T/AKT cells when treated with PI3K inhibitors (PI3Ki, $r = 0.7383$) or AKT inhibitors (AKTi, $r = 0.5534$), whereas HCC1806/AKT cells were less responsive to PI3K/AKT inhibition (Fig. 7A-B). Consistently, FRET-AKT dynamics clustering displayed the sensitivity to PI3K/AKT signaling inhibition in Hs578T/AKT cells, but resistance in HCC1806/AKT cells (Fig. 7C-D).

Altogether, our integrated FRET biosensor and kinase inhibitor screening dissects the RTK/MAPK-dependent proliferation in HCC1806 TNBC cells that are resistant to PI3K/AKT inhibition, and the PI3K/AKT-dependent proliferation in Hs578T TNBC cells that are RTKi/MEKi-resistant.

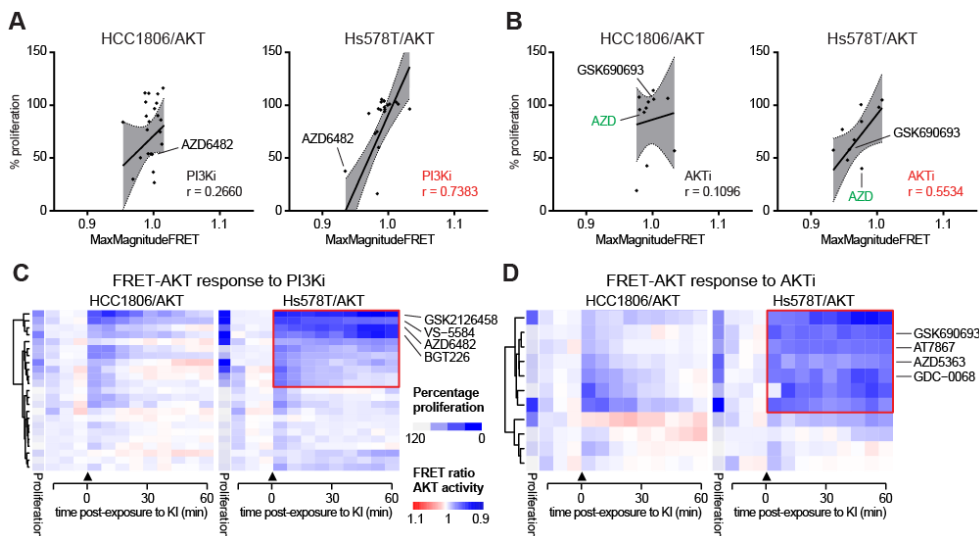


Fig. 7. Correlation between inhibition of FRET-AKT and cell proliferation by selective kinase inhibitors. (A-B) Association of MaxMagnitudeFRET with relative proliferation of KIs targeting PI3K (PI3Ki, **A**) and AKT (AKTi, **B**) in FRET-AKT reporter cells. 95% confidence band is shown in grey. Significance is set at Pearson correlation coefficient $r > 0.5$ (red). **(C-D)** Clustering of FRET-AKT activity dynamics against PI3Ki (**C**) and AKTi (**D**). Heatmaps were vertically clustered across KIs, annotated with relative proliferation and corresponding targets. FRET/CFP ratio was normalized to DMSO control. Arrow indicates when KIs were added.

3.5. MEKi-resistant and AKTi-resistant TNBC cells display differential FRET-ERK and FRET-AKT dynamics in response to RTK/MAPK and PI3K/AKT inhibition

To confirm the findings on kinase signaling dependencies in AKTi-resistant HCC1806 and RTKi/MEKi-resistant Hs578T TNBC cells, we further investigated the inhibitory effects of RTK/MAPK and PI3K/AKT inhibitors in escalating doses (0.316, 1 and 3.16 μM) on FRET-

ERK and FRET-AKT dynamics in the FRET-ERK and FRET-AKT biosensor cell lines. Treatment

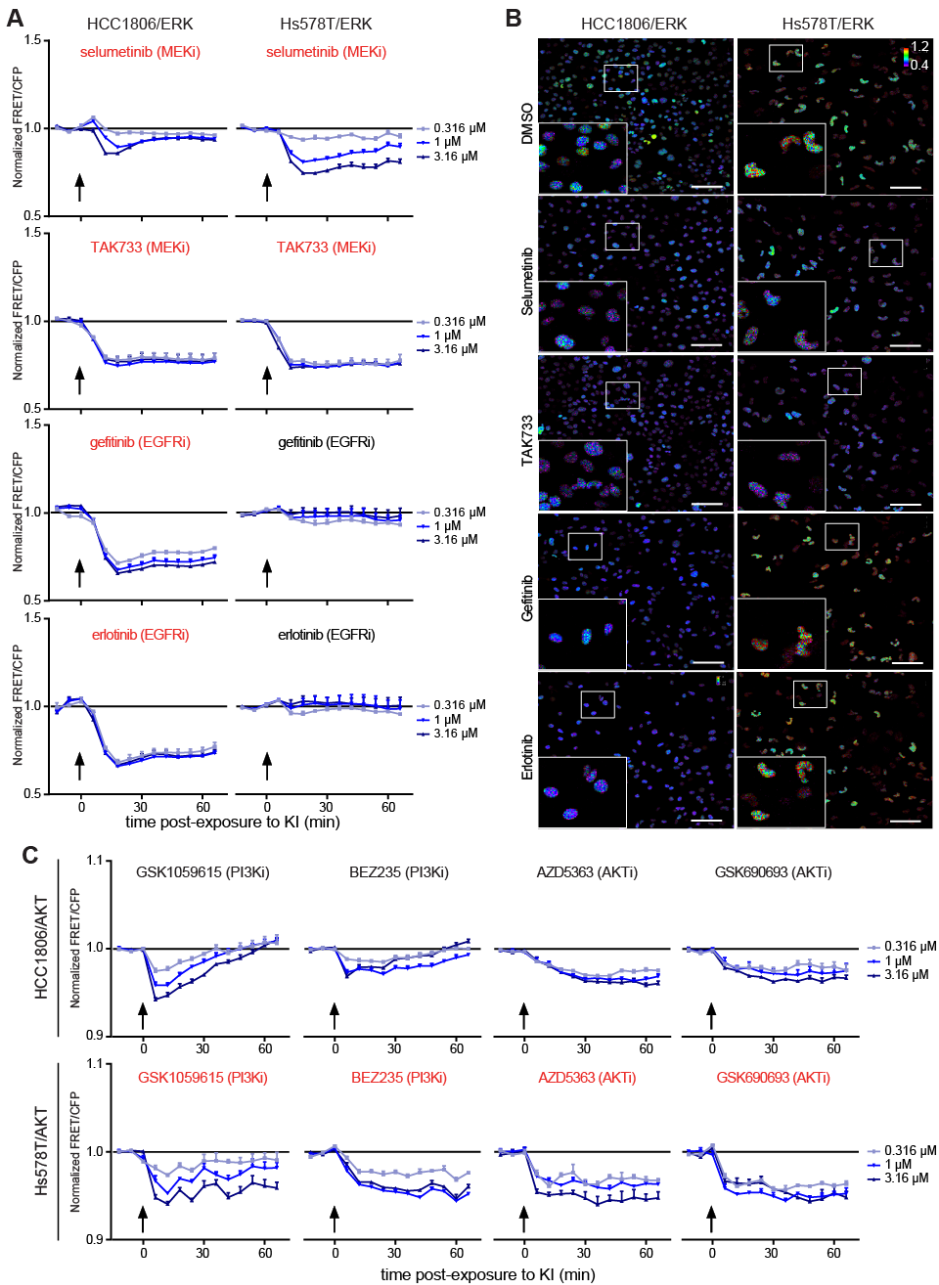


Fig. 8. Potency of selected kinase inhibitors on FRET-ERK and FRET-AKT activity. (A) Concentration response FRET-ERK activity dynamics for selumetinib, TAK733, gefitinib and erlotinib. (B) Representative images taken from (A) at 1 μ M. Raw FRET/CFP ratio was color-coded in rainbow scale. Scale bar = 100 μ m. (C) Concentration response of FRET-AKT activity dynamics for GSK1059615, BEZ235, AZD5363 and GSK690693. Three basal images were taken prior to KI treatment in dose range (μ M). KIs showing positive correlation between MaxMagnitudeFRET and proliferation are marked in red. Arrow indicates when KIs were added.

2

with MEKi, selumetinib decreased FRET/CFP ratio in HCC1806/ERK and more significantly in Hs578T/ERK cell lines in a dose dependent fashion, while TAK733 effectively inhibited FRET-ERK activity even at low dose (0.316 μ M) in both cell lines (Fig. 8A, upper panels). Distinctively, EGFRi gefitinib and erlotinib dramatically decreased FRET-ERK signal in HCC1806/ERK cells, but hardly ever in Hs578T/ERK cells (Fig. 8A, lower panels), revealing the EGFRi resistance in Hs578T cells. These differential FRET-ERK dynamic changes in HCC1806/ERK and Hs578T/ERK cells were captured, representatively upon 30 min exposure to MEKi selumetinib and TAK733 and EGFRi gefitinib and erlotinib at 1 μ M (Fig. 8B). Next, PI3Ki and AKTi conferred inhibitory effect on FRET-AKT activity in both HCC1806/ERK and Hs578T/AKT cell lines, yet, in different patterns. The inhibited FRET-AKT by PI3Ki GSK1059615 and BEZ235 in HCC1806/ERK cells was gradually recovered within one hour, whilst the FRET-AKT in Hs578T cells was steadily restrained in dose dependence (Fig. 8C, left panels). AKTi AZD5363 and GSK690693 suppressed FRET-AKT activity more effectively in Hs578T/AKT cells than in HCC1806/AKT cells (Fig. 8C, right panels). As a result, our FRET biosensor-based live imaging deciphered the ERK dynamic responsiveness to EGFRi in AKTi-resistant HCC1806 TNBC cells and the AKT dynamic responsiveness to PI3Ki and AKTi in MEKi-resistant Hs578T cells that are also highly refractory to EGFRi.

3.6. *EGFRi-refractory TNBC cells sustain ERK signaling for proliferation*

In EGFRi-refractory Hs578T TNBC cells, EGFRi failed to inhibit FRET-ERK activity, while the FRET-AKT activity was targetable by PI3Ki and AKTi, suggesting that the downstream ERK signaling bypasses EGFR inhibition, leading to resistance. Thus, we further addressed how the FRET-ERK dynamic activity is associated with proliferative responses to EGFRi, MEKi, PI3Ki and AKTi, respectively, in dose ranges. The proliferation assays demonstrated that Hs578T/ERK cells were highly resistant to EGFRi (gefitinib and erlotinib), maintaining low sensitivity to MEKi (selumetinib and TAK733) and highly responding to PI3Ki (BEZ235) and AKTi (AZD5363) (Fig. 9A, left). Contrastingly, the AKTi-resistant HCC1806/ERK cells were responsive to EGFRi and MEKi but relatively insensitive to PI3Ki and AKTi (Fig. 9A, right). Next, we assessed if the FRET-ERK activity dynamics would reflect the ERK phosphorylation status in Hs578T/ERK and HCC1806/ERK cells in response to representative inhibitors. Strikingly, EGFRi gefitinib eliminated ERK phosphorylation (p-ERK) in HCC1806/ERK cells, but left the downstream p-ERK signaling intact in Hs578T/ERK cells (Fig. 9B-C). MEKi suppressed ERK phosphorylation in both cell lines, correlating with downregulated FRET-ERK activity dynamics, while PI3Ki and AKTi conferred no significant changes on p-ERK status in the cells, as expected. Taken together, the FRET-ERK dynamic activity was indicative of ERK signaling and proliferation of TNBC cells in response to inhibition of signaling pathways, such as RTK, MAPK and PI3K/AKT.

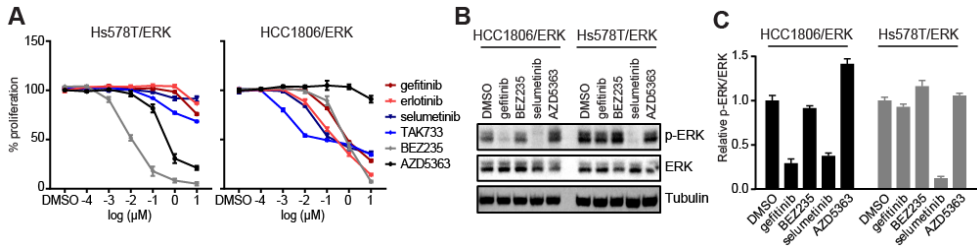


Fig. 9. Differential response of TNBC cells to inhibitors targeting different kinase signaling components. (A) Proliferative response of FRET-ERK reporter cells to EGFRi (gefitinib and erlotinib), MEKi (selumetinib and TAK733), PI3Ki BEZ235 and AKTi AZD5363 in a concentration range. **(B)** Effects of representative KI gefitinib, BEZ235, selumetinib and AZD5363 on ERK (AKT) phosphorylation in FRET-ERK (AKT) reporter cells. FRET reporter cells were treated with KIs at 1 μM for 30 min. **(C)** Quantification of phosphorylated ERK level, derived from **(B)**. The expression level was normalized to total ERK and further compared to that in DMSO-treated cells.

4. Discussion

TNBC is an aggressive disease with unfavorable prognosis^{104, 105}. Currently, there are no effective targeted therapies approved for the treatment of TNBC patients. Given the pivotal role of EGFR/MAPK and PI3K/AKT signaling in controlling cell growth, survival and proliferation, central nodes of these pathways, MEK and AKT, have been emerging as promising targets for cancer drug discovery^{134, 135}. MEK inhibitors and AKT inhibitors have been explored for the treatment of TNBC in the past decades. However, the clinical outcomes are unfavorable due to drug-induced activation of alternative survival signaling pathways^{58, 136}. Here we have established and systematically characterized a panel of FRET-ERK and FRET-AKT TNBC reporter cell lines. We have applied this FRET reporter panel in high-throughput screening to uncover contextual kinase signaling dependencies in TNBC that modulate AKT and ERK pathways. Thus, we identified ten signaling pathways associated with the proliferative response of TNBC to kinase drugs.

Different TNBC cell lines demonstrate alternative resistance to AKT or MEK inhibitors, suggesting dependencies on either ERK or AKT signaling for their enhanced proliferation. In AKTi-resistant cells, targeting various receptor tyrosine kinases, MAPKs, cell cycle-related kinases, PI3K/AKT and angiogenesis caused a downregulation of FRET-ERK dynamics, accompanied by attenuated proliferation. This included inhibitors targeting VEGFR (ZM 306416 and AEE788), ALK (AP26113), MEK (TAK733), cell cycle (AZD7762 and TAK901), and Src (dasatinib). MEKi-resistant cells were addicted to PI3K/AKT and cell cycle regulated FRET-AKT activity. Further, we note that targeting PI3K/AKT and angiogenesis pathways did suppress FRET-ERK activity.

The MAPK signaling and PI3K/AKT signaling are two canonical pathways of RTK signal transduction, functioning in a variety of cellular processes^{100, 137}. Transcriptomics and proteomics profiles on TNBC samples indicate that activation of both pathways is frequently observed, but can be attributed to variable reasons. Ras and Raf are rarely

mutated in TNBC^{19, 106}. However, activation of upstream RTKs and inactivation of negative regulators, such as NF1 mutation and DUSP4 loss, lead to active MAPK signaling^{58, 77, 138, 139}. Activation of PI3K pathway, either directly by PI3KCA mutation or indirectly by PTEN or INPP4B loss, is common in TNBC tumors^{19, 106, 140}. Our KI screening data have demonstrated that the effects of MAPK inhibition on TNBC cell proliferation positively correlate with their efficacy on ERK activity. The inhibitory effects of RTKi on cell proliferation and ERK activity are better correlated in RTKi/MEKi-resistant cells than AKTi-resistant cells. Inhibition of PI3K/AKT signaling is efficacious to suppress cell proliferation in RTKi/MEKi-resistant subgroups. Complementary to accumulating molecule signature studies, our findings on differential kinase dependencies using our FRET reporter panel, provide experimental evidence for the development and prioritization of precision medicine for TNBC cohorts.

Kinase drugs have been preferably pursued as promising targeted therapeutics due to the pivotal role of kinase molecules in signal transductions and corresponding cell biological processes^{111, 135, 141}. Given the hypothesis that kinases with enhanced expression or activating mutations hold the essentialities in cancer cell progression, gene expression signatures have been extensively studied and employed to identify common genetic background within cancer types^{142, 143}. However, a number of studies suggest that gene expression is rarely indicative of kinase activity, perturbation of which is a key factor for evaluating the effectiveness of kinase drugs^{144, 145}. In this study, establishment of high-content FRET-based live cell imaging enables dynamic quantitative detection of intracellular activity of ERK and AKT, two key elements in kinase signaling cascades. Our results illustrate that the influences on kinase activity incarnate the proliferative response of TNBC to kinase drugs in a temporal and direct way. We anticipate that FRET-based signaling reporters will contribute substantially to monitor the efficacy of candidate kinase inhibitors, but also will contribute to the further understanding of their mode-of-action in relation to crosstalk with well-defined signaling components in cancer, including ERK and AKT signaling.

In summary, our work describes an integrated protein kinase dependency identification and functional validation approach that identifies TNBC kinase addictions, potential targetable pathways and associated targeted therapeutics. We demonstrate the feasibility of FRET imaging-based high-content screening of intracellular kinase activity in assessing kinase specificity and possible signaling crosstalk. In particular, our study reveals the intact ERK kinase signaling which drives TNBC drug resistance against RTKi/MAPKi-targeted therapies. Besides RTKi and MAPKi, AKTi-resistant cells are also responsive to cell cycle inhibition via ERK downregulation. Future studies should aim at broadening the range of cancer relevant kinase biosensors and translating this approach to in vitro/in vivo models that are closer to the clinic, including cultures of patient-derived xenograft.

Acknowledgments

This work was supported by the ERC Advanced grant Triple-BC (grant no. 322737). JH was financially supported by the China Scholarship Council.

Supplementary data

Supplementary video 1. Basal FRET-ERK activity dynamics in serum-starved Hs578T/ERK cells.

Supplementary video 2. EGF (50 ng/ml) stimulated FRET-ERK activity dynamics in serum-starved Hs578T/ERK cells.

Supplementary video 3. Basal FRET-ERK activity dynamics in serum-starved HCC1806/ERK cells.

Supplementary video 4. EGF (50 ng/ml) stimulated FRET-ERK activity dynamics in serum-starved HCC1806/ERK cells.

Supplementary video 5. Effects of MEKi selumetinib (1 μ M) on FRET-ERK activity dynamics in the presence of EGF (50 ng/ml) in Hs578T/ERK cells.

Supplementary video 6. Basal FRET-AKT activity dynamics in serum-starved Hs578T/AKT cells.

Supplementary video 7. EGF (50 ng/ml) stimulated FRET-AKT activity dynamics in serum-starved Hs578T/AKT cells.

Supplementary video 8. Effects of AKTi AZD5363 (1 μ M) on FRET-AKT activity dynamics in the presence of EGF (50 ng/ml) in Hs578T/AKT cells.

Chapter 3

A kinome screen for lapatinib drug resistance identifies FYN as a suppressor of EGFR/PI3K/AKT signaling axis dependency in triple-negative breast cancer

Jichao He, Ronan P. McLaughlin, Yinghui Zhang, Bob van de Water

Manuscript in preparation

Abstract

Triple-negative breast cancer (TNBC) is molecularly intricate, with limited therapeutic options. Although approximately 80% of TNBC overexpresses epidermal growth factor receptor (EGFR), TNBC is generally resistant to EGFR targeted therapies, including EGFR tyrosine kinase inhibitors lapatinib, gefitinib and erlotinib. Understanding compensatory signaling mechanisms that mediate the EGFR inhibitor resistance may facilitate to harness effective targeted therapies for TNBC. Here, kinome RNA-interference loss-of-function screen and pharmacological inhibition profiling have defined the vulnerability of AKT/mTOR signaling in EGFR inhibitor resistant TNBC cells. Contrarily, EGFR/MAPK signaling is vulnerable for TNBC cells resistant to mTOR inhibition. EGFR inhibitor lapatinib and kinome siRNA combinatorial screening identified numerous kinase targets that alleviate lapatinib resistance, including FYN, KIT, HK2, NME6 and DCK. Intriguingly, silencing of FYN, a Src family kinase, enhanced EGFR autophosphorylation and downstream AKT phosphorylation. Consequently, pharmacological inhibition of different components of the EGFR/PI3K/AKT axis synergized with FYN depletion. Our results indicate FYN as an EGFR signaling suppressor mediating TNBC resistance to EGFR targeted therapies in TNBC cells that do have increased expression of EGFR. We suggest FYN expression as a potential vulnerability for EGFR inhibitor drug resistance in TNBC.

Introduction

Triple-negative breast cancer (TNBC) does not express progesterone receptor (PR), estrogen receptor (ER) and human epidermal growth factor receptor 2 (HER2) that are vulnerable to ER, PR and/or HER2-targeted therapies for other breast cancer types ¹⁰⁷. Although comprehensive genomic profiling has characterized more than six molecular subtypes of TNBC ⁸, none of them has benefited from molecularly targeted therapies. TNBC still relies on cytotoxic chemotherapies, yielding unfavorable prognoses, with high likelihood of distant recurrence and death during the first 3-5 years after diagnosis ⁴. Treatment of TNBC remains a profound clinical challenge. The lack of treatment options for TNBC makes identifying alternative TNBC vulnerable targets paramount ⁶.

Many of protein kinases have been defined to play essential roles in cancer initiation and progression and drug resistance ^{146, 147}. Proto-oncogenic kinases include receptor tyrosine kinases (RTK), BCR-ABL, PIK3CA and MAPK kinases driving proliferation and angiogenesis in cancer ¹¹¹. The epidermal growth factor receptor (EGFR) has been defined as a key oncogenic RTK, which coordinates multiple pro-mitogenic signal transduction cascades, principally the Ras-Raf-MEK-ERK, PI3K-AKT-mTOR and Src-STAT3 signaling pathways, to promote cell proliferation, motility, and survival ¹⁴⁸⁻¹⁵⁰. As frequent overexpression of EGFR is observed in various cancer types, such as lung and colorectal cancer and glioblastoma ^{148, 149, 151, 152}, EGFR has been representing an attractive therapeutic target for cancer targeted therapies ¹⁵³, eliciting high response rates improving patient clinical outcomes ^{25, 154}. Approximately >80% of TNBC tumors have increased expression of EGFR, hence EGFR targeted therapies have been clinically explored for treating TNBC patients ^{25, 155}. Also, therapies targeting MAPK/ERK and PI3K/AKT/mTOR kinases downstream of EGFR signaling have been trialed ^{156, 157}. Yet, the clinical benefits of these targeted therapies for TNBC have been disappointing, due to low response rates and resistance ¹⁵⁰. The mechanisms of TNBC resistance to targeted therapies are likely owing to mutations of the drug targets and compensation by interactive dysregulated signaling pathways ¹⁵⁸⁻¹⁶⁰, suggesting to explore alternative combinatorial targeted therapies blocking vulnerable kinase targets in compensatory signaling pathways.

More than 500 protein kinases are encoded in the human genome ^{161, 162}. Protein kinases are one of the most targeted groups of drug targets ¹⁴⁶. Our previous studies have shown that TNBC cells, regardless of molecular subtypes, are commonly resistant to EGFR inhibitors (EGFRi) ¹⁶³ and differentially responsive to MEK inhibitors (MEKi) and AKT inhibitors (AKTi) (van de Noord et al, submitted), as well as mTOR inhibitors (mTORi) (He et al, submitted). In this study, by means of high-throughput screen of 720 siRNAs targeting the whole kinome and kinase-related components, in combination with EGFRi lapatinib, we aimed to define alternative signaling pathways and kinase targets vulnerable for therapy-refractory TNBC cells and synergistically targetable with EGFR targeted

therapies. Our kinome-wide siRNA screen and validation of targeted effects by kinase inhibitors revealed that alternatively targeting AKT/mTOR and EGFR/MAPK pathways succumbed resistant TNBC cells to EGFRi and mTORi, and blocking basal cell cycle machinery effectively overcame the differential EGFRi- and mTORi-resistant phenotypes of TNBC cells. Combined drug and kinome siRNA screen identified several novel kinase targets, including FYN, KIT, HK2, NME6 and DCK, whose silencing sensitized EGFRi-refractory TNBC cells to the clinically applied EGFR targeted therapies, such as lapatinib (Lap), gefitinib (Gef) and erlotinib (Erl). Importantly, the Src family kinase FYN¹⁶⁴ was defined to act as a negative regulator of EGFR activity in the EGFRi-resistance of TNBC cells. Targeting FYN enhanced activation of EGFR and AKT signaling, facilitating the effects of EGFR/PI3K/AKT directed inhibitors on signaling inhibition, thereby restoring TNBC cell responsiveness. Our work demonstrated unique kinase dependencies in therapy-resistant TNBC cells and revealed FYN as a potential kinase target vulnerable for EGFRi-refractory TNBC.

Materials and methods

Reagents and antibodies

All kinase inhibitors were purchased from Selleckchem® (Huissen, the Netherlands). The phospho(Ser473)-AKT (9271), phospho(Thr202/Tyr204)-p44/42 MAPK (ERK1/2, 9101), phospho(Ser2448)-mTOR (5536S), phospho((Tyr1148))-EGFR (4404) and phospho(Thr37/46)-4EBP1 (2855) antibodies were from Cell Signaling TECHNOLOGY® (Bioké, Leiden, Netherlands). EGFR (1005) antibody was from Santa Cruz (Heidelberg, Germany). FYN antibody [N1C2] (GTX109428) was from GeneTex (Irvine, US). The antibody against tubulin (T-9026) and human epidermal growth factor (EGF, E9644) were from Sigma Aldrich (Zwijndrecht, the Netherlands).

Cell culture

Cell line Hs578T (ATCC-HBT-126) and MDA-MB-231 (ATCC-HBT-26) were purchased from ATCC. Cell line HCC1806, SUM229PE and SUM52PE were kindly provided by Prof. John W. M. Martens (Erasmus Medical Centre, Rotterdam, the Netherlands). All cell lines were authenticated by short tandem repeat (STR) profiling as previously described¹⁶⁵, and subjected to Mycoplasma test using the Mycosensor PCR kit (#302108, Stratagene). Cells were cultured in RPMI-1640 medium supplemented with 10% fetal bovine serum, 25 U/mL penicillin and 25 µg/mL streptomycin in a humidified incubator at 37°C with 5% CO₂.

SRB proliferation assay

A sulforhodamine B (SRB) colorimetric assay was used to measure total amount of proteins indicative of cell proliferation, as previously described¹²⁵.

High-throughput human kinome siRNA screen

The primary screen was carried out by use of kinase SMARTpool siRNA library containing 720 siRNAs targeting human kinome-wide 720 kinases and kinase-related components (GE Dharmacon, Lafayette, CO, USA). In the validation screen, SMARTpool siRNA and single siRNA_1, _2, _3 and _4 that comprise the SMARTpool mix were used to target each candidate hit. To silence target genes, 50 nM siGENOME Human SMARTpool siRNA mix was transfected into cells, which were seeded overnight in 96-well plate with optimized densities, by transfection reagent INTERFERin (Polyplus-Transfection SA, Illkirch-Graffenstaden, France) according to the manufacturer's instructions. A pool of 720 kinase siRNAs at stock concentration of 1 μ M, which has no effect on gene expression, was taken as non-targeting siRNA control (siCtrl). The medium was refreshed 24 h post-transfection and TNBC cells were transfected for 2 days and proliferated for 4 days under indicated condition. In drug and siRNA combination screen, drug solution was supplemented to cells 2 days post siRNA transfection at indicated concentration, followed by 4-day treatment. SRB colorimetric assay was used as read-out for cell proliferation. Primary kinome siRNA screen data were analyzed using an unbiased sample-based analysis as previously and presented in Z scores¹⁶⁶.

Western Blotting and gene expression data

Cells were seeded in 12-well plates at the appropriate density. For stimulation/starvation assays, medium was refreshed with serum-free medium (SFM) the following day and cells were starved overnight. Thereafter, cells were stimulated with 100 ng/ml EGF (Sigma; E9644) for 30 min in SFM. Cells were lysed with RIPA buffer containing 1% protease/phosphatase inhibitor cocktail (Sigma-Aldrich, P8340). Proteins were resolved by SDS-PAGE and transferred to polyvinylidene difluoride membranes. Membranes were blocked in 5% BSA in Tris-buffered saline with 0.05% Tween-20 (TBS-T), followed by overnight incubation with primary antibodies, washing, and 1 h incubation with HRP-conjugated secondary antibodies. Chemiluminescence was generated in the presence of HRP substrate and detected with an Amersham Imager 600 (GE Healthcare Life Sciences, Eindhoven, the Netherlands). Log₂-based RNA-seq expression profile of TNBC cell lines was retrieved from our own established data (Koedoot et al, submitted).

Gene network and pathway analysis

The STRING database (version 10.5) (<https://string-db.org>) was applied to analyze and integrate direct and indirect protein-protein interactions (PPI) and functional associations of screened kinase hits. The interaction networks were further analyzed and visualized using Cytoscape v3.7.0. Metascape portal¹⁶⁷ (<http://metascape.org>) that combines over 40 independent knowledgebases, such as GO Biological Processes, KEGG pathway, Reactome gene sets, Canonical Pathways, CORUM complexes; DAVID functional

annotation tool was used to visualize the functionally enriched pathways and identify MCODE (molecular complex detection) complex of kinase targets, statistically significant ($p < 0.05$) with ≥ 3 targets per cluster.

Statistical analysis

Pearson correlation analysis was performed using GraphPad Prism 7. Statistical analysis of all experimental data was performed using two-way ANOVA (* $p < 0.05$, ** $p < 0.01$, *** $p < 0.001$). All experiments were performed in at least three independent biological replicates. Data were expressed as mean \pm SEM. Significance was set at $p < 0.05$. The hierarchical clustering in heatmap was performed using CRAN pheatmap package in RStudio (version 0.99.887).

Results

TNBC cells display differential phenotypic responses to EGFR and mTOR targeted therapies

TNBC patients have not been benefited from targeted therapies in the clinic, owing to the heterogeneous nature of TNBC¹⁰⁷. Despite frequent overexpression of EGFR in $\sim 80\%$ TNBC tumors^{150, 168, 169}, targeting EGFR is ineffective for treating TNBC patients^{170, 171}. To

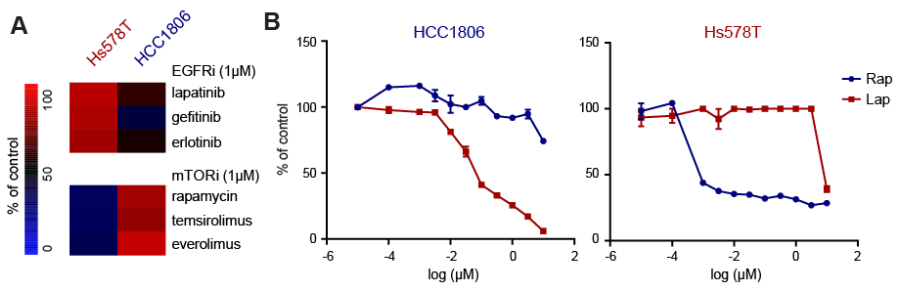


Figure 1. Differential responses of TNBC Hs578T and HCC1806 cells to EGFR inhibitors (EGFRi) and mTOR inhibitors (mTORi). (A) Resistance of Hs578T cells to EGFRi (lapatinib, gefitinib, erlotinib) and HCC1806 cells to mTORi (rapamycin, everolimus, temsirolimus), at 1 μM . (B) Dose responses of Hs578T and HCC1806 to lapatinib (Lap) and rapamycin (Rap). Cells were treated with inhibitors at indicated concentrations for 4 days, followed by SRB proliferation assay. Proliferation of cells was presented as % of control, normalized to non-treatment condition with DMSO.

understand the phenotypic responses of TNBC cells to targeted therapies, we have previously screened several clinically applied kinase-targeting small molecules across ~ 20 TNBC cell lines. Consistent to the clinical results, our previous study has demonstrated the common resistance in $>85\%$ of TNBC cell lines to various EGFRi, including Lap, gefitinib (Gef) and erlotinib (Erl)¹⁶³, as shown representatively for the TNBC cell line Hs578T (Figure 1A). Exceptionally, one TNBC cell line HCC1806 was found to display sensitivity to the EGFR targeted therapies. Intriguingly, the EGFRi-sensitive HCC1806 cells were strongly

resistant to different mTORi, such as rapamycin (Rap), temsirolimus and everolimus, whereas the EGFRi-refractory Hs578T cells were highly responsive to the mTOR-targeted therapies (Figure 1A). The EGFRi-refractory Hs578T cells and the mTORi-refractory HCC1806 cells were phenotypically responsive in proliferation inhibition to mTORi Rap and EGFRi Lap, respectively, in dose dependent manner (Figure 1B). These differential phenotypic responses of TNBC cells to EGFR and mTOR targeted therapies implicated alternative kinase dependencies in the refractory TNBC cells, rationalizing the discovery of vulnerable kinase targets bypassing inhibition of EGFR-related or mTOR-related signaling, to combat TNBC resistance.

Kinome siRNA screen reveals specific vulnerable kinase targets in EGFRi- and mTORi-resistant TNBC cells

To identify alternatively vulnerable kinase targets in the circumstance of EGFRi-resistance of TNBC, we next performed human kinome-wide siRNA screen targeting 720 protein kinases and kinase-related components in the EGFRi-refractory and mTORi-sensitive Hs578T cells, compared to the EGFRi-sensitive and mTORi-resistant HCC1806 cells. The

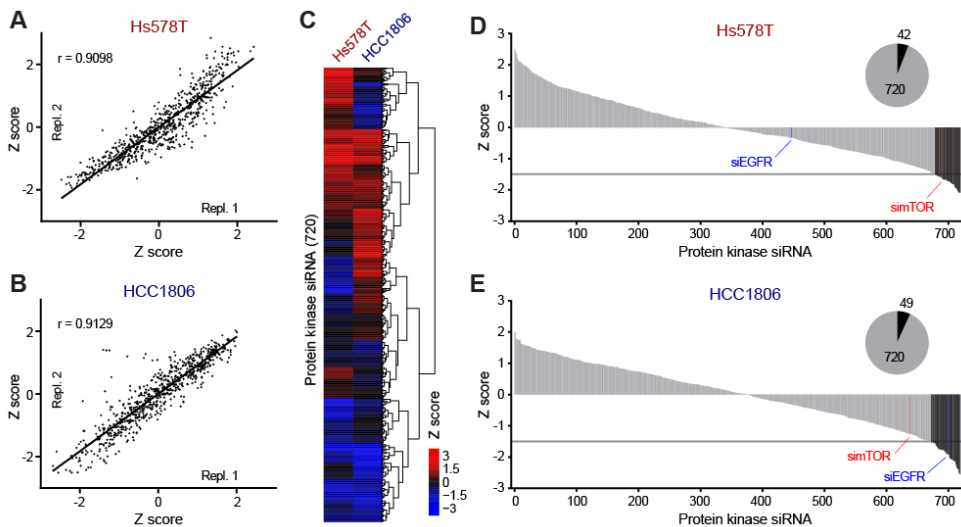


Figure 2. Kinome siRNA screen of EGFRi-resistant Hs578T and mTORi-resistant HCC1806 TNBC cells. (A-B) Effect of replicate kinome siRNA screens of Hs578T cells (A) and HCC1806 (B) cells was presented in Z scores. Cells were transfected with siRNAs for 2 days, and then refreshed and cultured for 4 days, followed by SRB proliferation assay. Pearson correlation coefficient r was representative for reproducibility of replicate screens in Hs578T ($r = 0.9098$) and HCC1806 ($r = 0.9129$) cells. (C) Heatmap clustering displaying differential targeting effects of kinome-wide siRNAs on Hs578T and HCC1806 cells. Color in blue indicated inhibitory effect on proliferation; in black, no effect; in red, enhanced effect. (D) Ranking of individual siRNA targeting effect on Hs578T cell proliferation. (E) Ranking of individual siRNA targeting effect on HCC1806 cell proliferation. The effect with Z score < -1.5 (black bars) was considered significant on proliferation inhibition. The significant hits were numbered in pie charts. The effects of siRNA targeting EGFR (siEGFR) and siRNA targeting mTOR (simTOR) were indicated.

targeting effect of each siRNA on cell proliferation was presented in Z score, displaying high reproducibility in the replicate screens of Hs578T (Pearson coefficient $r = 0.9098$) (Figure 2A) and HCC1806 ($r = 0.9129$) cells (Figure 2B). Hierarchical clustering revealed distinct vulnerabilities of Hs578T and HCC1806 cells to the kinome RNA interference (Figure 2C; Supplementary Table S1), indicating the different kinase dependencies within these TNBC cell lines. Of 720 kinases, 42 vulnerable kinase targets were screened showing significant targeted effects (Z score < -1.5) on proliferation inhibition of Hs578T cells (Figure 2D), and 49, on HCC1806 proliferative inhibition (Figure 2E).

Consistent to the phenotypic responses to EGFRi and mTORi kinase inhibitors (Figure 1), the EGFRi-resistant Hs578T cells were highly prone to mTOR siRNA (simTOR) silencing (Figure 2D), while the mTORi-resistant HCC1806 cells were strongly sensitized by EGFR siRNA (siEGFR) silencing (Figure 2E). Remarkably, among 42 kinase targets that were vulnerable for the EGFRi-refractory Hs578T cells, mTOR was centered in the protein-protein interaction (PPI) network, and the cell cycle and mTOR pathways were the most vulnerable (Figure 3A), involving the cell cycle kinases PLK1, CDKN2D, CHEK1 and WEE1 and the mTOR signaling components RPS6KA2, STRADA and mTOR (Supplementary Table S2). Within the PPI network of 49 vulnerable kinase targets for the mTORi-resistant HCC1806 cells, EGFR was tightly connected with other components, and the pathways downstream EGFR signaling, such as MAPK pathway, Ras pathway and PI3K/AKT, and the FoxO signaling pathways, were significantly enriched (Figure 3B; Supplementary Table S2). Commonly, 12 kinases were vulnerable for both cell lines, including, MAP3K9, CHEK1, WEE1, RPS6KA2, GUCY2D, RELA, PMVK, AURKA, CAMKIINALPHA, PCTK3, PLK1, CDC2L1, which are functionally involved in cell cycle pathway (Figure 3C).

Next, we reasoned if pharmacological inhibition of the enriched signaling clusters above could attenuate proliferation of the TNBC cells. To this end, we treated the cells with groups of kinase inhibitors pharmacologically targeting EGFR/MAPK, AKT/mTOR and cell cycle signaling, respectively. In line with the findings of kinome siRNA screen, the kinase inhibitor response profiling exhibited that the EGFRi-refractory Hs578T cells were responsive to inhibition of AKT/mTOR signaling by different AKT inhibitors (AKTi) and mTORi (Figure 3D), remaining resistant to diverse EGFRi and less responsive to various MEK inhibitors (MEKi) targeting MAPK signaling (Figure 3E). In contrast, the mTORi-resistant HCC1806 cells were sensitive to EGFR/MAPK inhibition by the EGFRi and MEKi and relatively resistant to AKT and mTOR inhibition. Consistently, both cell lines were sensitive to pharmacological inhibitors targeting cell cycle protein kinases, such as PLK, CDK and Chk (Figure 3F).

The results above indicated that alternative addictions to AKT/mTOR signaling and EGFR/MAPK signaling pathways might confer therapy-refractory phenotypes on TNBC cells. Obstruction of mTOR-centralized network may sensitize the EGFRi-refractory Hs578T cells, while blockage of EGFR/MAPK signaling dependency in the mTORi-resistant HCC1806

cells may restore responses to mTOR-targeted therapies. Targeting PLK, CDK and Chk signaling in the basal cell cycle machinery makes the TNBC cells responsive, suggesting the vulnerabilities of the cell cycle related kinase targets for the refractory TNBC cell types.

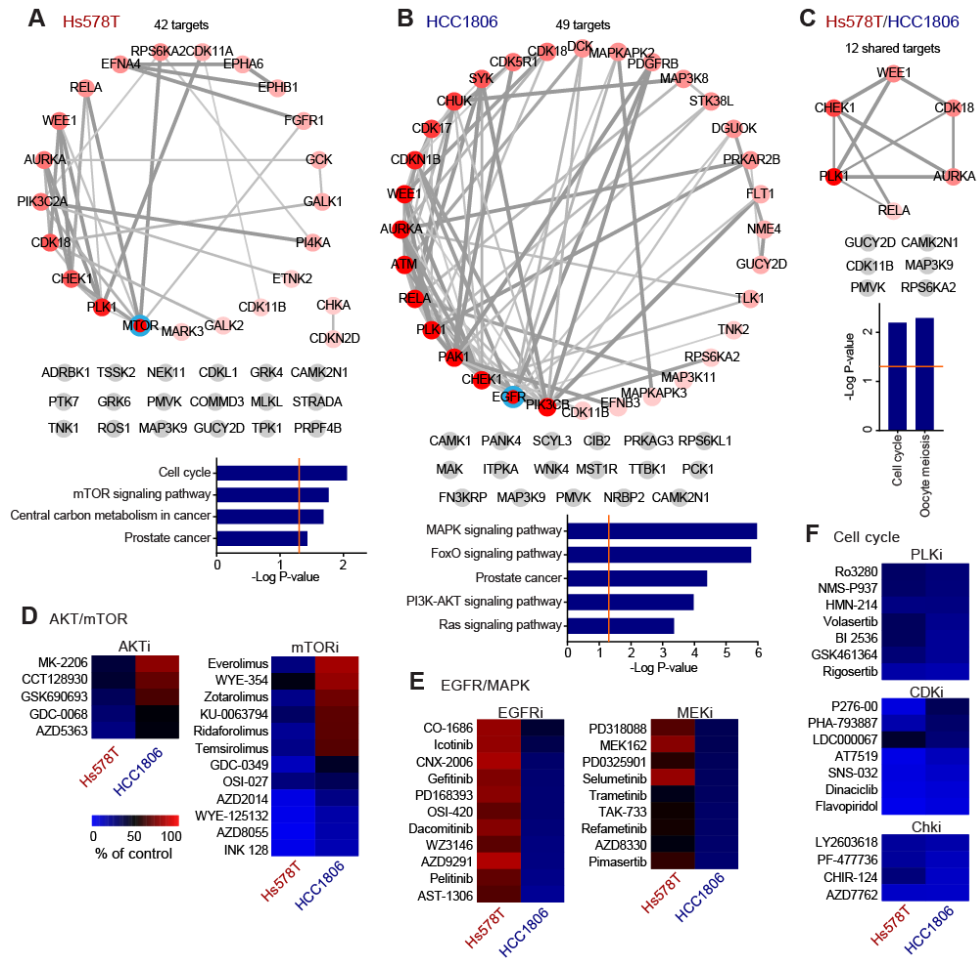


Figure 3. Distinct kinase dependencies of EGFRi-refractory Hs578T cells and mTORi-resistant HCC1806 cells. (A-C) STRING protein-protein interaction (PPI) network and KEGG pathway enrichment of 42 kinase targets vulnerable for EGFRi-resistant Hs578T **(A)**, 49 for mTORi-resistant HCC1806 cells **(B)**, and 12 for both Hs578T and HCC1806 cells **(C)**. The primary targets EGFR and mTOR were circled in blue. Edge thickness indicated the interaction score. Red color signified the connected kinases. Unconnected kinases were marked in grey. **(D-F)** Proliferative responses of Hs578T and HCC1806 cells to AKT inhibitors (AKTi) and mTORi **(D)**, to EGFRi and MEK inhibitors (MEKi) **(E)**, and to cell cycle related PLK1 inhibitors (PLKi), CDK inhibitors (CDKi) and Chk inhibitors (Chki) **(F)**. Cells were treated with inhibitors at 1 μ M for 4 days, followed by SRB proliferation assay.

Lapatinib and kinome siRNA combination screen identifies vulnerable kinase targets sensitizing TNBC cells to EGFR inhibition

Cancer drug resistance is a multifaceted process involving different mechanisms, such as target alteration, alternative cell surface receptors, escape from apoptosis, and DNA damage repair, hence combination of targeted therapies has been applied to sensitize resistant cancer cells⁷⁵. Resistance to EGFR targeted therapies is a common phenotype of TNBC, despite high levels of EGFR expression and clear inhibition of EGFR in TNBC tumor cells^{170, 171}, suggesting alternative survival signaling pathways bypassing EGFR inhibition,

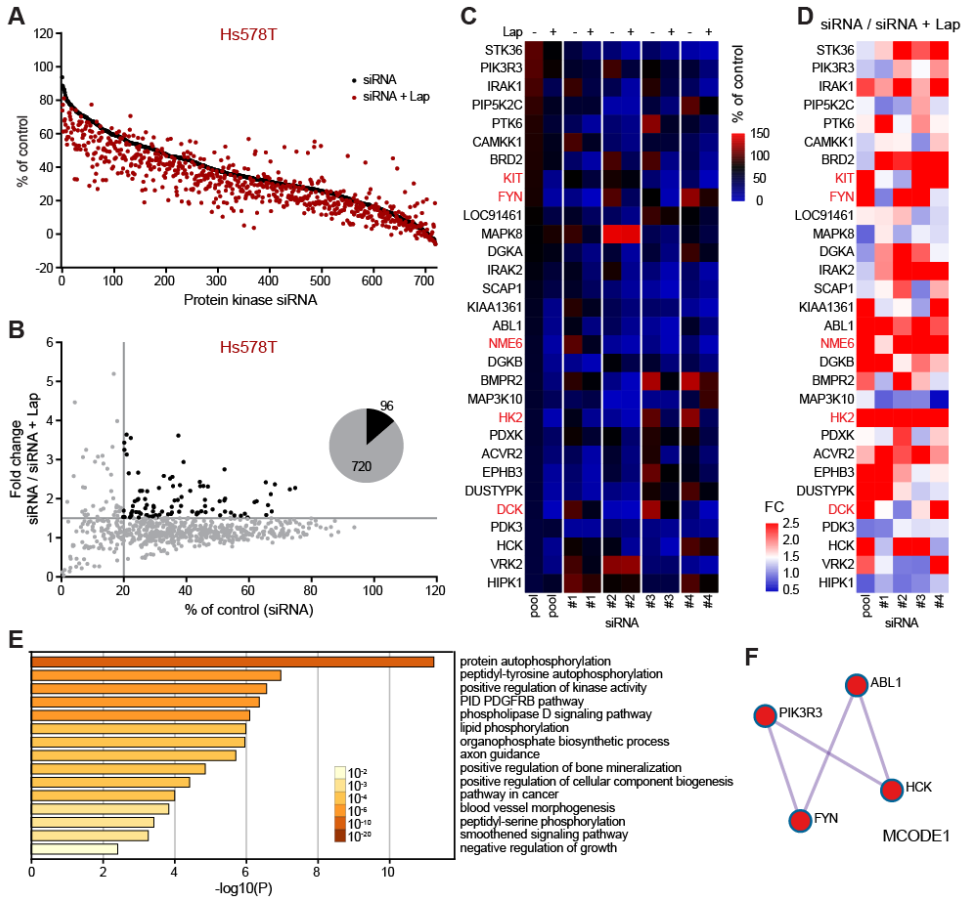


Figure 4. Combined lapatinib and kinome siRNA screen of EGFRi-refractory Hs578T cells. (A) Effect of siRNA and combined siRNA and lapatinib (siRNA + Lap) on Hs578T cell proliferation. Cells were transfected with siRNAs for 2 days, followed by 4-day treatment with Lap at 1 μ M or DMSO as control. Percentage proliferation (% of control) was relative to siCtrl + DMSO control. **(B)** Fold change (FC) of proliferation in comparison of siRNA alone to siRNA + Lap combination (siRNA / siRNA + Lap). 96 primary hits with FC > 1.5 were selected, significantly synergizing with Lap to inhibit proliferation. **(C)** Deconvolution screen of Lap synergistic hits with SMARTpool siRNA and individual (1, 2, 3 and 4) siRNAs. Heatmap showed top 30 hits enabling > 50% of proliferation under SMARTpool siRNA silencing alone. **(D)** FC of proliferation (siRNA / siRNA + Lap) controlled by the 30 hits. Five Lap synergistic hits with significant effect by SMARTpool and $\geq 2/4$ individual siRNAs (FC > 1.5) were marked in red. **(E)** Metascape bar graph viewing top enrichment clusters of the 30 hits. Color scale represented statistical significance by p-values in log base 10, Log₁₀(P). **(F)** MCODE algorithm displaying the most densely connected hits.

3

such as AKT/mTOR as shown above. Therefore, to identify kinome-wide alternative kinase targets that are synergistically targetable with EGFR inhibition, thereby understanding the mechanisms underlying EGFRi resistance in TNBC cells, we performed kinome siRNA screen in combination with EGFRi Lap (at a clinically relevant dose, 3.16 μM ¹⁷²) in the EGFRi-refractory Hs578T cells. The results showed that the majority of kinases were vulnerable by siRNA silencing to enhance the inhibitory effect of Lap on Hs578T cell proliferation (Figure 4A). We selected kinases, whose silencing per se controlled >20% of proliferation and enhanced 1.5 fold change (FC) of inhibition when combined with Lap (siRNA / siRNA + Lap), as potential synergistic hits. Consequently, 96 hits were selected as potential targets vulnerable for Lap resistance in Hs578T cells (Figure 4B; Supplementary Table S3). These hits were further validated for their vulnerabilities by deconvolution screen with SMARTpool siRNA and 4 deconvoluted siRNAs. 30 hits were further ranked by their SMARTpool siRNA direct silencing effect on >50% of proliferation control (Figure 4C, Supplementary Table S4) and selected for their siRNA silencing effect significantly synergizing Lap with FC ratio (siRNA / siRNA + Lap) greater than 1.5 (Figure 4D), being considered the most vulnerable kinase targets sensitizing TNBC cells to EGFRi Lap.

Next, Metascape pathway enrichment analysis¹⁶⁷ identified 14 clusters where the 30 Lap synergistic kinase targets were significantly enriched (Figure 4E). The most statistically enriched cluster was related to protein autophosphorylation, involving 60% of the Lap synergistic kinase targets (18/30), including FYN, ABL1, EPHB3, HCK, IRAK1, KIT, MAP3K10, PTK6, VRK2, DSTYK, PKDCC, PIK3R3, PIP4K2C, CAMKK1, HK2, BMPR2, PDK3 and SKAP1 (Supplementary Table S5). Peptidyl-tyrosine autophosphorylation and positive regulation of kinase activity clusters were highly ranked, involving 12 (FYN, ABL1, HCK, PTK6, PIK3R3, MAPK8, EPHB3, IRAK1, SKAP1, KIT, IRAK2 and BMPR2) and 18 (FYN, ABL1, IRAK1, IRAK2, KIT, MAP3K10, DSTYK, CAMKK1, MAPK8, PIK3R3, HCK, STK36, SKAP1, PTK6, PDK3, VRK2, HIPK1 and DGKB), respectively. Remarkably, MCODE (Molecular Complex Detection) algorithm identified a tyrosine autophosphorylation network node where FYN, ABL1, HCK and PIK3R3 were densely connected (Figure 4F) and frequently enriched in the phosphorylation and kinase activity related clusters, suggesting their essential implications in TNBC resistance to EGFR targeted therapies.

Lapatinib synergistic kinase target FYN negatively regulates EGFR/AKT signaling

Among the 30 significant Lap synergistic targets, FYN, KIT, HK2, NME6 and DCK displayed on-target silencing effects by pooled and deconvoluted siRNAs ($\geq 2/4$) to synergize EGFRi Lap (Figure 4C-D). These five targets were further validated for their targeting effects in combination with Lap at 3.16 μM , compared to non-targeting siRNA control (siCtrl) (Figure 5A). Ligand EGF binding results in EGFR autophosphorylation and activation of downstream signaling¹⁷³. As Lap synergistic targets were largely involved in regulation of autophosphorylation and kinase activity (Figure 4E, Supplementary Table S5), we then

further tested their targeting effects on EGFR signaling activation in EGF stimulation. Silencing of these Lap synergistic kinase targets, except for KIT, generally upregulated EGF-induced EGFR phosphorylation at Y1148, a major autophosphorylation site of EGFR¹⁷³, as detected by anti-phospho-EGFR (pY1148) antibody. Of them, the targeting effect of FYN on EGFR signaling upregulation was most significant, implying its strong negative regulation on EGFR activity (Figure 5B-C). Downstream of the upregulated EGFR signaling by FYN silencing upon EGF stimulation, phosphorylation of AKT, rather than ERK or mTOR, was increased (Figure 5B-C). Consistently, FYN silencing significantly enhanced the pharmacological inhibitory effect on cell proliferation by EGFRi Lap, Gef and Erl, PI3K inhibitors (PI3Ki) BEZ235 (BEZ) and AKTi AZD5363, not by MEKi selumetinib (Sel) and Src inhibitors (Srci) dasatinib (Das) (Figure 5D). Yet, while FYN knockdown strongly synergized the pharmacological inhibitory effect of EGFRi Lap on proliferation, simultaneous FYN and EGFR silencing did not lead to the similar synthetic lethal effect (Figure 5E), further suggesting the essential impact of FYN on EGFR signaling activation. However, co-silencing of FYN and AKT showed a synergistic effect, similarly to the effect of FYN silencing with EGFRi Lap (Figure 5E).

FYN and the PI3K regulatory subunit, PIK3R3, were tightly interactive in the tyrosine autophosphorylation MCODE network (Figure 4F). Together, the results above suggested that FYN negatively regulated EGFR signaling pathway and downstream AKT effector. Hence, targeting FYN released EGFR/PI3K/AKT signaling, thereby restoring responses of TNBC cells to EGFR/PI3K/AKT-directed treatments, independently of MAPK signaling.

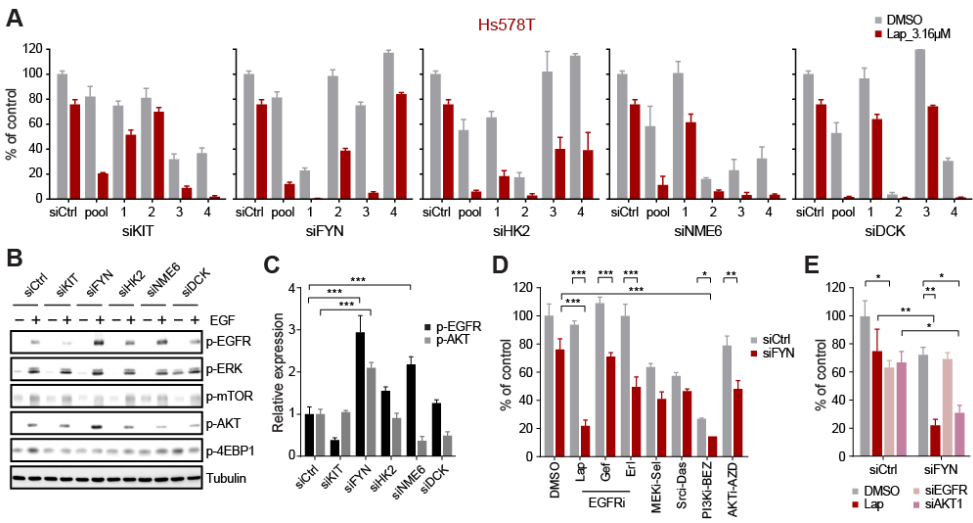


Figure 5. FYN silencing enhanced EGFR/PI3K/AKT signaling in EGFRi-refractory Hs578T cells. (A) Validation of Lap synergistic hits KIT, FYN, HK2, NME6 and DCK in EGFRi-refractory Hs578T cells. Cells were transfected with SMARTpool or 4 single siRNAs for 2 days prior to 4-day Lap treatment. **(B)** Silencing effects of Lap synergistic hits on EGF-induced EGFR signaling. Hs578T cells were transfected with SMARTpool siRNAs for 2 days, starved

overnight, and then exposed to EGF (100 ng/ml) for 30 min. **(C)** Quantification of EGFR and AKT phosphorylation level in response to EGF, relative to tubulin, data derived from **(B)**. **(D)** Effects of FYN silencing on Hs578T cellular response to EGFRi (Lap, Gef and Erl), MEKi selumetinib (Sel), Src inhibitor (Srci) dasatinib (Das), PI3Ki BEZ235 (BEZ), and AKTi AZD5363 (AZD). **(E)** Co-silencing Effects of FYN and EGFR or AKT on Hs578T cell proliferation (two-way ANOVA * $p < 0.05$, ** $p < 0.01$, *** $p < 0.001$).

FYN silencing-mediated lapatinib synergy associates with active EGFR/PI3K/AKT signaling

Next, we questioned whether FYN silencing-mediated Lap synergy was associated with expression and activation of EGFR and the downstream active AKT signaling in TNBC cells. We chose three TNBC cell lines, Hs578T, MDA-MB-231 and SUM229PE, with high EGFR expression, and one EGFR negative TNBC cell line SUM52PE as negative control (Figure 6A). All these TNBC cell lines expressed overall similar levels of FYN, with Hs578T cells showing the highest expression. Downstream active p-AKT was positively detected in SUM52PE and Hs578T cell lines, but were largely absent in MDA-MB-231 and SUM229PE cell lines (Figure 6B), consistent with our previous findings (van de Noord et al, submitted). Treatment with the EGFR inhibitors lapatinib, gefitinib and erlotinib did not affect SUM52PE cells, as they lack expression of EGFR. In contrast, Hs578T, MDA-MB-231 and SUM229PE were commonly resistant to the EGFR targeted therapies, despite the presence of EGFR (Figure 6B-C), recapitulating our previous findings¹⁶³. FYN is a member of Src family¹⁶⁴. Treatment with inhibitors for FYN (FYNi) PP1, PP2 and saracatinib (Sar), which also potently inhibit other Src family members (Selleckchem®), did not cause any cellular responses (Supplementary Figure S1A), exhibiting common resistance of these TNBC cell lines to single FYN inhibition. Moreover, the FYNi PP1, PP2 or Sar did also not synergize with EGFRi Lap to inhibit proliferation of Hs578T cells (Supplementary Figure S1B), suggesting that FYN kinase activity does not bypass EGFR signaling inhibition. Remarkably, siRNA silencing of FYN significantly synergized with EGFRi Lap, PI3Ki BEZ and AKTi AZD in the EGFR positive and p-AKT positive Hs578T cells, but not in the EGFR negative SUM52PE and the p-AKT negative MDA-MB-231 and SUM229PE cells (Figure 6E). FYN silencing enhanced upstream EGFR and downstream AKT phosphorylation (Figure 5B), and synergized with knockdown of AKT, but not EGFR, to inhibit proliferation (Figure 5E). Together, these results indicated that EGFR expression and phosphorylation and EGFR-activated downstream PI3K/AKT signaling were essential for FYN silencing-mediated sensitization of TNBC cells to EGFR targeted therapies, such as Lap, as illustrated (Figure 6E), further suggesting FYN as a potential target vulnerable for TNBC resistance to EGFR inhibition. This combinatorial effect of FYN and EGFR targeting seems highly TNBC context dependent, and warrants strategies for stratifying drug sensitivity for individual TNBC patients.

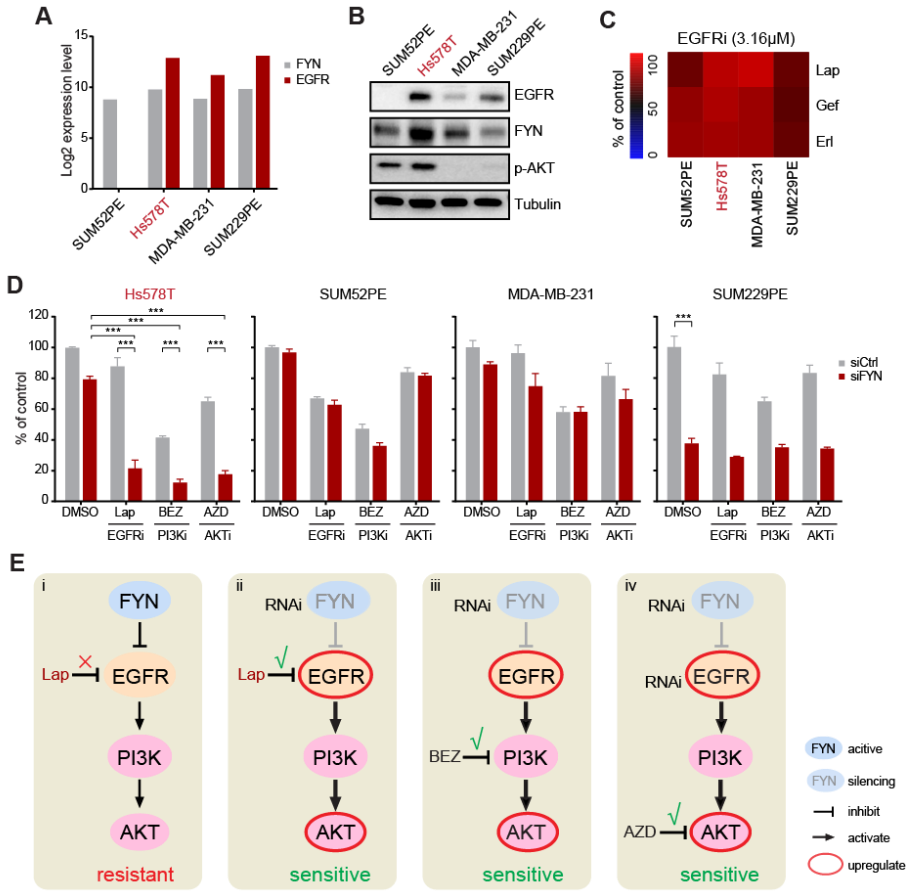


Figure 6. Association of FYN silencing-mediated lapatinib synergy with EGFR and p-AKT expression. (A) Log2-based RNA-seq gene expression levels of FYN and EGFR in SUM52PE, Hs578T, MDA-MB-231 and SUM229PE TNBC cell lines. (B) Expression of EGFR, FYN, and phosphorylated AKT (p-AKT) in the TNBC cell lines. (C) Proliferative responses of the TNBC cell lines to EGFRi Lap, Gef and Erl. Cells were treated with EGFRi at 1 μM for 4 days, followed by SRB proliferation assay. (D) Effects of FYN silencing on cellular responses of the TNBC cell lines to EGFRi Lap, PI3Ki BEZ and AKTi AZD (two-way ANOVA * $p < 0.05$, ** $p < 0.01$, *** $p < 0.001$). (E) Diagram illustrating mechanisms underlying FYN silencing-mediated Lap synergy. FYN negatively regulated EGFR activity, limiting downstream PI3K/AKT signaling, rendering TNBC cells refractory to EGFRi Lap (i). RNA interfering (RNAi) of FYN released the negative regulation of EGFR, amplifying EGFR signaling responsiveness to EGFRi Lap (ii). Release of EGFR activity from FYN RNAi enhanced downstream AKT signaling, leading to sensitivity to PI3Ki BEZ (iii) and AKTi AZD (iv).

Discussion

TNBC commonly expresses high level of EGFR^{150, 151}. However, in most cases the TNBC disease is poorly responsive to EGFR targeted therapies^{25, 174}. Various resistance mechanisms can operate in cancer, such as increased drug efflux, mutations of the drug targets, DNA damage repair, and alternation of signaling pathways to evade cell death^{24, 174, 175}. Activated downstream pathways, primarily the Ras-Raf-MEK-MAPK and PI3K-AKT

pathways, are causatively one of the major resistance mechanisms to EGFR tyrosine kinase inhibitors in lung cancer ^{24, 175}. The molecular mechanism of TNBC resistance to EGFR targeted therapies is yet uncertain. In this study, our siRNA-based kinome-wide loss of function screen revealed numerous vulnerable kinase targets mediating proliferative phenotypes of EGFRi-refractory TNBC cells. Among these kinase targets, mTOR was the most vulnerable and centralized in the interactive signaling network. These kinases fell mainly into cell cycle (such as PLK1, CHEK1 and WEE1) and mTOR signaling (such as RPS6KA2 and mTOR) pathways, and cancer-related metabolism process (including FGFR1 and GSK3). Treatment with inhibitors targeting AKT/mTOR signaling attenuated proliferation of EGFRi-refractory TNBC cells. In addition, we defined addiction to EGFR/MAPK signaling in one mTORi-resistant TNBC cell line. These results indicated that TNBC cells develop alternative addictions, for instance, to AKT/mTOR signaling pathway, to gain resistant phenotypes against EGFR targeted therapies. Exploration of the kinase targets vulnerable for EGFRi-refractory phenotype of TNBC cells may further facilitate understanding the resistance mechanisms and identifying selective targeted therapies against the alternative kinase addictions in TNBC cells. Importantly, vulnerabilities of EGFRi- and mTORi-resistant TNBC cells to inhibitors targeting cell cycle kinases, such as PLK, CDK and Chk, reflected the dependency of TNBC cells on basal cell cycle machinery for maintaining cell proliferation.

To overcome EGFRi-refractory phenotypes of cancer cells, another option is to define potential combinatorial inhibition of alternative signaling activations to enhance cellular responsiveness to EGFR targeted therapies. Clinical data confirmed that PIK3CA oncogenic mutation resulted in dramatically suppressed sensitivity of lung adenocarcinomas to EGFRi ¹⁷⁶. A genome-wide loss-of-function screen identified PI3K hyperactivation was associated with lapatinib resistance of HER2-positive breast cancer cells and could be reversed by PI3Ki BEZ235 ¹⁷⁷. Loss of PTEN, which mediates activation of AKT, contributes to erlotinib resistance in colorectal cancer ¹⁷⁸. Our EGFRi lapatinib and kinome siRNA combination screen identified a group of kinases vulnerable for lapatinib resistance of TNBC cells. The majority of the kinases were functionally enriched in regulation of protein phosphorylation and kinase activity. Among them, the kinases ABL1, FYN, HCK, IRAK1, KIT, PIK3R3, PTK6 and SKAP1 were most commonly clustered and annotated to regulate tyrosine autophosphorylation, an essential process that RTKs and non-receptor tyrosine kinases undergo to be self-phosphorylated and activated. These results suggested that these signaling regulatory components might regulate autophosphorylation and activation of EGFR, leading to resistance of TNBC cells to EGFR targeted therapies. Therefore, targeting these vulnerable kinase targets may potentially unleash effective EGFR inhibition by EGFR tyrosine kinase inhibitors, such as gefitinib, erlotinib and lapatinib, for treating the refractory TNBC.

Our subsequent EGFRi lapatinib and siRNA deconvolution screen has functionally validated a few kinases, including FYN, KIT, HK2, NME6 and DCK, as potential vulnerable targets for lapatinib resistance of TNBC cells. Most importantly, silencing of these kinases, particularly FYN, a member of Src family kinases (SFKs), enhanced the ligand EGF binding-induced autophosphorylation of EGFR and activation of downstream PI3K/AKT signaling, thereby enabling EGFRi lapatinib to effectively inhibit EGFR/PI3K/AKT signaling and restoring the responsiveness of TNBC cells. SFKs are non-receptor tyrosine kinases, including Src, Fyn, Yes, Blk, Yrk, Frk, Fgr, Hck, Lck, Srm, and Lyn¹⁷⁹. SFKs intensively integrate with transmembrane RTKs and transduce RTK signaling to downstream effectors, such as PI3K, AKT and STAT3, promoting cell proliferation, survival, migration, invasion and drug resistance^{179, 180}. FYN is overexpressed in various cancers, including prostate cancer, head and neck carcinoma and melanoma^{181, 182}. Yet, the role of FYN overexpression in cancer is to be well defined. One study presents that overexpression of FYN in prostate cancer supports FYN as a novel potential target for prostate cancer therapy¹⁸¹, whereas another shows that loss of FYN expression in prostate cancer and high levels of FYN in benign prostatic hyperplasia propose FYN as a potential tumor suppressor¹⁸³. Functionally, in breast cancer, while FYN knockdown does not attenuate tumor cell proliferation and tumor growth rate of basal type breast cancer MDA-MB-231 cells, depletion of FYN suppresses metastatic ability of MDA-MB-231 tumor cells¹⁸⁴. FYN promotes mesenchymal phenotypes of basal type breast cancer cells through epithelial-mesenchymal transition via STAT5/NOTCH2 signaling node¹⁸⁴. Increased FYN activity blocks EGFR mitogenic signaling to suppress growth of keratinocytes¹⁶⁴. Phospho-proteomics profiling has linked FYN, as well as LYN and LCK, to EGFRi lapatinib resistance in a cohort of HER2 positive breast tumors following lapatinib treatment¹⁸⁵. Here, our results have defined FYN as a negative regulator of EGFR signaling, specifically on autophosphorylation and kinase activity of EGFR, mediating lapatinib resistance in TNBC cells. Depletion of FYN enhanced EGF-induced EGFR autophosphorylation and downstream AKT phosphorylation. FYN silencing synergized with lapatinib in EGFR-positive but not in EGFR-negative TNBC cells, while co-silencing of FYN and EGFR in EGFR-positive TNBC cells did not support the synergistic effect, suggestive of the regulatory effect of FYN on EGFR phosphorylation level but not EGFR expression. Particularly, the synergistic effect of FYN silencing and EGFR pharmacological inhibition by lapatinib required active AKT signaling, indicating a prerequisite of an intact EGFR/PI3K/AKT signal route for the FYN silencing-mediated synergy. Our work reveals that FYN-mediated EGFR/PI3K/AKT signaling is one mechanism of TNBC resistance against EGFR targeted therapies, supporting FYN as a potential vulnerable target for EGFRi-refractory TNBC.

Acknowledgments

This work was supported by the ERC Advanced grant Triple-BC (grant no. 322737). JH was financially supported by the China Scholarship Council.

Supplementary data

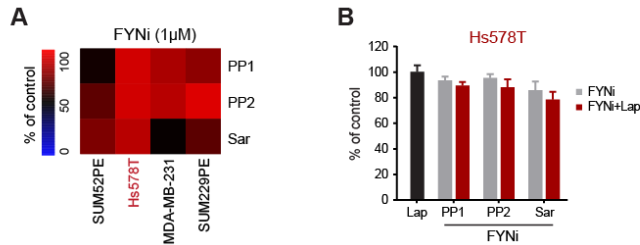


Figure S1. Proliferative responses of TNBC cells to FYN inhibitors (FYNI) PP1, PP2 and saracatinib (Sar) alone (A) and in combination with EGFRi Lap (B). Cells were treated with FYNI at 1 μ M alone or in combination with Lap at 3.16 μ M for 4 days, followed by SRB proliferation assay.

Table S1. Differential targeting effects of kinome-wide siRNAs on Hs578T and HCC1806 cells.

Table S2. KEGG pathway enrichment of direct targeting kinases in Hs578T and HCC1806 cells.

Pathway Enrichment of 42 kinase targets in Hs578T cells				
Category	Term	-logP	PValue	Symbols
KEGG_PATHWAY	hsa04110:Cell cycle	2.0567	0.008776	PLK1, CDKN2D, CHEK1, WEE1
KEGG_PATHWAY	hsa04150:mTOR signalling pathway	1.7665	0.017121	RP56KA2, STRADA, MTOR
KEGG_PATHWAY	hsa05230:Central carbon metabolism in cancer	1.6858	0.020618	FGFR1, GCK, MTOR
KEGG_PATHWAY	hsa05215:Prostate cancer	1.4293	0.037217	FGFR1, RELA, MTOR
Pathway Enrichment of 49 kinase targets in HCC1806 cells				
Category	Term	-logP	PValue	Symbols
KEGG_PATHWAY	hsa04010:MAPK signaling pathway	5.9751	1.06E-06	EGFR, RP56KA2, RELA, MAP3K8, MAPKAPK3, PDGFRB, PAK1, MAPKAPK2, CHUK, MAP3K11
KEGG_PATHWAY	hsa04068:FoxO signaling pathway	5.7906	1.62E-06	PRKAG3, EGFR, CDKN1B, PIK3CB, PLK1, ATM, CHUK, PCK1
KEGG_PATHWAY	hsa05215:Prostate cancer	4.3985	3.99E-05	EGFR, CDKN1B, PIK3CB, RELA, PDGFRB, CHUK
KEGG_PATHWAY	hsa04151:PI3K-Akt signaling pathway	3.9773	1.05E-04	EGFR, CDKN1B, FLT1, PIK3CB, RELA, PDGFRB, CHUK, SYK, PCK1
KEGG_PATHWAY	hsa04014:Ras signaling pathway	3.3618	4.35E-04	EGFR, FLT1, PIK3CB, RELA, PDGFRB, PAK1, CHUK
Pathway Enrichment of 12 kinase targets in both Hs578T and HCC1806 cells				
Category	Term	-logP	PValue	Symbols
KEGG_PATHWAY	hsa04114:Oocyte meiosis	2.2891	0.00514	RP56KA2, PLK1, AURKA
KEGG_PATHWAY	hsa04110:Cell cycle	2.1952	0.00638	PLK1, CHEK1, WEE1

Table S3. 96 Lap synergistic kinase targets for EGFRi-refractory Hs578T cells.

Table S4. Deconvolution screen of 96 Lap synergistic kinase targets in Hs578T cells.

Table S5. Metascape gene annotation and pathway enrichment of 30 Lap synergistic kinase targets.

Pathway Enrichment							
GroupID	Category	Term	Description	LogP	Log(q-value)	InTerm_InList	Genes Symbols
1_Summary	GO Biological Processes	GO:0046777	protein autophosphorylation	-11.2472622	-6.930	9/235	25, 2049, 2K3, SKAP1
2_Summary	GO Biological Processes	GO:0038083	peptidyl-tyrosine autophosphorylation	-6.96820337	-3.253	4/37	25, 2534, 3K2, BMPR2
3_Summary	GO Biological Processes	GO:0033674	positive regulation of kinase activity	-6.57270683	-3.126	8/574	25, 2534, 3PK1, DGKB
4_Summary	Canonical Pathways	M186	PID PDGFRB PATHWAY	-6.36614423	-3.003	5/129	25, 2534, 30CC, HIPK1
5_Summary	KEGG Pathway	hsa04072	Phospholipase D signaling pathway	-6.099466	-2.861	5/146	1606, 1607PHB3, H2K
6_Summary	GO Biological Processes	GO:0046834	lipid phosphorylation	-5.99472614	-2.823	4/64	1606, 1607MAPK8, KIT
7_Summary	GO Biological Processes	GO:0090407	organophosphate biosynthetic process	-5.96452684	-2.823	8/691	1606, 1633AK1, IRAK2
8_Summary	KEGG Pathway	hsa04360	Axon guidance	-5.71144786	-2.649	5/175	25, 659, 2036, MAPK8
9_Summary	GO Biological Processes	GO:0030501	positive regulation of bone mineralization	-4.85987918	-2.048	3/39	92, 659, 91, IRAK1, KIT
10_Summary	GO Biological Processes	GO:0044089	positive regulation of cellular component biogenesis	-4.42485898	-1.789	6/541	25, 2049, 3I1, PIP4K2C
11_Summary	KEGG Pathway	hsa05200	Pathways in cancer	-4.00905126	-1.506	5/395	25, 3815, 5K, ACVR2A
12_Summary	GO Biological Processes	GO:0048514	blood vessel morphogenesis	-3.84175921	-1.410	6/690	25, 659, 20, 4K2C, HCK
13_Summary	GO Biological Processes	GO:0018105	peptidyl-serine phosphorylation	-3.42436367	-1.195	4/289	4294, 5165PK8, VRK2
14_Summary	GO Biological Processes	GO:0007224	smoothened signaling pathway	-3.27014482	-1.093	3/133	4294, 2714K36, HIPK1
15_Summary	GO Biological Processes	GO:0045926	negative regulation of growth	-2.4177288	-0.475	3/264	659, 5753, ME6, AB11

Chapter 4

Multi-targeted kinase inhibition alleviates mTOR inhibitor resistance in triple-negative breast cancer

Jichao He, Ronan P. McLaughlin, Vera van der Noord, John A. Foekens, John W. M. Martens, Gerard van Westen, Yinghui Zhang, Bob van de Water

Published in *Breast Cancer Res Treat.* 2019 Aug 6. doi: 10.1007/s10549-019-05380-z

Abstract

Purpose

Owing to its genetic heterogeneity and acquired resistance, triple-negative breast cancer (TNBC) is not responsive to single-targeted therapy, causing disproportional cancer-related death worldwide. Combined targeted therapy strategies to block interactive oncogenic signaling networks are being explored for effective treatment of the refractory TNBC subtype.

Methods

A broad kinase inhibitor screen was applied to profile the proliferative responses of TNBC cells, revealing resistance of TNBC cells to inhibition of the mammalian target of rapamycin (mTOR). A systematic drug combination screen was subsequently performed to identify that AEE788, an inhibitor targeting multiple receptor tyrosine kinases (RTKs) EGFR/HER2 and VEGFR, synergizes with selective mTOR inhibitor rapamycin as well as its analogs (rapalogs) temsirolimus and everolimus, to inhibit TNBC cell proliferation.

Results

The combination treatment with AEE788 and rapalog effectively inhibits phosphorylation of mTOR and 4EBP1, relieves mTOR inhibition-mediated upregulation of cyclin D1, and maintains suppression of AKT and ERK signaling, thereby sensitizing TNBC cells to the rapalogs. siRNA validation of cheminformatics-based predicted AEE788 targets has further revealed the mTOR interactive RPS6K members (RPS6KA3, RPS6KA6, RPS6KB1 and RPS6KL1) as synthetic lethal targets for rapalog combination treatment.

Conclusions

mTOR signaling is highly activated in TNBC tumors. As single rapalog treatment is insufficient to block mTOR signaling in rapalog-resistant TNBC cells, our results thus provide a potential multi-kinase inhibitor combinatorial strategy to overcome mTOR-targeted therapy resistance in TNBC cells.

Keywords

Multi-kinase inhibitor; mTOR-targeted therapy; Drug resistance; Triple-negative breast cancer (TNBC); Polypharmacology

Background

Triple-negative breast cancer (TNBC) constitutes a small subtype (10-20%) of breast cancer, but causes the majority of breast cancer-related deaths^{104, 186}. As defined by the absence of ER and PR expression and HER2 overexpression, TNBC is not curable by hormone receptor or HER2-targeted therapies¹⁸⁷. Furthermore, TNBC is highly heterogeneous. Gene expression profiling has further classified TNBC into six unique molecular subtypes, namely basal-like (BL1 and BL2), mesenchymal (M), mesenchymal stem-like (MSL), immunomodulatory (IM), and luminal androgen receptor-like (LAR) subtype⁸. The TNBC molecular signatures have been explored for targeted therapies in clinical trials, including those targeting receptor tyrosine kinases (RTKs, e.g. EGFR, VEGFR, c-Met), PI3K/AKT, Ras/MAPK, JAK/STAT, cell cycle regulators^{107, 188}. Yet, TNBC has not benefited from above mono-targeted therapies so far, due to intrinsic or acquired resistance¹⁰⁷.

The mammalian target of rapamycin (mTOR), a conserved serine/threonine protein kinase, is a central regulator of cell growth and proliferation, by sensing and integrating multiple signals from growth factors and nutrient signals^{189, 190}. mTOR hyperactivity is frequently observed in TNBC compared to other breast cancer subtypes and is often correlated with poor prognosis, underpinning the potential of mTOR-targeted therapy for TNBC treatment^{39, 134, 191}. Although mTOR-targeted interventions, such as rapamycin and its analogs (rapalogs) temsirolimus and everolimus, delay progression and extend survival, patients with TNBC eventually develop resistance to mTOR inhibitors with undesired outcome^{112, 134}. Evidence has shown that rapalog treatment could release mTOR negative feedback on upstream kinases and activate compensatory pathways, for instance, PI3K/AKT and MAPK/ERK signaling pathways, thereby bypassing mTOR inhibition¹⁹²⁻¹⁹⁴. This observation underscores the need for alternative combinatorial therapeutic approaches for TNBC treatment.

Since oncogenic pathways incorporate multiple signaling components and axes to promote tumor malignancy, monotherapy may not be sufficient for long-term control of TNBC^{134, 192, 195}. Hence, simultaneously targeting different signaling molecules represents a promising strategy to impede tumor growth and progression^{190, 196}. Several reports have documented that co-targeting growth factor receptors and mTOR exerts cooperative anti-cancer effects in various cancer types, including TNBC¹⁹⁷⁻²⁰¹. However, these studies focus on a particular combination in the questioned cancer type. Little is known about the interactive kinases involved in rapalog resistance and the mechanisms of the combinatorial effect remain unclear. Here, we systematically screened a broad collection of kinase inhibitors across a large panel of TNBC lines treated with rapamycin. Our data demonstrated that multiple targeted kinase inhibition, for instance, by inhibitor AEE788, sensitizes TNBC cells to various mTOR inhibitors, rapamycin, temsirolimus and everolimus. Integrated cheminformatics study and siRNA validation revealed additional putative targets of AEE788, which interact closely with mTOR signaling. Most importantly, our

study provided an efficacious approach for exploring cancer combination treatment. Moreover, the combinatorial therapy is more effective than single drug application and thus demonstrates a therapeutic advantage over either agents as a monotherapy in TNBC treatment.

Methods

Cell culture

TNBC cell lines used were representative for different TNBC subtypes, including basal-like 1 (BL1) HCC38, HCC1143, HCC1937 and MDA-MB-468, basal-like 2 (BL2) HCC70, HCC1806 and SUM149PT, mesenchymal (M) BT549, mesenchymal stem-like (MSL) Hs578T, MDA-MB-231, MDA-MB-436 and SUM159PT, luminal androgen receptor (LAR) MDA-MB-453 and SUM185PE, and unclassified BT20, SKBR7, SUM52PE, SUM229PE and SUM1315MO2. All human TNBC cell lines were cultured in RPMI-1640 medium supplemented with 10% fetal bovine serum, 25 U/mL penicillin and 25 µg/mL streptomycin in a humidified incubator at 37°C with 5% CO₂. Normal breast cell line MCF10A was kindly provided by Prof. dr. Peter ten Dijke (LUMC, Leiden, the Netherlands) and maintained in DMEM/F12 (Gibco) supplemented with 5% horse serum (Gibco), 20ng/ml epidermal growth factor (EGF) (Upstate), 100ng/ml cholera toxin (Calbiochem), 0.5 g/ml hydrocortisone (Sigma), 10 g/ml insulin (Sigma), 100U/ml penicillin and 50 g/ml streptomycin (Gibco). Kidney cell line RPTEC was cultured in mixed F12/DMEM (1:1 ratio) medium and grown for over 10 days after confluency to be differentiated.

Reagents and antibodies

The library of 378-kinase inhibitors (L1200), rapamycin, temsirolimus, everolimus, AEE788, gefitinib, PD184352, palbociclib, and LY2835219 inhibitors were purchased from SelleckChem (Huissen, Netherlands). The phospho(Ser473)-AKT (9271), phospho(Thr202/Tyr204)-p44/42 MAPK (ERK1/2, 9101), phospho(Ser2448)-mTOR (5536S), phospho(Thr37/46)-4EBP1 (2855), phospho((Tyr1148))-EGFR (4404), 4EBP1 (8594), Cyclin B1 (4135), mTOR (4517), Beclin-1 (3738), AKT (9272) and p44/42 MAPK (ERK1/2, 4695) antibodies were from Cell Signaling (Bioké, Leiden, Netherlands). Cyclin D1 (sc-20044) and CDK4 (sc-601) antibodies were from Santa Cruz (CA, USA), The antibody against tubulin (T-9026) and human epidermal growth factor (EGF, E9644) were from Sigma Aldrich (Zwijndrecht, The Netherlands). The antibody against GRP78/BiP (610978) was from BD Biosciences (NJ, USA). The LC3B (NB100-2220) antibody was from Novus biologics (Colorado, USA).

Kinase inhibitor library combination screen

One day post-seeding into 96-well plates, cells were treated with individual kinase inhibitors alone or combined with rapamycin at 1 μ M. After 4-day treatment, proliferation was evaluated by sulphorhodamine B (SRB) colorimetric assay¹²⁵.

siRNA transfection

To silence target genes, 50 nM siGENOME Human SMARTpool siRNA mix (GE Dharmacon, Lafayette, CO, USA) was transfected into cells by transfection reagent INTERFERin (Polyplus-Transfection SA, Illkirch-Graffenstaden, France) according to the manufacturer's instructions. A pool of 720 kinase siRNAs at stock concentration of 1 μ M, which has negligible effect on gene expression, was taken as control. The medium was refreshed 24 h post-transfection and transfected cells were used for experiments 48 h post-transfection.

Annexin V/Propidium Iodide apoptosis assay

To detect apoptosis, a live cell imaging of Annexin V-Alexa633/Propidium Iodide (AnV/PI) labeling was performed in real time. Cells were treated as indicated and labeled with AnV (250 ng/ml) that conjugates to phosphatidyl serine on the membranes of apoptotic cells, and PI (100 nM) that intercalates with DNA in apoptotic or necrotic cells. At the time points of 24, 48, 72 and 96 h, the AnV and PI in-taken cells were captured with a Nikon Eclipse Ti confocal microscope. Simultaneously, the nuclei of live cells were stained with DNA dye Hoechst 33342 (200 ng/ml) and imaged for cell density. Quantitative image analysis was performed with CellProfiler (v2.1.1). AnV and PI apoptosis fraction was calculated by normalization of AnV and PI positive cells to the total cell number.

Immunofluorescence assay

SUM149PT and HCC1143 cells were fixed 24 h after treatment with ice cold methanol for 15 minutes, and were subsequently rinsed 3 times for 5 minutes with PBS. Afterwards, the cells were incubated with blocking solution (10% normal goat serum, 0.3% Triton-100 in PBS) for 1 h, rinsed 3 times for 5 min with PBS, followed by overnight incubation with primary antibody (1:300), washing, and 1 h incubation with second antibody. Nuclei staining with Hoechst 33342 was performed as a final step together with the rinsing steps. The antibodies were diluted in antibody staining solution (1% BSA, 0.3% Triton-100 in PBS). All images were taken with confocal microscope Eclipse Ti-E from Nikon.

Synergy assessment

Combination Index (CI) was used to define synergism ($CI < 1$), additive effect ($CI = 1$) and antagonism ($CI > 1$) of combination drug treatment. The concentration of the single drug that inhibits 50% of cell proliferation (IC_{50}) was determined by fitting the dose-response curve using GraphPad Prism 7.0 software. The CI was calculated using the formula " $CI = C_A$,

$50/IC_{50,A} + C_{B,50}/IC_{50,B}$, where $C_{A,50}$ and $C_{B,50}$ are the concentration of drug A and B used in combination to achieve 50% drug effect.

Western Blotting

Cells were seeded in 6-well plates at the appropriate density. For stimulation/starvation assays, medium was refreshed with serum-free medium (SFM) the following day and cells were starved overnight. Thereafter, cells were pre-treated with drug solutions for 4 hours, then stimulated with 100 ng/ml EGF (Sigma; E9644) for 5 minutes in SFM. Cells were lysed with RIPA buffer containing 1% protease/phosphatase inhibitor cocktail (Sigma-Aldrich, P8340). Proteins were resolved by SDS-PAGE and transferred to polyvinylidene difluoride membranes. Membranes were blocked in 5% BSA in Tris-buffered saline with 0.05% Tween-20 (TBS-T), followed by overnight incubation with primary antibodies, washing, and 1 h incubation with HRP-conjugated secondary antibodies. Chemiluminescence was generated in the presence of HRP substrate and detected with an Amersham Imager 600 (GE Healthcare Life Sciences, Eindhoven, the Netherlands). Whenever relevant, the intensity of protein band was quantified using ImageJ software.

Real time PCR (qPCR) assay

RNA was isolated from TNBC cells using RNeasy (Qiagen). cDNA was generated from 400 ng total RNA, using RNeasy Plus Kit from Qiagen. Real-time qPCR was performed in triplicate, using the SYBRGreen PCR MasterMix (Applied Biosystems) on a 7900HT fast real-time PCR system (Applied Biosystems). The primer sequences used were: forward *ATCAAGTGTGACCCGGACTG*, reverse *CTTGGGGTCCATGTTCTGCT* (human CCND1); forward *CTGGTAAAGTGATATTGTTGCCAT*, reverse *TGGAATCATATTGGAACATGTAAACC* (human GAPDH). Relative mRNA levels after correction for GAPDH control mRNA were expressed using the $2^{-\Delta\Delta CT}$ method.

Putative target prediction, validation and network analysis

Candidate kinase targets of AEE788 were predicted by ligand-based target prediction model in ChEMBL database (version 23) and validated by siRNA knockdown plus rapamycin treatment. Bioactivity data for single protein targets in ChEMBL was used to train and validate two Naive Bayesian multi-label classifier models (at 1 μ M and 10 μ M bioactivity cutoffs respectively). Specifically, the model learns what sub-structural features of ligands correlate with activity against a certain target and assigns a score to each of these features. Bioactivity data was filtered for the presence of a pChEMBL value and only data with confidence score 9 was used. The model sums the individual feature scores for all the targets and comes up with a sorted list of likely targets with the highest scores. Validated gene targets showing higher FC (fold change) than control siRNA were taken as input to perform protein-protein interaction analysis in NetworkAnalyst

(<http://www.networkanalyst.ca/NetworkAnalyst/faces/home.xhtml>) using IMEx Interactome database. KEGG pathway database was used to generate gene network.

Statistical analysis

Kinase inhibitor (KI) library screen data were analyzed using an unbiased sample-based analysis with the formula “Z score = (individual KI sample - mean of all KI samples)/standard deviation of all KI samples”. The effect of individual KIs on cell proliferation inhibition was considered significant when their Z score < -1.5. Pearson correlation analysis was performed using GraphPad Prism 7.0. Statistical analysis of all experimental data was performed using two-way ANOVA (* $p < 0.05$, ** $p < 0.01$, *** $p < 0.001$). Data were expressed as mean \pm SEM. Significance was set at $p < 0.05$. The hierarchical clustering in heatmap was performed using CRAN pheatmap package in RStudio (version 0.99.887).

Results

TNBC cell lines are differentially responsive to mTOR inhibitor rapalogs

To gain insights into TNBC dependency on mTOR signaling integration for proliferation and cell survival, a KI library (Selleckchem®) containing 378 small molecular inhibitors targeting various kinase signaling pathways was screened across 19 TNBC cell lines (Suppl. Table S1), which are representative for the six transcriptome-based subtypes of TNBC⁸. All TNBC cell lines were exposed to individual inhibitors at 1 μ M for 4 days, followed by measurement of cell proliferation. The effect of each inhibitor on proliferation was assessed by Z scores normalized to overall proliferative response. TNBC cell lines were largely resistant to the majority of the kinase inhibitors, without any clear correlation to the TNBC molecular subtypes (Fig. 1a). The proliferative response towards mTOR inhibitors was variable among TNBC cell lines. We distinguished 11 TNBC cell lines insensitive to different mTOR inhibitors (Fig. 1b), including rapamycin (Rap) and its analogues (i.e. rapalogs), zotarolimus, everolimus, ridaforolimus and temsirolimus. HCC1806 and SUM149PT were most resistant to rapalogs, while Hs578T was most sensitive.

Rapalogs are highly selective allosteric inhibitors of mTOR, by binding to FKBP12/rapamycin-binding domain to block mTOR Ser2448 phosphorylation and function^{202, 203}. mTOR Ser2448 is a predominant phosphorylation residue for mTOR kinase activity in response to mitogen-derived stimuli²⁰³. Therefore, we examined the inhibitory effect of rapamycin (Rap), temsirolimus (Tem) and everolimus (Eve), on Ser2448-mTOR phosphorylation with a focus on rapalog-resistant TNBC cell lines HCC1806 and SUM149PT and rapalog-sensitive Hs578T TNBC cells. The rapalogs potently inhibited phosphorylation of mTOR in the sensitive Hs578T cells, but not or less effectively in the resistant HCC1806 and SUM149PT cells, respectively (Fig. 1c, d). These data suggest that mTOR kinase activity and its sustained phosphorylation render the TNBC cells resistant to rapalogs.

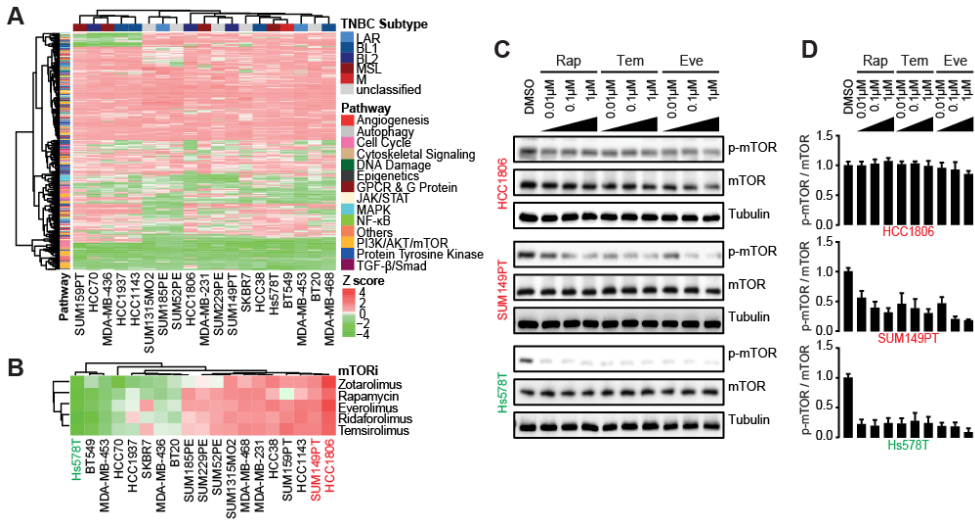


Fig. 1 Resistance profiling of TNBC cell lines to mTOR inhibitor rapalogs. **a** Heatmap presenting the responses of 19 TNBC cell lines to 378 kinase inhibitors. Data were shown based on the effect of individual KI on proliferation (relative Z scores), subtype-annotated cell lines (clustered horizontally) and pathway-annotated inhibitors (clustered vertically). Strong inhibitory effect on proliferation was indicated in green and weak in red. **b** Response clustering of TNBC cell lines to mTOR inhibitors (mTORi). **c** Concentration range effects of rapalogs rapamycin (Rap), temsirolimus (Tem) and everolimus (Eve) on mTOR phosphorylation, in rapalog-resistant HCC1806 and, SUM149PT TNBC cells, compared to rapalog-sensitive Hs578T cells. Cells were treated with rapalogs in concentration range (μM) for 4 h. **d** Quantitative comparison of phosphorylated mTOR level to total mTOR level in rapalog-treated resistant and sensitive TNBC cells.

Combinatorial drug screen identifies kinase inhibitors sensitizing TNBC cells to mTOR inhibition

Next, to identify kinase inhibitors synergizing with mTOR inhibition in rapalog refractory TNBC cells, we further performed a drug screen with rapamycin (at 1 μM) in combination with the 378 kinase inhibitors (also tested at 1 μM) in the resistant SUM149PT cells. Pearson correlation coefficient r displayed high reproducibility of two replicate screens for KI ($r = 0.9509$) and KI and rapamycin (KI + Rap, $r = 0.9115$), respectively (Fig. 2a, b). Comparison of KI + Rap combinatory effect to the single KI effect on proliferation inhibition uncovered 9 potent KIs (Fig. 2c), which significantly enhanced inhibitory effect of rapamycin on proliferation of SUM149PT cells (Fig. 2d). These included one MEK inhibitor PD184352 and 8 RTK inhibitors, AEE788, afatinib, AC480, AZD8931, AZD9291, AST-1306, ZM 306416 and gefitinib that are described to target single or multiple EGFR/HER2 and VEGFR RTKs (Fig. 2e). We also performed rapamycin combination screen in the resistant HCC1806 cells in parallel. As HCC1806 cells were responsive to EGFR inhibitors, only additive effects were observed (Suppl. Fig. S1c; Suppl. Fig. S2).

These data implicate that while the resistant SUM149PT cells poorly respond to inhibitors of EGFR or VEGFR and mTOR inhibitor rapamycin alone, concurrent blockage of

upstream EGFR or VEGFR RTK activity or MEK signaling transduction, and downstream mTOR signaling could converge re-sensitization of TNBC cells.

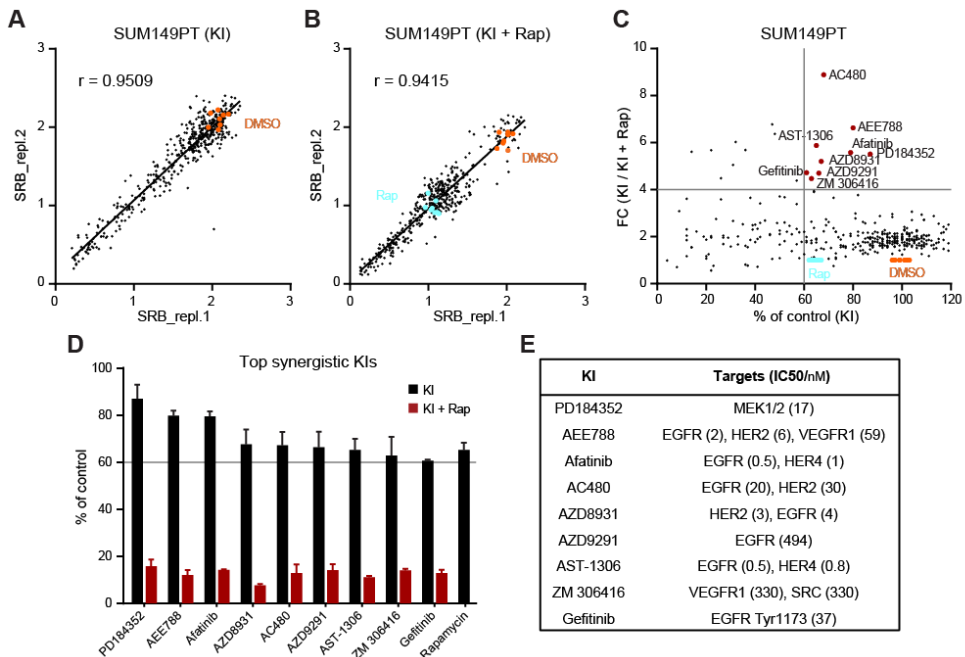


Fig. 2 Identification of kinase inhibitors which sensitize TNBC cells to rapamycin. **a, b** Pearson correlation coefficient r showing reproducibility of replica screen of 378 kinase inhibitors alone (KI, **a**) or combined with rapamycin (KI + Rap, **b**). SUM149PT cells were treated for 4 days with $1 \mu\text{M}$ KI individuals alone or combined with $1 \mu\text{M}$ Rap. Orange dots, DMSO control. Cyan dots, Rap only. **c** Effect comparison of KI alone to KI combined with Rap on proliferation of SUM149PT cells. The percentage of proliferation (% of control) was relative to DMSO. The ratio of percentage of proliferation was shown as fold change (FC, KI versus KI + Rap). Top synergistic inhibitors were marked in red. **d** Selected inhibitors reducing 40% proliferation with $\text{FC} > 4$ (extracted from Figure 2C, red dots) when combined with rapamycin. Error bars indicate screen replicates. **e** Kinase targets of the selected inhibitors and IC_{50} values of the inhibitors on corresponding targets (SelleckChem®).

Multi-targeted RTK inhibitor AEE788 enhances proliferative inhibition and cell death in rapalog-resistant TNBC cells

Next, we further validated the combinatorial effect of the most promising combinations on proliferative inhibition in the rapalog-resistant SUM149PT cells. We focused on the MEK inhibitor PD184352, EGFR inhibitor gefitinib and the multi-targeted RTK inhibitor AEE788. Cells were treated with rapamycin in a concentration range alone or combined with different concentrations of PD184352, gefitinib or AEE788. AEE788 synergized with rapamycin to inhibit SUM149PT cell proliferation in dose-dependent manner (Fig. 3a, top panel). In contrast, PD184352 and gefitinib (Suppl. Fig. S1a, b) displayed a more additive effect when combined with rapamycin. The synergistic effects of AEE788 and rapalogs, Rap, Tem and Eve, were further confirmed in SUM149PT as well as another rapalog-

resistant TNBC cell line HCC1143 (Fig. 3a). AEE788 significantly reduced the half-maximal

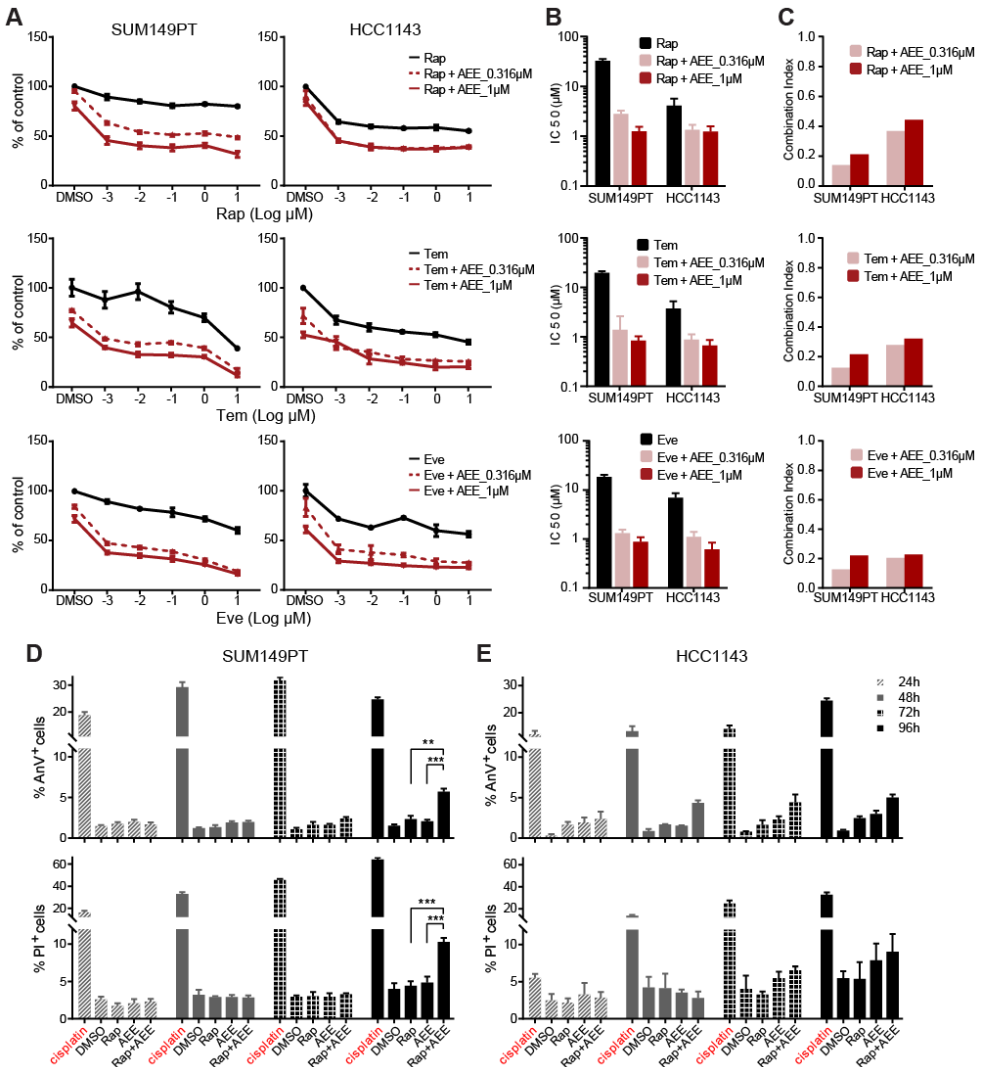


Fig. 3 Synergistic effect of AEE788 and rapalogs on proliferative inhibition and cell death in rapalog-resistant TNBC cells. **a** Proliferative response of rapalog-resistant SUM149PT (left panel) and HCC1143 (right panel) TNBC cells, to rapalogs Rap, Tem and Eve in concentration range alone or combined with 0.316 μM and 1 μM AEE788 respectively. **b** IC₅₀ values (μM) of rapalogs in combination with AEE788, inducing 50% of proliferation inhibition in SUM149PT and HCC1143 cells. **c** Combination index (CI) of rapalog and AEE788 in SUM149PT and HCC1143 cells. CI < 1 indicates synergism. **d, e** Combinatorial effects of Rap and AEE788 on SUM149PT (left panel, **d**) and HCC1143 (right panel, **e**) cell death. Cells were subjected to Annexin V/Propidium Iodide (AnV/PI) apoptosis assays after treatment for 24, 48, 72 and 96 h. Cisplatin (100 μM) was used as positive control. (two-way ANOVA * $p < 0.05$, ** $p < 0.01$, *** $p < 0.001$)

inhibitory concentrations (IC₅₀) of the rapalogs in both SUM149PT and HCC1143 cell lines (Fig. 3b). Combination index (CI) analysis detected the strong synergy of AEE788 and

rapalogs, overall with CI values < 0.5 (Fig. 3c). To detect the combinatorial effects of AEE788 and rapamycin on TNBC cell death, we performed Annexin V/Propidium Iodide apoptosis assay in SUM149PT and HCC1143 cell lines. Besides proliferative inhibition, the combination significantly enhanced apoptosis and necrosis 96 h post-treatment in SUM149PT cells (Figure 3d), and enhanced the monotherapy-induced apoptosis in HCC1143 cells, albeit not statistically significant (Figure 3e). Next, we evaluated the combinatorial effects on normal mammary cells MCF10A and renal cells RPTEC. Importantly, neither monotherapy nor combination significantly suppressed proliferation or induced cell death of MCF10A and RPTEC cells, suggesting that the combo effects might be cancer cell specific and less toxic in normal mammary and renal cells (Suppl. Fig. S3). Altogether, the KI combination not only inhibited TNBC cell proliferation, but also enhanced the monotherapy-induced apoptosis and necrosis, with minimal effects on normal mammary and renal cells.

Co-treatment of rapamycin and AEE788 abolishes mTOR phosphorylation and sustains downregulation of ERK and AKT signaling in TNBC cells

mTOR belongs to a complex network of regulatory feedback loops responsible for controlling upstream proliferative signaling pathways. The major upstream signaling in control of mTOR activity involves PI3K/AKT and MAPK/ERK, the two canonical pathways downstream of RTKs¹⁸⁹. Resistance to mTOR inhibition in cancer has been linked to activation of upstream PI3K/AKT and MAPK/ERK signaling, following rapalog treatment¹⁹⁴. Next, we investigated the synergistic effect of AEE788 and rapamycin on PI3K/AKT and MAPK signaling in TNBC cells. Treatment with AEE788 alone inhibited ERK and AKT phosphorylation in the resistant SUM149PT and HCC1143 cells (Fig. 4a). Single treatment with rapamycin slightly increased p-ERK in SUM149T and p-AKT in HCC1143 cells. The phosphorylation levels of mTOR and the target of mTOR, 4EBP1, were not affected by either AEE788 or rapamycin alone, further indicating the sustained mTOR signaling in the resistant TNBC cells. However, co-treatment of AEE788 and rapamycin almost completely abolished mTOR phosphorylation, whilst ERK and AKT phosphorylation remained inhibited (Fig. 4a, b). The synergistic effect of AEE788 and rapamycin on p-4EBP1 inhibition was marginal (Fig. 4a).

As AEE788 has been described as an EGFR/VEGFR dual RTK inhibitor, we further evaluated the co-treatment effect of AEE788 and rapamycin on EGFR RTK signaling activity in both resistant SUM149PT and HCC1143 cells upon EGF stimulation (Fig. 4c). EGF treatment caused the activation of the EGF-receptor as evidenced by increased p-EGFR and downstream p-ERK and p-AKT. AEE788 effectively blocked EGF-stimulated phosphorylation of these components, in both SUM149PT and HCC1143 cells. It has been reported that 4EBP1 has multiple phosphorylation sites and an increase in 4EBP1 phosphorylation is accompanied by a decrease in its electrophoretic mobility²⁰⁴⁻²⁰⁶. EGF

also effectively caused enhanced p-mTOR and p-4EBP1. Rapamycin could inhibit 4EBP1 phosphorylation by EGF in both cell lines but with no (SUM149PT) or limited (HCC1143) effects on mTOR activation; and, reversely, AEE788 could inhibit mTOR activation but with marginal effects on 4EBP1 phosphorylation. However, co-treatment with AEE788 and rapamycin particularly could shut-down the EGF-mediated phosphorylation of mTOR and 4EBP1 signaling.

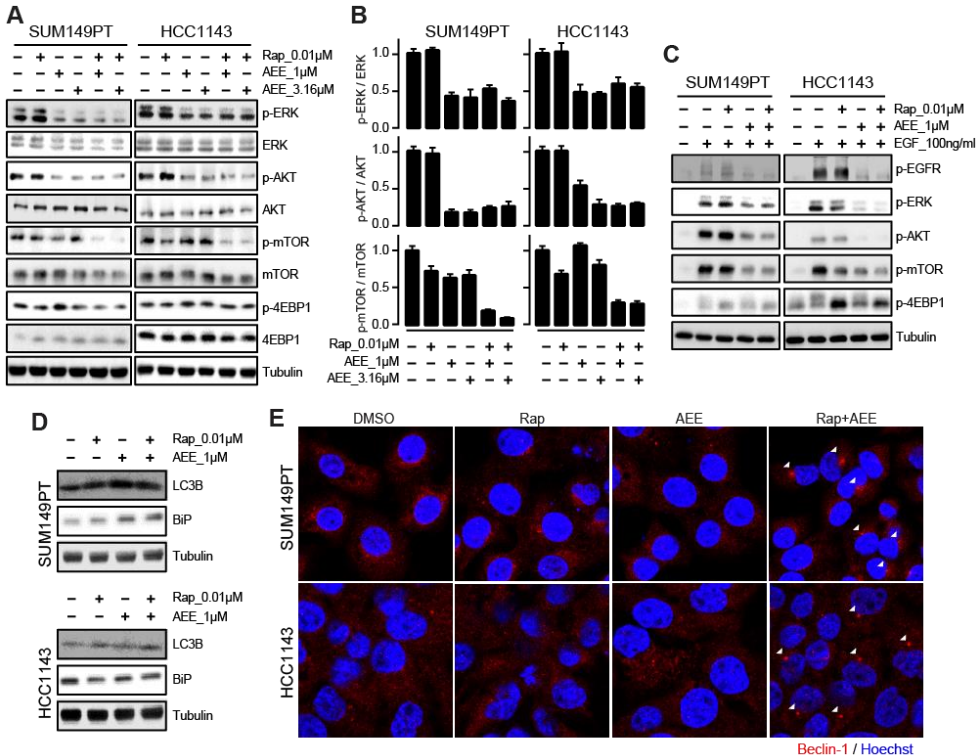


Fig. 4 Combinatorial effect of AEE788 and rapamycin on mTOR signaling inhibition in rapalog-resistant TNBC cells. **a** Effects of AEE788 and Rap co-treatment on mTOR phosphorylation, upstream AKT and ERK and downstream 4EBP1 signaling in rapalog-resistant SUM149PT and HCC1143 cells. Cells were treated with 1-3.16 μ M AEE788 and 0.01 μ M Rap alone or combined as indicated for 4 h. **b** Quantification of phosphorylated ERK to total ERK (top row), phosphorylated AKT to total AKT (middle row) and phosphorylated mTOR to total mTOR (bottom row) in SUM149PT and HCC1143 treated with AEE788 and Rap alone or combined as indicated. **c** Effects of AEE788 and Rap co-treatment on EGF-stimulated signaling transduction in SUM149PT and HCC1143 cells. Cells were starved in serum-free medium overnight, pre-treated for 4 h with AEE788 and Rap alone or combined as indicated, followed by exposure to 100 ng/ml EGF for 5 min. 4EBP1 can be phosphorylated at several sites, as indicated by multiple bands. The bottom band is the unphosphorylated form of 4EBP1. **d** Effects of AEE788 and Rap co-treatment for 24 h on autophagy (LC3B) and ER stress (BiP). **e** Effects of AEE788 and Rap co-treatment on Beclin-1 accumulation. Cells were subjected to immunofluorescence assay 24 h post-treatment. White arrows indicate the induction of Beclin-1.

Several cellular processes have been linked to the immunogenicity of cell death, including autophagy and ER stress²⁰⁷⁻²¹⁰. Given that mTOR is a key regulator of autophagy,

we then tested the combination effect of autophagy in TNBC cells. Interestingly, the combination sustained the elevated LC3B level induced by monotherapy and demonstrated accumulated Beclin-1 expression 24 h post-treatment in both SUM149PT and HCC1143 cells (Fig. 4d, e). The combination increased the expression level of BiP, a key regulator of ER stress, 24 h post-treatment in SUM149PT cells, but not so much in HCC1143 cells (Fig. 4d), suggesting the involvement of immunogenic cell death-related events in TNBC cells by the combination treatment.

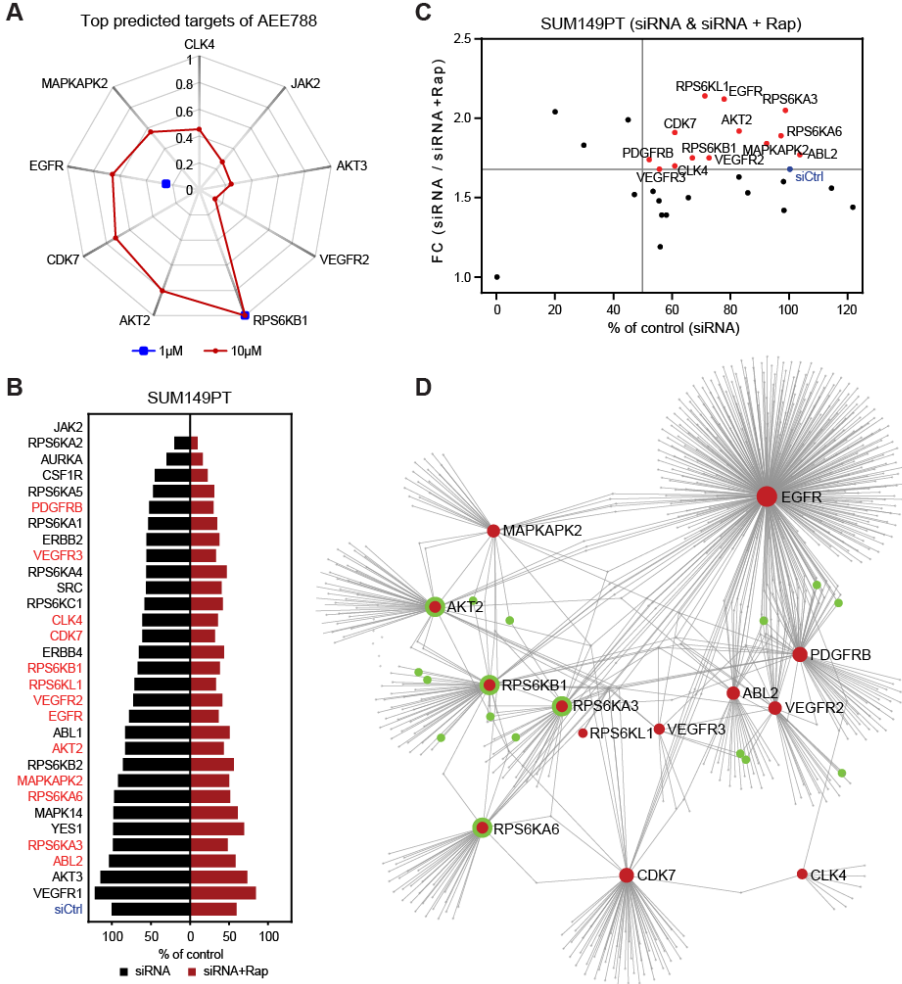


Fig. 5 Validation of AEE788 potential targets synergizing with rapamycin in rapalog-resistant TNBC cells. a Radar chart displaying highly predicted targets of AEE788 in ChEMBL_23 database with 1 μ M (blue) and 10 μ M (red) as cutoff. **b** Screen of AEE788 targets with siRNA alone (siRNA) or in combination with 0.01 μ M rapamycin (siRNA + Rap) in SUM149PT cells. siCtrl, siRNA control. **c** siRNA silencing effect of AEE788 targets synergizing with rapamycin. The ratio of percentages of proliferation was shown as FC (siRNA versus siRNA + Rap). Targets with

silencing effect over siCtrl (FC > 1.7, blue) were marked in red. **d** Protein-protein interactions of AEE788 targets (red) by NetworkAnalyst. Proteins interacting with mTOR signaling pathway were marked in green.

Silencing of AEE788 targets enhances mTOR inhibition in TNBC cells

Although AEE788 has been described as an inhibitor targeting multiple RTKs, we wondered whether the effect of AEE788 could be related to unanticipated polypharmacology, thus impacting through additional mechanisms of mTOR signaling. We used a cheminformatics approach to predict candidate alternative kinase targets of AEE788. ChEMBL is an open large-scale bioactivity database that contains comprehensive target inhibition information of thousands of drug-like molecules, including kinase inhibitor activity, allowing well-informed prediction of structure-based alternative kinase target prediction^{211, 212}. We firstly performed ligand-based target prediction for AEE788. With 1 μ M and 10 μ M activity cutoffs, 9 kinases showed high prediction scores and as such putative targets of AEE788, including RPS6KB1, AKT2, CDK7, EGFR, MAPKAPK2, CLK4, JAK2, AKT3 and VEGFR2 (Fig. 5a). To refine the scale of target list, we selected kinases showing prediction score greater than 0.1 and kinases with an IC₅₀ of AEE788 smaller than 1 μ M according to the publically available data²¹³. As a result, 30 putative kinase targets were selected. To validate the potential contribution of these kinases in the interaction with rapamycin, we performed a targeted rapamycin and siRNA synthetic lethal screen in SUM149PT cells (Fig. 5b). The synthetic lethal screen revealed 13 candidate targets (Fig. 5c). We anticipated that these validated targets would take part in connected signaling networks and, therefore, would all individually impact on the rapamycin sensitivity. Indeed, protein-protein interaction network analysis revealed a close interaction of the various putative kinase targets of AEE788 (Fig. 5d; Suppl. Table S2). Interestingly, the well-known mTOR target RPS6KB1 as well as other RPS6K family members RPS6KA3, RPS6KA6 and RPS6KL1, were mapped in the network, supporting the synergistic drug interaction of AEE788 with rapamycin on mTOR signaling. In addition, ABL2 and PDGFRB were predicted and validated as potential targets involved in rapamycin synergy. Of relevance, rapalog-resistant TNBC cell lines SUM149PT, HCC1143, SUM159PT and HCC38 poorly responded to inhibitors targeting the verified targets of AEE788, including EGFR, VEGFR, PDGFR, ABL and S6K (Suppl. Fig. S2). Taken together, the above data suggests that AEE788 synergizes with rapamycin in suppressing TNBC cell proliferation by targeting several EGFR, VEGFR, PDGFR, ABL and different S6K kinases that are all connected to mTOR signaling.

AEE788 abolished rapalog-upregulated cyclin D1 expression in TNBC cells

Finally, we looked into the mechanism how AEE788 and rapalogs impact on cell proliferation. Inhibition of mTOR by rapamycin blocks cell cycle progression and cell proliferation has been linked to disruption of the cyclin dependent kinase 4 (CDK4)-cyclin

D1 complex²¹⁴. Therefore, we next addressed the role of cyclin D1 in the synergistic effect of AEE788 and rapalogs on proliferation of rapalog-resistant SUM149PT and HCC1143 TNBC cell lines. Unexpectedly, we observed that rapalogs Rap, Tem and Eve did not

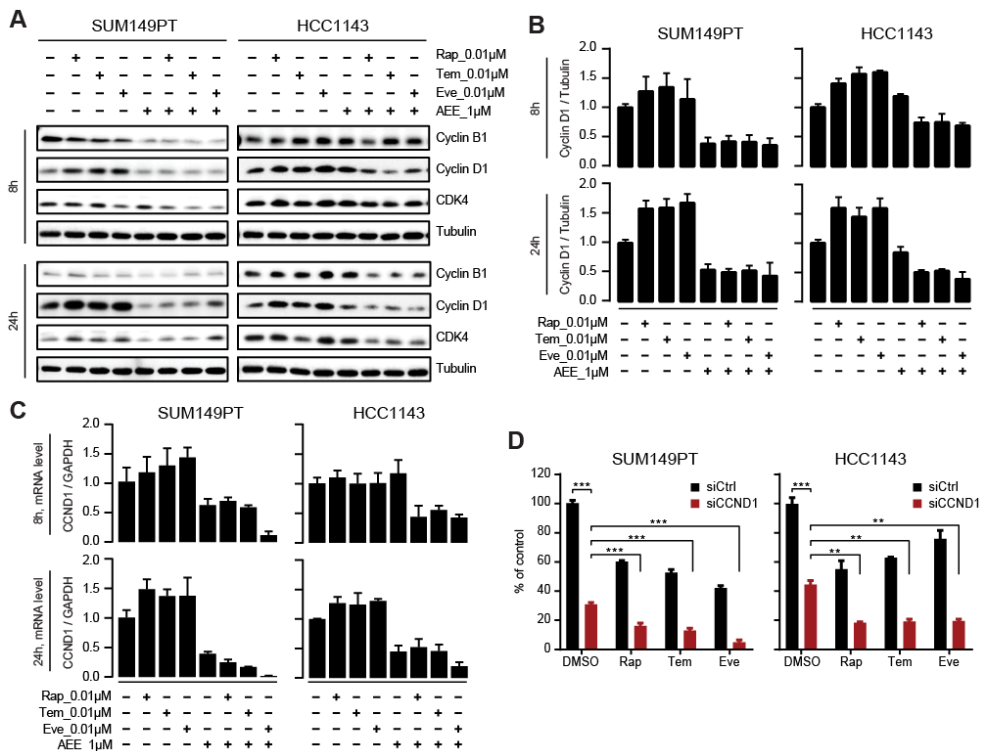


Fig. 6 Co-treatment with AEE788 prevents rapalog-induced cyclin D1 upregulation in resistant TNBC cells. a Combinatorial effects of AEE788 and rapalogs (Rap, Tem and Eve) on expression of cell cycle regulatory proteins in SUM149PT and HCC1143 cells. Cells were treated with 1 μM AEE788 and 0.01 μM rapalogs (Rap, Tem and Eve) alone or combined as indicated, for 8 h and 24 h, respectively. **b** Cyclin D1 protein expression levels relative to tubulin in SUM149PT and HCC1143 cells treated with AEE788 and rapalogs alone or combined as indicated. **c** Cyclin D1 mRNA expression level relative to GAPDH in SUM149PT and HCC1143 cells treated with AEE788 and rapalogs alone or combined as indicated. **d** Effect of CCND1 siRNA silencing (siCCND1) on proliferation inhibition of SUM149PT and HCC1143 cells treated with 0.01 μM rapalogs or DMSO control (two-way ANOVA * $p < 0.05$, ** $p < 0.01$, *** $p < 0.001$). siCtrl, siRNA control. Significant effect of rapalogs treatment alone on proliferative inhibition was observed (** $p < 0.01$).

suppress but upregulated cyclin D1 protein expression and mRNA levels of CCND1 (the gene encoding cyclin D1) in SUM149PT and HCC1143 TNBC cells after short- (8 h) and long-term (24 h) treatment (Fig. 6a-c). This suggests a positive-feedback loop activation upon rapalog treatment, thereby counteracting the anti-proliferative effect of rapalogs. Rapalogs slightly increased CDK4 levels, but did not affect cyclin B1 expression in the TNBC cells (Fig. 6a). When co-treated with AEE788, the rapalog-induced cyclin D1 upregulation was blocked at both the mRNA and protein levels (Fig. 6a-c). Moreover, co-treatment of

AEE788 and rapalogs led to downregulation of cyclin B1 and CDK4 expression in both TNBC cell lines (Fig. 6a). These results suggested that AEE788 synergized with rapalog to abrogate cyclin D1 upregulation thereby inhibiting cell proliferation. Next, we silenced cyclin D1 by siRNA-based CCND1 knockdown in SUM149PT and HCC1143 cells, in combination with rapalogs Rap, Tem and Eve, respectively. While silencing cyclin D1 alone considerably impaired SUM149PT and HCC1143 cell proliferation, this inhibitory effect was significantly enhanced when combined with rapalogs Rap, Tem or Eve (Fig. 6d). In support of a role of CDK4/cyclin D1 in the resistant phenotype of rapamycin, an enhanced inhibition on proliferation was observed in SUM149PT and HCC1143 cells when co-treated with rapamycin and selective CDK4/6 inhibitor palbociclib or LY2835219 (Suppl. Fig. S3), albeit not as effective as AEE788.

Discussion

mTOR acts as a central regulator of multiple signaling networks in control of cell growth, proliferation and survival^{189, 215}. mTOR signaling is frequently upregulated in malignant tumors, including TNBC, highlighting the potential of mTOR kinase targeted therapy in cancer modulation^{112, 134, 189, 190}. However, patients with TNBC often experience mTOR targeting failure due to acquired resistance and activation of bypass surviving pathways^{192, 194, 216}. Our drug combination screen revealed that co-treatment with AEE788, a multiple RTK-targeted inhibitor, restores the sensitivity of TNBC cells towards the clinically applied mTOR inhibitors (rapamycin, temsirolimus and everolimus). The effect of AEE788 is likely due to polypharmacology to shut down the crosstalk among receptors as well as mTOR pathway within signaling networks in the resistant scenario. The combination of targeted agents profoundly improves therapeutic efficacy and overcome resistance that might develop under single-agent therapy.

mTOR inhibition can relieve distinct negative feedback loops that normally serve to attenuate upstream RTKs, PI3K and MAPK signaling, leading to rapalog resistance²¹⁷. As such, mTOR inhibition alone is not sufficient to overcome the entire oncogenic program propagated from the alternate proliferative signaling pathways. By exploiting high-throughput kinase drug combination screen, our study has identified the effective kinase inhibitor, AEE788, that can block compensatory mechanisms conferring aberrant cell cycle progression upon rapalog treatment. The repression of EGFR/VEGFR and mTOR related pathways in concert seemingly reverts processes predominantly responsible for uncontrolled TNBC tumor proliferation. Our results are in line with the above observations that co-inhibition of upstream RTKs (such as EGFR, VEGFR, PDGFR and IGF1R), PI3K and MAPK signaling transduction and mTOR signaling elicited enhanced therapeutic efficacy in various cancer types.

Sustained mTOR signaling drives resistance to targeted therapeutics in cancer treatment²¹⁶. In TNBC tumor cells, mTOR signaling is frequently upregulated²¹⁸. We

demonstrated that while rapalogs alone were insufficient to inhibit the sustained mTOR signaling in resistant TNBC cells, co-treatment of rapalogs with the multi-targeted RTK inhibitor AEE788 synergistically blocked mTOR phosphorylation in SUM149PT and HCC1143 cells. Interestingly, SUM149PT cells have been characterized for the constitutively activated EGFR via a self-sustaining amphiregulin autocrine loop, and subsequently, altered receptor signaling and gene expression ^{219, 220}. While the KI combination blocked the EGF-mediated downstream EGFR signaling in both SUM149PT and HCC1143 cells, further considerations need be taken on whether the synergy is associated with RTK signaling cascades mediated by particular protein kinase receptor ligands (such as EGF, amphiregulin etc). Another mechanism of resistance to mTOR inhibition in cancer is the rapalog-mediated activation of upstream PI3K/AKT and MAPK/ERK signaling ¹⁹⁴. Co-treatment with AEE788 and rapamycin maintained the inhibitory effect on AKT and ERK signaling in TNBC cells. These data suggest that AEE788 and rapamycin synergistically inhibit the sustained mTOR activity in TNBC cells, thus blocking mTOR's potential feedback loop on activation of alternative ERK and AKT proliferative signaling pathways.

Polypharmacology, the action of drugs against multiple targets ¹⁹⁶, is commonly observed in drug development including the effective marketed kinase inhibitors ²²¹. Our ChEMBL-based cheminformatics analysis demonstrated that AEE788 is a kinase inhibitor that likely targets several kinases; this is consistent with other reports using protein kinase assays ^{198, 222}. Complementary to a recent kinobeads study on target landscape of clinical kinase drugs ²²¹, our cheminformatics approach presented that the multi-targeted RTK inhibitor AEE788 likely interacts with EGFR, VEGFR, ABL2, PDGFRB and several mTOR signaling pathway components, including AKT and S6K family members. Subsequent siRNA-based knockdown of these various kinases, e.g. RTKs (EGFR, VEGFR2/3 and PDGFRB), AKTs (AKT2 and AKT3) and RPS6Ks (RPS6KA3, RPS6KA6, RPS6KB1 and RPS6KL1), MAPKAPK2, ABL2 and CDK7 sensitized rapalog-resistant TNBC cells to rapamycin. Several reports have demonstrated the synergistic effects of targeting EGFR or MEK on anti-mTOR therapies in TNBC ^{199, 223-225}. However, our study demonstrated that simultaneous use of EGFRi gefitinib or MEKi PD184352 only exerts additive effects on rapamycin-mediated proliferative inhibition, suggesting that AEE788-rapalog synergy results presumably from multi-targeted kinase inhibition. These data support the anticipated polypharmacology of AEE788 as the mode-of-action of the synergy with rapalogs. Further studies are required to determine the detailed kinome target landscape of AEE788 in TNBC.

mTOR pathway regulates cell growth through its downstream effectors, such as 4EBP1 and RPS6KB1 ^{189, 215}. Another primary way that mTOR confers its regulatory effects on cell proliferation is to upregulate expression of the cell cycle regulator cyclin D1 ²²⁶. CCND1, the cyclin D1 encoding gene, is frequently amplified in breast cancer, and depletion of cyclin D1 suppresses breast cancer progression ^{137, 227}. In response to mTOR

inhibition, however, cyclin D1 is elevated by everolimus in various types of cancer ^{200,201}. Consistently, we found that treatment with rapalogs (rapamycin temsirolimus and everolimus) commonly upregulated cyclin D1 in rapalog-resistant TNBC cells, indicating an alternative activation of cyclin D1 proliferative signaling pathway after mTOR inhibition. Considering that cyclin D1 was lost in the presence of the AEE788-rapalog combination, AEE788 seems to compensate the undesired effects of rapalog, further highlighting the therapeutic advantage of the drug combination. Interestingly, while we discovered the AEE788-rapamycin interaction through a wider screening effort in TNBC cells, our findings were further supported by the observations on the synergistic effects of AEE788-everolimus combination in prostate, germ and renal tumor cell lines ^{198,200,201}. Moreover, a xenograft-bearing mice study also documented the beneficial action of AEE788-everolimus combination in glioblastoma tumor regression ²²⁸. However, these studies did not further the mode-of-action of AEE788. Since AEE788 is recognized as a multiple targeting kinase inhibitor, their observations were limited to EGFR/VEGFR, lacking of the notion on other potentially targeted candidate kinases. Our study, for the first time, revealed the synergy on rapalogs treatment in TNBCs and its underlying polypharmacology by utilizing integrated systematic screen and cheminformatics approach. Moreover, either genetic or pharmacological ablation of cyclin D1 significantly enhanced mTOR-inhibition mediated proliferative inhibition. This is concordant with the recent reports on the synergistic anti-cancer activity of combined CDK4/6 and mTOR targeting ²²⁹⁻²³¹.

In conclusion, our work supports that polypharmacology to target multiple kinase targets in combination with rapalog treatment may offer a distinct combinatorial benefit to TNBC patients that are otherwise resistant to mTOR-targeted therapeutics.

Acknowledgments

JH was financially supported by the China Scholarship Council.

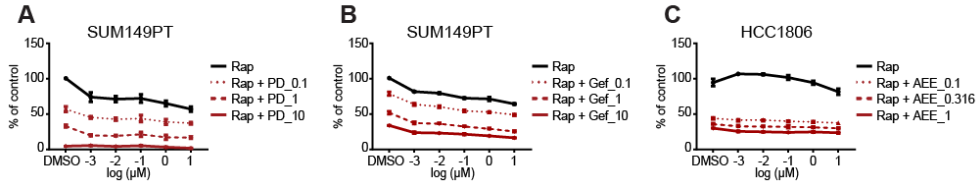
Funding

This work was supported by the European Research Council Advanced grant Triple-BC (grant no. 322737) and the Dutch Cancer Society project (grant nr 2011-5124). GvW was supported by the Dutch Scientific Council (NWO domain AES Veni 14410).

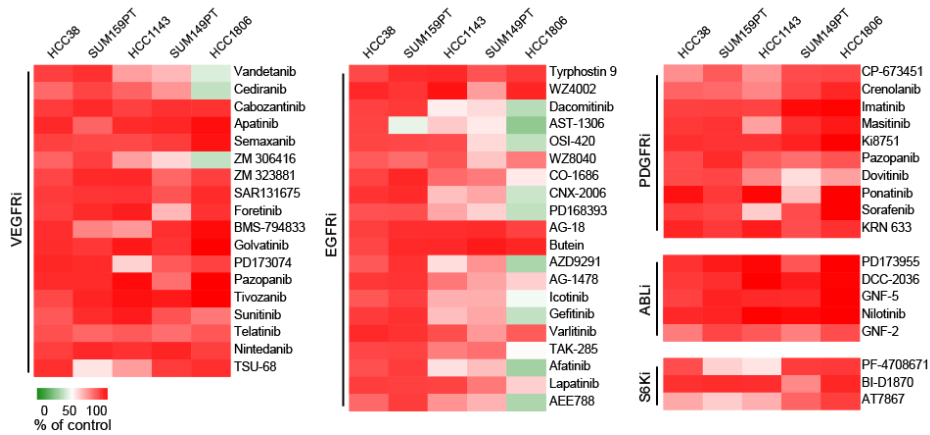
Author contributions

JH, YZ and BvdW conceived and designed the experiments. YZ and BvdW supervised the research. JH, RM, VvdN and YZ performed the experiments. JM and JF co-supervised the research. GvW performed ligand-based target prediction. JH, YZ and BvdW wrote the manuscript. All authors read, reviewed and approved the final manuscript.

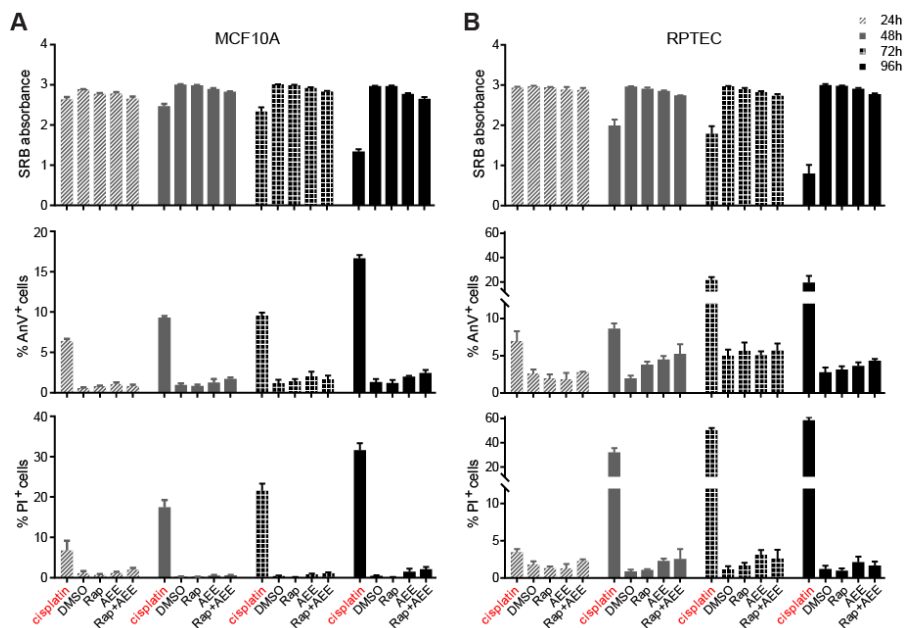
Supplementary material



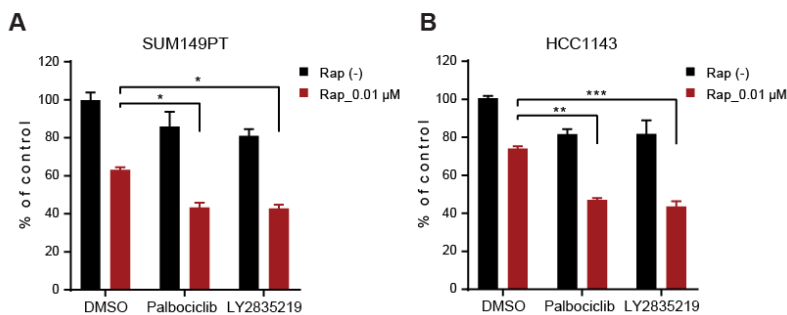
Suppl. Fig. S1 Effects of co-treatment with PD184352, gefitinib or AEE788 on rapamycin-mediated proliferative inhibition in TNBC cells. SUM149PT (a, b) and HCC1806 (c) cells were treated with Rap in dose range alone or combined with PD184352 (PD), gefitinib (Gef) or AEE788 (AEE) at indicated concentrations for 4 days, followed by SRB proliferation assay.



Suppl. Fig. S2 Proliferation response of rapalog-resistant TNBC cell lines towards VEGFR, EGFR, PDGFR, ABL and S6K inhibitors. TNBC cells were treated with KI at 1 μ M for 4 days, followed by SRB proliferation assay. Strong inhibitory effect on proliferation was indicated in green and weak in red.



Suppl. Fig. S3 Combinatorial effect of rapamycin and AEE788 on proliferation and cell death of MCF10A (a) and RPTEC (b) cells. Proliferative response (upper panel, SRB absorbance), early apoptosis (middle panel, AnV⁺) and late apoptosis/necrosis (bottom panel, PI⁺) of MCF10A and RPTEC cells, to Rap alone or combined with AEE788 respectively. Cisplatin (100 μ M) was used as positive control.



Suppl. Fig. S4 Combinatorial effect of rapamycin and inhibitors targeting CDK4/6-Cyclin D1 complexes on proliferation of rapalog-resistant SUM149PT (a) and HCC1143 (b) TNBC cells. Cells were treated Rap alone, or in combination with selective CDK4/6 inhibitor palbociclib or LY2835219 at 0.01 μ M for 4 days (two-way ANOVA * $p < 0.05$, ** $p < 0.01$, *** $p < 0.001$).

Suppl. Table S1 Molecular subtypes of TNBC cell lines.

basal-like 1 (BL1)	basal-like 2 (BL2)	mesenchymal (M)	mesenchymal stem-like (MSL)	luminal androgen receptor (LAR)	unclassified
HCC1937	HCC1806	BT549	Hs578T	MDA-MB-453	BT20
HCC1143	SUM149PT		SUM159PT	SUM185PE	SKBR7
HCC38	HCC70		MDA-MB-231		SUM52PE
MDA-MB-468			MDA-MB-436		SUM229PE
					SUM1315MO2

Suppl. Table S2 Node table in protein-protein interactions of AEE788 potential targets.

Id	Node	Degree	Betweenness	Id	Node	Degree	Betweenness
P00533	EGFR	391	178881.7	P46934	NEDD4	6	4332.63
P09619	PDGFRB	74	20524.36	P03372	ESR1	5	7738.14
P50613	CDK7	66	35914.58	P12931	SRC	5	3009.24
P23443	RPS6KB1	56	26521.88	P29353	SHC1	5	2745.16
P31751	AKT2	53	26567.47	P62993	GRB2	5	910.52
Q9UK32	RPS6KA6	38	19388.73	Q16543	CDC37	4	7079.36
P35968	VEGFR2	38	11501.12	P42224	STAT1	4	2445.99
P51812	RPS6KA3	37	14817.52	P05067	APP	4	2088.79
P42684	ABL2	36	12328.21	P46108	CRK	4	516.6
P49137	MAPKAPK2	32	12761.96	P19174	PLCG1	4	516.6
P35916	VEGFR3	11	2613.92	P16333	NCK1	4	516.6
P07900	HSP90AA1	9	14538.16	O94875	SORBS2	3	2467.85
P08238	HSP90AB1	9	14538.16	Q16539	MAPK14	3	1871.29
POCG48	UBC	8	16809.34	P27361	MAPK3	3	827.61
Q9HAZ1	CLK4	8	4077.61	P48740	MASP1	3	726.74
...				...			
...				...			
Q96HN2	AHCYL2	1	0	P08151	GLI1	1	0

Chapter 5

Integrative analysis of genomic amplification-dependent expression and loss-of-function screen identifies ASAP1 as a driver gene in triple-negative breast cancer progression

Jichao He, Ronan P. McLaughlin, Lambert van der Beek, Sander Canisius, Lodewyk Wessels,
John W. M. Martens, John A. Foekens, Yinghui Zhang, Bob van de Water

Manuscript in preparation

Abstract

The genetically heterogeneous triple-negative breast cancer (TNBC) continues to be an intractable disease, due to lack of effective targeted therapies. Gene amplification is a major event in tumorigenesis. Genes with amplification-dependent expression are being explored as therapeutic targets for cancer treatment. In this study, we have applied ADMIRE (Analytical Multi-scale Identification of Recurring Events) analysis and transcript quantification in the TNBC genome across 222 TNBC tumors (n = 118 TCGA and n = 104 Metabric) and identified 148 candidate genes with positive correlation in copy number gain (CNG) and gene expression. siRNA-based loss-of-function screen of the candidate genes has validated EGFR, MYC, ASAP1, IRF2BP2 and CCT5 genes as drivers promoting proliferation in different TNBC cells. MYC, ASAP1, IRF2BP2 and CCT5 display frequent CNG and concurrent expression over 2173 breast cancer tumors (cBioPortal dataset). More frequently are MYC and ASAP1 amplified in TNBC tumors (> 30%, n = 320). In particular, high expression of ASAP1, the ADP-ribosylation factor (Arf) GTPase-activating protein, is significantly related to poor metastatic relapse free survival of TNBC patients (n = 257, bc-GenExMiner). Furthermore, we have revealed that silencing of ASAP1 modulates numerous cytokine and apoptosis signaling components, such as IL1B, TRAF1, AIFM2 and MAP3K11 that are clinically relevant to survival outcomes of TNBC patients. ASAP1 has been reported to promote invasion and metastasis in various cancer cells. Our findings that ASAP1 is an amplification-dependent TNBC driver gene promoting TNBC cell proliferation, functioning upstream apoptosis components and correlating to clinical outcomes of TNBC patients, support ASAP1 as a potential actionable target for TNBC treatment.

Keywords

Recurrent copy number gain; Driver gene; Whole transcriptome sequencing; Triple-negative breast cancer; ASAP1

Background

Triple-negative breast cancer (TNBC) represents a particularly proliferative and aggressive subtype of breast cancer, associated with large size of tumors, high mitotic rate of tumor cells, high tumor grade and metastasis, causing poor prognosis and high mortality rate of patients¹⁰⁷. TNBC constitutes 15-20% of breast cancer, being clinically characterized by the lack of expression of estrogen receptor (ER), progesterone receptor (PR) and the absence of amplification of human epidermal growth factor receptor 2 (HER2), which are the known drivers of other breast cancer types²³². The absence of actionable targets defined in TNBC cells leads to clinical failure of targeted therapies in TNBC patients. Cytotoxic chemotherapy remains the conventional systemic treatment for TNBC patients, resulting in adverse effects and unfavorable outcomes^{77, 233}. Identification of actionable targets for TNBC treatment is a continuous effort.

Gene copy number alterations (CNAs) are a hallmark in the cancer genome⁴⁹. Gains or losses of gene copy are important somatic genomic aberrations contributing to tumorigenesis¹⁰⁶. Changes in gene copy number result in corresponding changes in expression of the affected genes, causing phenotypes²³⁴. Copy number gains (CNGs), increasing from the two DNA copies present in normal diploid genome, sometimes to several hundred copies (known as amplification), are observed to frequently occur on cancer driver genes^{235, 236}. Oncogenic driver genes with increase in DNA copy number and expression have been identified and explored as potential drug targets for targeted therapies in cancer²³⁷. For instance, the *HER2* gene, which is amplified in ~30% of primary breast cancers²³⁸, has been proven as an actionable target for trastuzumab antibody targeted therapy and lapatinib inhibitor targeted therapy treating patients with HER2-amplified breast cancer²³⁹. Therefore, identification of CNG-driven genes and their amplification-dependent overexpression provides opportunities for discovering potential cancer driver genes as therapeutic targets for therapy-refractory cancer.

A number of studies have demonstrated the genomic heterogeneity in TNBCs, being dominated by substantial mutational burdens, including CNAs and genomic rearrangements^{106, 240}. CNA genomic profiling based on separate TNBC sample groups have reported the TNBC-related recurrent CNAs on various chromosome regions²⁴¹. Yet, integrative analysis of CNG frequency and CNG-driven gene expression in the TNBC genome is limited.

In this study, we applied the ADMIRE (Analytical Multi-scale Identification of Recurring Events) algorithm to identify candidate driver genes that are frequently amplified by recurrent CNGs, in correlation with their RNA expression levels, in 222 triple-negative tumors from TCGA (n=118)¹⁹ and Metabric (n=104)²³² datasets. As a result, 148 genes were identified, with a significant and positive correlation in their gene amplification and expression. These amplification-driven genes were subsequently validated by loss-of-function screen for their biological function in TNBC cell proliferation,

followed by assessment of their expression and amplification in broad breast cancer cell lines and tumors, and evaluation of their clinical relevance using multiple large public breast cancer datasets^{242,243}. Consequently, we characterized the known oncogenes MYC and EGFR and the novel candidate genes ASAP1, IRF2BP2 and CCT5 as cancer drivers in promoting proliferation of TNBC cells. MYC and ASAP1 were observed to be more frequently amplified and highly expressed in TNBC than non-TNBC tumors. Specifically, high expression of ASAP1, an ADP-ribosylation factor (Arf) GTPase-activation protein regulating cell motility and invasiveness²⁴⁴, is significantly relevant to poor metastatic relapse-free survival (MRFS) of patients with TNBC tumors, not non-TNBC tumors. Transcriptome analysis further revealed that ASAP1 regulates various cytokine and apoptosis signaling components that are significantly associated with TNBC prognosis. Our work discovered ASAP1 as an amplification-dependent gene driving TNBC proliferation, survival and progression, supporting the potentiality of ASAP1 as a therapeutic target for the treatment of TNBC.

Methods

Cell culture

Human TNBC cell lines BT549, Hs578T and SUM149PT were cultured in RPMI-1640 medium supplemented with 10% fetal bovine serum, 25 U/mL penicillin and 25 µg/mL streptomycin in a humidified incubator at 37°C with 5% CO₂.

Selection of amplification-dependent candidate driver genes in TNBC genome by integrated ADMIRE copy number region analysis and transcript expression quantification

ADMIRE analysis²⁴⁵ was performed to detect genomic regions with recurrent copy number gains across 222 triple-negative tumors (n=118 from TCGA; n=104 from Metabric). Segmented copy number profiles for both TCGA¹⁹ and the discovery set of Metabric²³² were obtained and used as input for the ADMIRE analysis. ADMIRE was configured to control its false discovery rate at 0.01. The recurrently altered copy number regions identified by ADMIRE were filtered in order to enrich regions most likely to harbor driver genes. Importantly, ADMIRE regions may be nested within larger regions, where the higher nesting levels correspond to more focal and more frequently altered regions. Our filtering only kept the regions detected at the highest nesting level. In addition, regions were kept only if they spanned at least one, but no more than 100 genes. Next, the genes contained in those regions were identified and selected as candidate driver genes, if their mRNA expression profile showed a positive correlation with their copy number. For this, the RNA-Seq data for TCGA analyzed using RSEM transcript quantification and the microarray expression data for Metabric were applied. The correlation was tested using Spearman correlation, where the Log-ratio copy number estimates were correlated with

the expression values. Correction for multiple testing was performed by controlling the false discovery rate at 0.1. The ADMIRE analysis and the subsequent filtering steps were performed separately for TCGA and Metabric, after which the resulting gene lists were merged.

siRNA-mediated loss-of-function screen

The primary screen was carried out by use of siGENOME Human SMARTpool siRNAs (GE Dharmacon, Lafayette, CO, USA) targeting 148 ADMIRE candidate driver genes. In the validation screen, SMARTpool siRNA and single siRNA₁, ₂, ₃ and ₄ that comprise the SMARTpool mix were used to validate each candidate hit. Cells were seeded overnight in 96-well plate at an optimized density for BT549 (8,000 cells/96-well), Hs578T (8,000 cells/96-well) and SUM149PT (10,000 cells/96-well), and transfected with 50 nM siRNA by transfection reagent INTERFERin (Polyplus-Transfection SA, Illkirch-Graffenstaden, France) according to the manufacturer's instructions. We used a pool of 720 kinase siRNAs at stock concentration of 1 μ M in our laboratory as a negative control (siCtrl), this has no significant effect on expression of any single kinase genes; siRNA against KIF11 was used as positive control. The medium was refreshed 24 h post-transfection and TNBC cells were transfected for 2 days and proliferated for 4 days under indicated condition. SRB colorimetric assay was used as read-out for cell proliferation.

SRB proliferation assay

A sulforhodamine B (SRB) colorimetric assay was used to measure total amount of proteins indicative of cell proliferation, as previously described¹²⁵.

Real time RT-qPCR assay

RNA was isolated from TNBC cells, which were transfected with corresponding siRNA for 72 h, using RNeasy (Qiagen). cDNA was generated from 400 ng total RNA, using RNeasy Plus Kit from Qiagen. Real-time RT-qPCR was performed in triplicate, using the SYBRGreen PCR MasterMix (Applied Biosystems) on a 7900HT fast real-time PCR system (Applied Biosystems). The primer sequences used were: forward *CAGCCGGCGCTTCCC*, reverse *ATCAGAAAACGACCGGGACC* (human ASAP1); forward *CTGGTAAAGTGGATATTGTTGCCAT*, reverse *TGGAATCATATTGGAACATGTAACC* (human GAPDH). Relative mRNA levels after correction for GAPDH control mRNA were expressed using the $2^{-\Delta\Delta CT}$ method.

DNA copy number alteration and mRNA expression profiling of candidate genes in breast cancer cell lines and tumors

DNA copy number data of candidate genes in 20 TNBC cell lines were obtained from online resources²⁴⁶. Log₂-based RNA expression profiles of candidate genes in 52 breast cancer cell lines was retrieved from our own established RNA-Seq data. Copy number

alterations (CNAs) and mRNA expression of candidate hits in 2173 breast tumors were obtained from dataset “METABRIC, Nature 2012 & Nat Commun 2016” in cBioPortal (<http://www.cbioportal.org/>), an open-access resource for interactively exploring multidimensional cancer genomics ²⁴³ and the largest dataset with available DNA copy number (n = 2173) and mRNA expression (n = 1904) profiles. The 2173 breast tumor samples were filtrated by the immunohistochemistry (IHC) status of estrogen receptor (ER), progesterone receptor (PR), and human epidermal growth factor receptor 2 (HER2), resulting in 320 triple-negative tumors.

Human whole transcriptome analysis of ASAP1 silencing effect

TNBC cells were seeded into 96-well plate and transfected with optimal SMARTpool siRNA targeting ASAP1 (siASAP1), and siRNA control (siCtrl), as described above. The experiment was performed in biological triplicate. 72 h later, cells were washed with PBS and lysed in 80 μ l 1 \times BioSpyder lysis buffer. Lysates were frozen at - 80 °C and shipped to BioSpyder technologies on dry ice for human whole transcriptome targeted RNA sequencing TempO-Seq analysis. Expression data for 21,111 transcripts were generated (BioSpyder Technologies, Inc., Carlsbad, CA, United States). Normalization and differential expression analysis were performed using DESeq2 package. Specifically, each siASAP1 condition was paired with the corresponding control siCtrl and the counts for each sample were normalized using the DESeq2 estimateSizeFactors function. Differential expression of each treatment relative to its respective control was measured using the Wald test. With baseMean of counts < 10 filtered, genes that were regulated by siASAP1 with significance (p value < 0.05 and absolute Log₂ FC > 1) were considered significantly differentially expressed genes (DEGs).

Gene functional enrichment analysis of ASAP1-regulated genes

The DEGs, up- or down-regulated by silencing ASAP1, were uploaded to Metascape ¹⁶⁷, an oriented resource combining functional enrichment, interactome analysis, gene annotation and membership research to leverage over 40 independent knowledgebases within one integrated portal (<http://metascape.org>). Pathway and process enrichment analysis was carried out with ontology sources of KEGG pathway, GO Biological Processes, Reactome Gene Sets, Canonical Pathways and CORUM. All genes in the genome were used as the enrichment background. Terms with p-value < 0.01, a minimum count of 3, and an enrichment factor (a ratio between the observed counts and the counts expected by chance) > 1.5 were collected and grouped into clusters based on their membership similarities. To further capture the relationship between the terms of pathways and processes, network of enriched terms were visualized using Cytoscape, where each node represents an enriched term and is colored by its cluster ID. Furthermore, if network contains between 3 and 500 proteins, protein-protein interaction enrichment analysis was

carried out with BioGrid, InWeb_IM and OmniPath to identify densely connected network components, presented in MCODE (Molecular Complex Detection) network node.

Assessment of clinical relevance of candidate genes to survival prognosis of breast cancer patients

The functionally validated candidate driver genes were further evaluated using Kaplan-Meier analysis for their relation to overall survival (OS) of 1981 breast cancer patients according to their gene expression²⁴³. Microarray DNA expression results from BrCa Gene-Expression Miner (bc-GenExMiner) were used to classify prognostic association of ASAP1 expression levels with metastatic relapse free survival (MRFS) of 257 TNBC patients (n=257) and ER+ BC patients (n=2519) using “optimal” splitting criterion²⁴². The ASAP1-regulated DEGs involved in cytokine, lipid metabolism and apoptosis pathways were assessed for their relation to relapse-free survival of TNBC patients by Kaplan-Meier plotter using “Auto select best cutoff”²⁴⁷. Mean expression of DEGs was used to assess their prognostic significance.

Statistical analysis

Pearson correlation analysis was performed using GraphPad Prism 7. Statistical analysis of all experimental data was performed using two-way ANOVA (* p < 0.05, ** p < 0.01, *** p < 0.001). Data were expressed as mean ± SEM. Significance was set at p < 0.05. The hierarchical clustering in heatmap was performed using CRAN pheatmap package in RStudio (version 0.99.887).

Results

ADMIRE analysis of TNBC genomes identifies TNBC candidate driver genes with recurrent copy number gain and correlated expression

Recurrent CNAs have been recognized as the result of natural selection in tumor evolution, and hence the recurrently altered regions are likely to harbor cancer driver genes²⁴⁸. In order to identify candidate driver genes for TNBC, we applied ADMIRE, a robust algorithm for the discovery of broad and focal recurring events²⁴⁵, to detect genomic regions with frequent CNAs in a set of TNBC tumors (n = 118 for TCGA; n = 104 for Metabric). Aggregated DNA copy number profiles (Figure 1A) assisted in pinpointing recurrently altered regions (Figure 1B). Genes contained in the focal regions were further assessed with copy number and expression correlation analysis, as exemplified for the proto-oncogene MYC and the RNA genes CASC8 (Cancer Susceptibility 8) and PVT1 (MYC activator) (Figure 1C). Genes showing positive correlation in mRNA expression levels and copy numbers were filtered out as candidate drivers (Figure 1D). The ADMIRE analysis and the subsequent filtering steps were performed separately for TCGA and Metabric cohorts. Subsequently, 148 genes were selected as candidate driver genes for TNBC (Additional file

1: Table S1). Next, functional enrichment analysis displayed the significant implication of

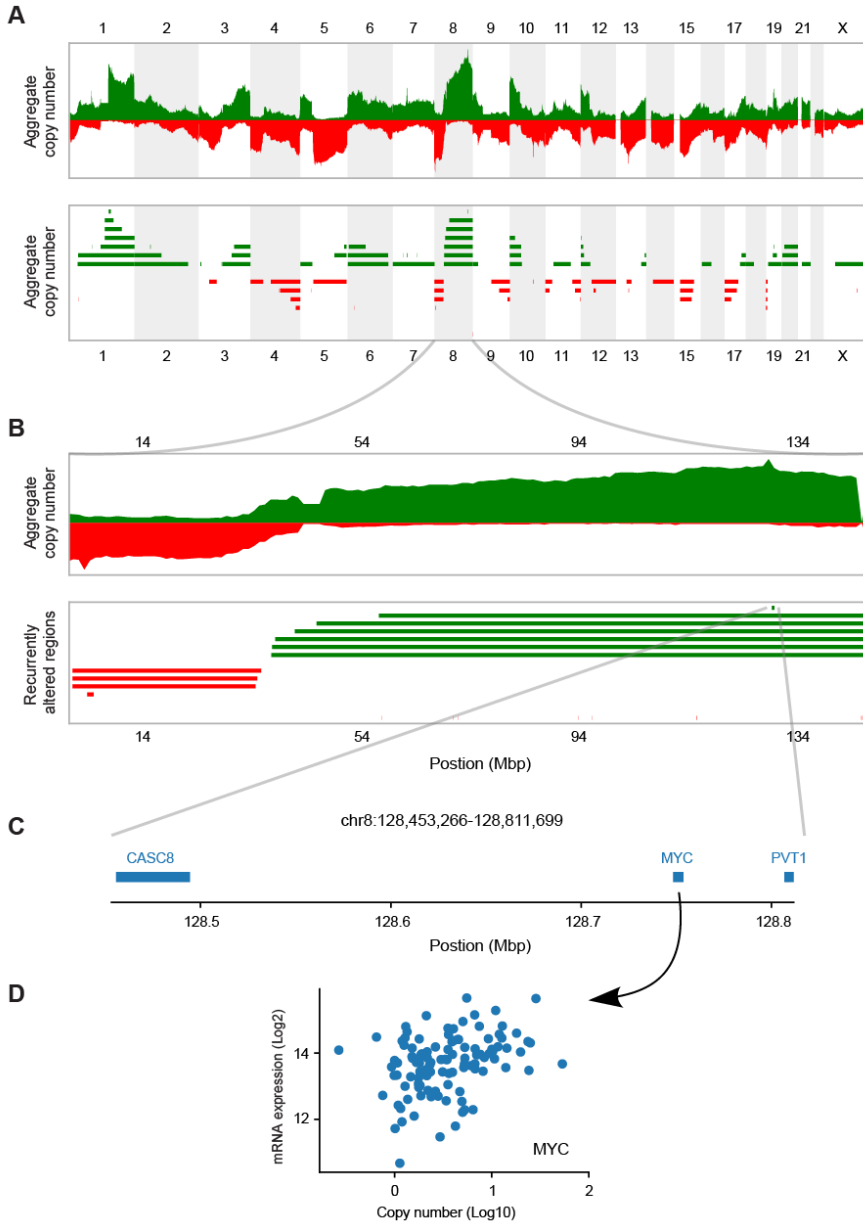


Figure 1. Schematic selection of candidate driver genes with increases in copy number and expression in TNBC genome. (A) Discovery of genomic regions with recurrent copy number alterations using ADMIRE analysis. The top panel shows the aggregate copy number profile across 222 triple-negative breast tumors (n = 118 for TCGA; n = 104 for Metabric). The bottom panel shows the significant recurrent copy number regions, with gains in green and losses in red. **(B)** Zoomed in fragment of panel A, focusing on chromosome 8. The bottom panel reveals the small focal recurrent copy number gain on 8q for further analysis. **(C)** The genes contained in the focal region identified in panel B. **(D)** Scatterplot exemplifying the positive correlation of MYC gene expression with its copy number in TNBC patients.

the 148 genes in 18 KEGG pathways (Additional file 2: Figure S1). The 148 gene set was enriched in cancer-related pathways, including Central carbon metabolism in cancer, Proteoglycans in cancer, Pathways in cancer, Melanoma, Prostate cancer and Endometrial cancer. Moreover, these candidate drivers were implicated in various oncogenic signaling pathways that control cell growth, survival and motility, such as ErbB, PI3K-Akt, Ras, MAPK and Wnt pathways. Altogether, our ADMIRE genomics approach collected 148 candidate TNBC drivers that are frequently amplified by recurrent CNGs in the TNBC genome and significantly enriched in pathways that fuel cancer progression.

Loss-of-function screen validates the TNBC candidate driver genes in TNBC cell proliferation

As a first step, we assessed the biological function of the 148 candidate genes in control of TNBC cell proliferation by siRNA-mediated loss of function screen in two TNBC cell lines, mesenchymal-like BT549 and basal-like SUM149T. High reproducibility was achieved for the duplicate screens in BT549 ($r = 0.9212$) and SUM149PT ($r = 0.9127$) (Figure 2A). Genes whose silencing controlled proliferation less than 60% were considered as candidate hits with significance (Figure 2B). Consequently, 41 primary hits were screened for BT549 and 20 for SUM149PT cell line (Figure 2B-C). In total, 46 primary hits were selected, of which 15 were common (Figure 2D; Additional file 3: Table S2).

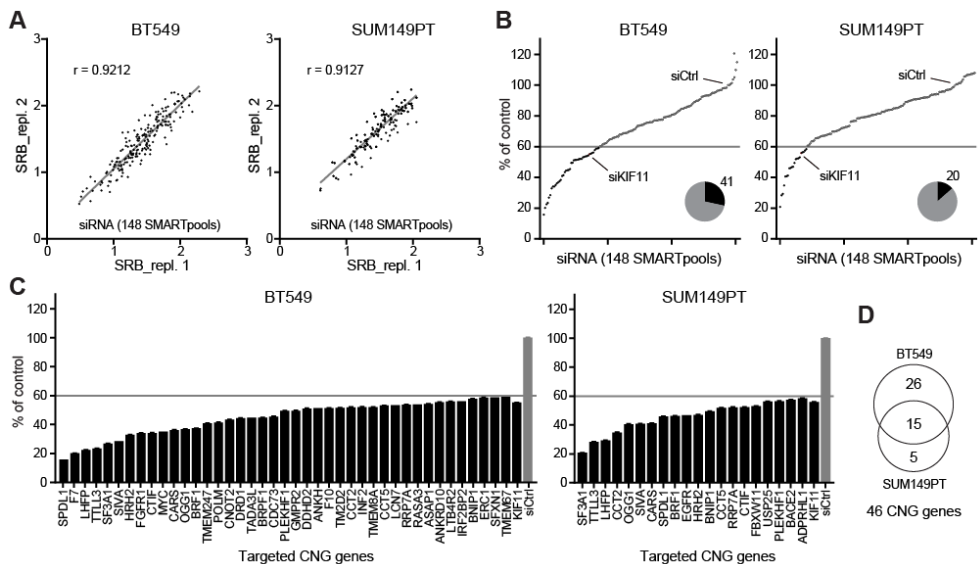


Figure 2. siRNA-mediated loss-of-function screen of candidate driver genes in TNBC cells. (A) Replicate siRNA screens of candidate driver genes in TNBC cell lines BT549 and SUM149T. siRNA silencing effect of candidate gene on cell proliferation was assessed 96 h after transfection and presented with sulforhodamine B (SRB) colorimetric raw values. **(B)** Normalized percentage of proliferation control by siRNA silencing. The number of genes (black) whose silencing led to >40% proliferative inhibition was indicated in the pie chart, as primary hits.

(C) Ranking and listing of the primary hits significantly controlling proliferation of BT549 and SUM149PT TNBC cell lines. siRNA targeting KIF11, positive functional control; siCtrl, non-targeting siRNA control. siRNA silencing effect on proliferation was relative to siCtrl. Error bars indicate variation of screen replicates. **(D)** Overlap primary hits in BT549 and SUM149PT TNBC cell lines.

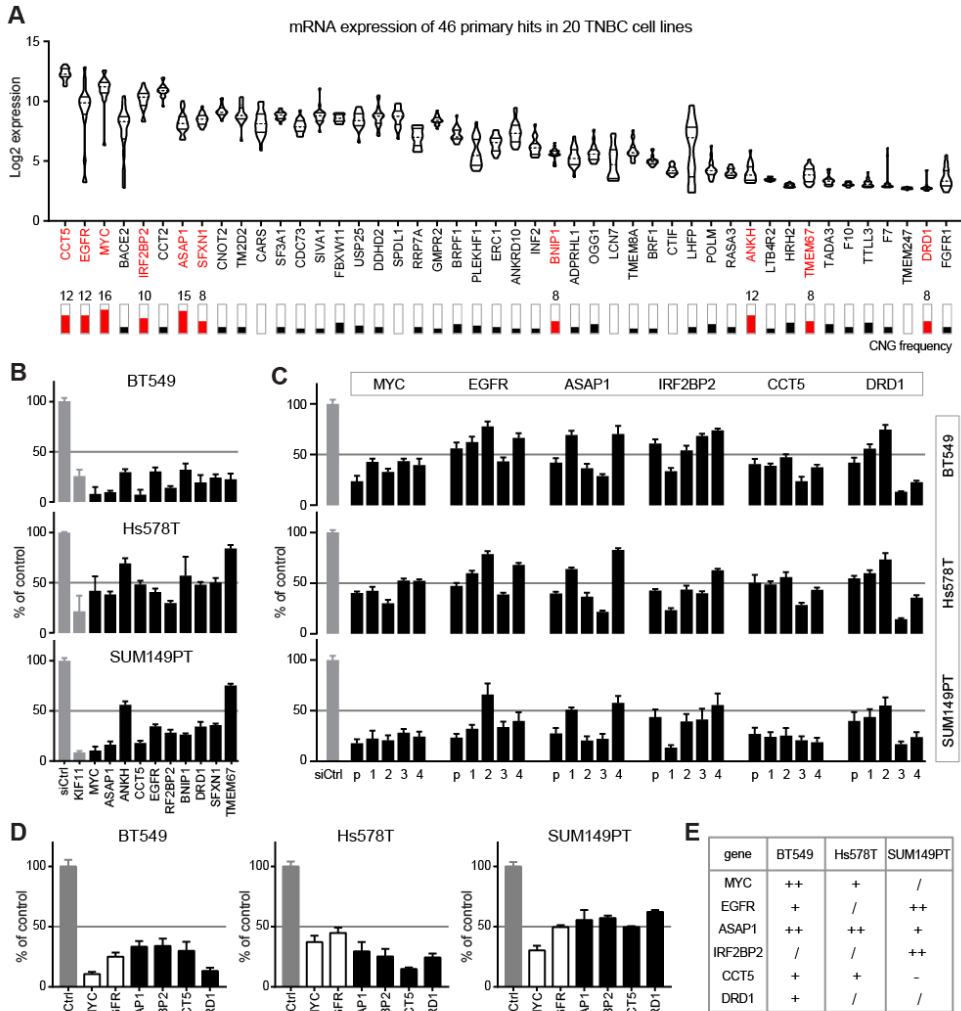


Figure 3. Validation of candidate driver genes with concurrent copy number gain (CNG) and overexpression in TNBC cells. (A) mRNA expression of 46 primary hits in 20 TNBC cell lines. Violin plot indicates Log₂ mRNA expression level of 46 primary hits in 20 TNBC cell lines retrieved from RNA-Seq analysis. Bars indicate CNG frequency of the hits in 20 TNBC cell lines. Genes with frequent CNG in $\geq 8/20$ TNBC cell lines were marked in red. **(B)** siRNA validation of primary candidate hits with high frequent CNG in BT549, Hs578T and SUM149PT TNBC cell lines. SMARTpool siRNAs were used to target each hit. KIF11 was taken as positive control. **(C)** siRNA deconvolution validation of six candidate driver hits. The effects of SMARTpool (p) siRNA and single siRNA₁, ₂, ₃ and ₄ on hits were compared for their proliferation control (%) in the TNBC cell lines. **(D)** Percentage of control proliferation (%) by optimized SMARTpool siRNAs targeting the six candidate hits. **(E)** CNA of the six

candidate driver genes in TNBC cell panel. “++”, high CNG; “+”, CNG; “/”, no copy number alteration; “-”, copy number loss.

Next, we examined the CNG frequency of the 46 primary hits in 20 TNBC cell lines, representative for diverse molecular subtypes of TNBC. Ten candidate hits were found with CNG frequency across ≥ 8 TNBC cell lines (Figure 3A, lower panel). The CNG recurrence for MYC was found in 16/20 of TNBC cell lines, ASAP1 in 15/20, ANKH, CCT5 and EGFR in 12/20, IRF2BP2 in 10/20, BNIP1, DRD1, SFXN1 and TMEM67 in 8/20, respectively. We also evaluated the mRNA expression level of the 46 primary hits in the 20 TNBC cell line panel in our established RNA-Seq data (Figure 3A, upper panel). Given the nature of heterogeneity of TNBC, the correlation of expression and copy number of the primary hits varied among cell lines.

To further validate the 10 candidate hits for their function in proliferation, we performed siRNA silencing in three TNBC cell lines, BT549, SUM149T and one more mesenchymal-like cell line Hs578T. Silencing of 6 hits, ASAP1, CCT5, IRF2BP2, DRD1 and two known oncogenes MYC and EGFR, potently inhibited proliferation ($> 50\%$) in all three cell lines (Figure 3B), suggesting their driving role in TNBC cell proliferation. Deconvolution siRNA screen confirmed the effect of single siRNAs ($\geq 2/4$) on the proliferation-driving hits, mostly achieving $> 50\%$ of proliferation inhibition, ruling out the off-targeting effect of pooled siRNAs (Figure 3C). The optimized pooled siRNA silencing further validated the function of the driver hits in proliferation control ($> 50\%$) (Figure 3D). Of note, the inhibitory effects on cell proliferation by silencing these six hits were, in general, concordant with CNA status in these cell lines (Figure 3E).

Collectively, our RNAi-based functional screen validated the ADMIRE-identified candidate driver genes and defined the role of MYC, EGFR, ASAP1, IRF2BP2, CCT5 and DRD1 in controlling proliferation of TNBC cells.

Frequent amplification of ASAP1 in TNBC is significantly relevant to poor clinical outcome

We next sought to address the correlation between CNA frequencies and expression levels of MYC, EGFR, ASAP1, IRF2BP2, CCT5 and DRD1 in broad breast cancer cell lines and breast tumors and the clinical relevance of the genes to patients with breast cancer. RNA-Seq analyses of the transcriptome from our 52 BC cell lines demonstrated that the Log2-based mRNA expression levels of MYC, EGFR, ASAP1 and CCT5 were higher in TNBC than non-TNBC cell lines (Additional file 4: Table S3), while similar high IRF2BP2 and low DRD1 were expressed in both cell types (Figure 4A). The difference of EGFR expression in TNBC and non-TNBC cells was of significance. Next, we obtained Z score-based mRNA expression data for the hits in 1904 breast cancer (BC) tumors from cBioPortal database^{232, 243, 249}. MYC, EGFR, ASAP1 and IRF2BP2 were highly expressed in TNBC, compared to non-TNBC

tumors (Figure 4B). CCT5 expression was found lower in TNBC than non-TNBC breast

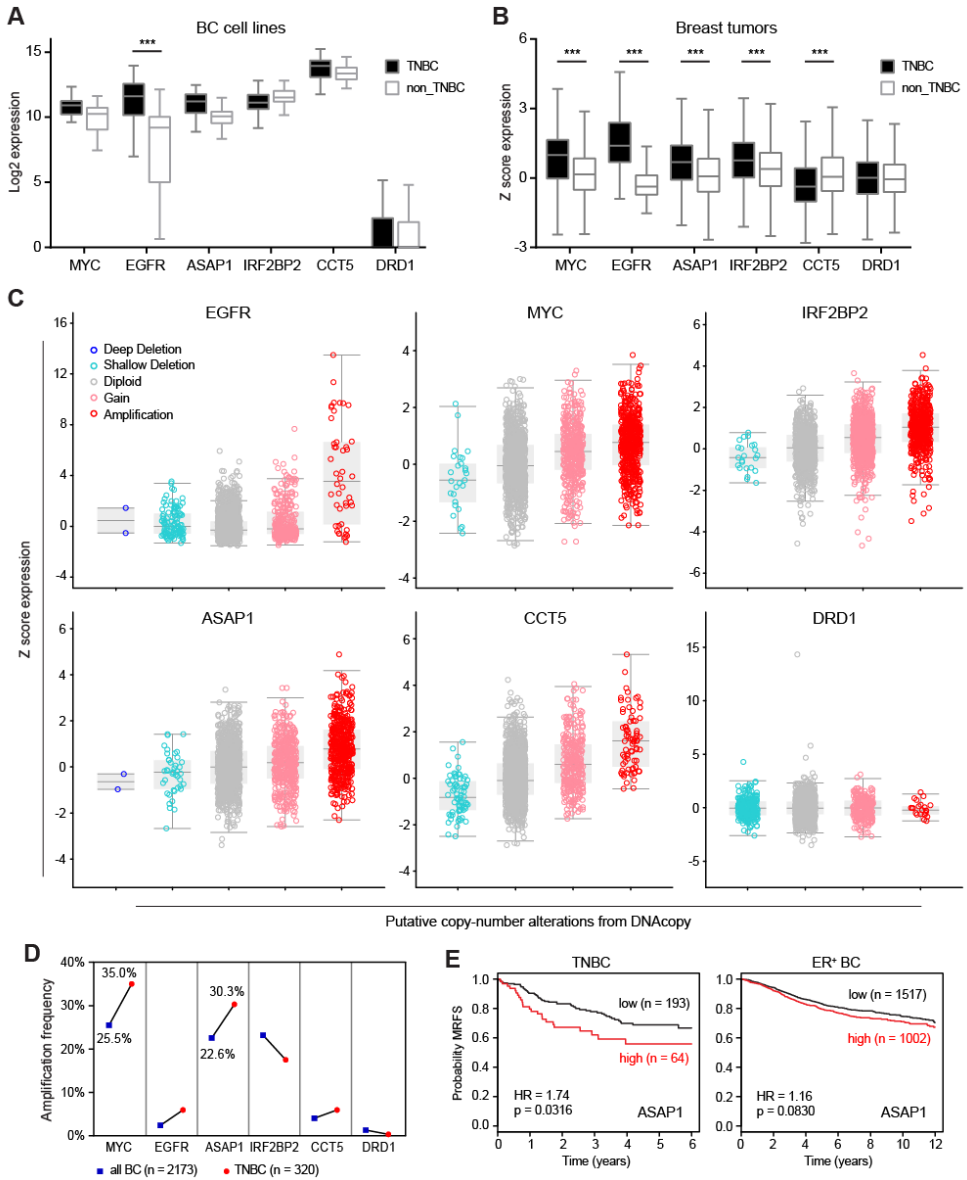


Figure 4. ASAP1 amplification and overexpression in TNBC in association with poor clinical outcome. (A) Log₂-based mRNA expression of the six candidate hits in 52 breast cancer (BC) cell lines. Log₂ values were obtained from established RNA-Seq data (two-way ANOVA *** $p < 0.001$). **(B)** Z score-based mRNA expression of the hits in 1904 BC tumors. Data were retrieved from the dataset “METABRIC, Nature 2012 & Nat Commun 2016” in cBioPortal dataset. **(C)** Correlation between CNA and gene expression of the candidate hits in the cohort of 1904 BC tumors. Different copy-number amplifications (shallow deletion, diploid, gain, amplification) are presented per gene. **(D)** Amplification frequency of the candidate hits in the cohort of 2173 BC tumors. Data were retrieved from the dataset “METABRIC, Nature 2012 & Nat Commun 2016” in cBioPortal dataset. **(E)** Metastatic relapse-

free survival (MRFS) Kaplan-Meier (KM) curve of ASAP1 in TNBC (n = 257) and ER⁺ BC (n = 2519) cohorts analyzed by bc-GenExMiner v4.2.

tumors, and DRD1 showed no significant difference. We further illuminated the correlation between CNAs and expression levels of the genes in the cohort of 1904 BC tumors. While CNA events in deep or shallow depletion rarely or less occurred, EGFR, MYC, IRF2BP2, ASAP1 and CCT5 (except for DRD1) often underwent copy gain and amplification, acquiring CNA-driven expression in the breast tumors (Figure 4C). Moreover, MYC, ASAP1 and IRF2BP2 were amplified in > 20% of all 2173 BC tumors (Figure 4D). Particularly, MYC and ASAP1 amplifications emerged more frequently in TNBC tumors (> 30%), suggesting TNBC subtype-related MYC and ASAP1 amplifications. Prognostic analysis demonstrated the association of the CNA-driven hits with overall survival of the cohort of 1981 BC patients^{232, 249}, indicating the significant implication of MYC and ASAP1 in poor disease outcomes (Additional file 5: Figure S2). More specifically, high ASAP1 expression was revealed to be related to worse MRFS of patients with TNBC (n=257), but not ER⁺ BC (n=2519) (Figure 4E), as assessed in the cohorts of BC patients²⁴². Together, we characterized MYC and ASAP1 as CNA-driven genes with frequent amplification and concurrent high expression in BC tumors. The CNA-driven amplification and expression of ASAP1 exhibited significant clinical impact particularly on TNBC progression.

Transcriptomic analysis of the impact of ASAP1 depletion on gene expression in TNBC cells

Amplification or deletion of a gene copy may affect the expression of genes located outside the amplified/deleted region itself via indirect mechanisms^{250, 251}. The ASAP1 gene, located at chromosome 8q24.1, encodes an Arf GTPase-activating protein (GAP) that induces hydrolysis of GTP bound to Arf proteins. ASAP1 has been reported to be involved in signal transduction, membrane trafficking and cytoskeleton remodeling²⁵² and promote proliferative, invasive and metastatic phenotypes of various cancer cells^{244, 253}. Whether CNA-driven ASAP1 amplification and overexpression influence gene expression at a genome-wide level in cancer cells is not addressed. To this end, we performed TempO-Seq-based targeted whole genome RNA sequencing in the three TNBC cell lines BT549, Hs578T and SUM149PT that harbor ASAP1 amplification and high expression (Figure 3E). The cells were transfected with siRNA targeting ASAP1 (siASAP1) or non-targeting siCtrl in biological triplicate, respectively. The transcriptome TempO-Seq assays were run at a read depth of 6.8M per sample (Additional file 6: Figure S3A), achieving reproducibility with Pearson r values over 0.95 (Additional file 6: Figure S3B). Principal components analysis (PCA) of global changes in gene expression clustered various gene expression patterns across cell lines and transfections (Additional file 6: Figure S3C). Using DESeq2 package in R, the Log₂ normalized transcriptome profiles displayed the differential effects of ASAP1

depletion on gene expression in the TNBC cells (Figure 5A). Silencing of ASAP1 by siASAP1 decreased > 45% of ASAP1 mRNA levels in the TNBC cells (Figure 5B, left panel), warranting the effective knockdown of ASAP1 itself (Log₂ FC -0.7 to -1.5) in the TempO-Seq transcriptome panels (Figure 5B, right panel). Genes with 2-fold changes (absolute Log₂ FC ≥ 1) in down- or up-regulation (p-value < 0.05) were selected in BT549 (311 down / 495 up), Hs578T (133 down / 117 up) and SUM149PT (500 down / 401 up) cells, respectively (Figure 5C). Venn diagrams extracted differentially expressed genes (DEGs) that were significantly down- or up-regulated by ASAP1 depletion in the TNBC cell lines (Figure 5D; Additional file 7: Table S4). Consequently, 95 DEGs were downregulated, and 79 DEGs upregulated in ≥ 2/3 of the TNBC cell lines, in total 174 DEGs, which were considered as common DEGs that were susceptible to the depletion of the amplification-dependent ASAP1.

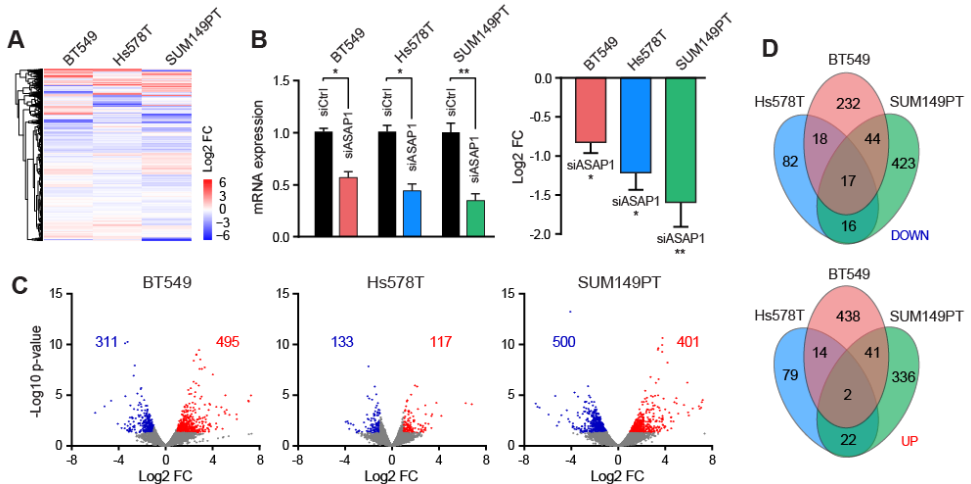


Figure 5. Targeted whole transcriptome analysis of ASAP1 depletion-induced transcription reprogramming in TNBC cells. (A) Transcriptome expression profiling in BT549, Hs578T and SUM149PT TNBC cells after siRNA-mediated depletion of ASAP1 (siASAP1). Log₂ fold change (Log₂ FC), siASAP1 versus siCtrl. (B) Targeting effect of siASAP1 on ASAP1 gene expression. Left panel, knockdown efficiency assessment by RT-qPCR (two-way ANOVA * $p < 0.05$, ** $p < 0.01$). TNBC cells were transfected with optimized SMARTpool siRNAs for 72 h. GAPDH was used as internal reference. Right panel, Log₂ FC of ASAP1 upon knockdown. (C) Volcano plot of differentially expressed genes (DEGs) in ASAP1-depleted BT549, Hs578T and SUM149PT cells. The red and blue dots indicate down- and up-regulated DEGs, respectively, with p-value < 0.05 and absolute Log₂ FC > 1. (D) Venn diagram of down- and up-regulated DEGs in BT549, Hs578T and SUM149PT TNBC cell lines. Upper panel, down-regulated DEGs; lower panel, upregulated DEGs. Common DEGs denote DEGs popping-up in at least two cell lines.

ASAP1 regulates cytokine and apoptosis signaling components that are associated with TNBC prognosis

Next, to evaluate the biological functions of 174 common DEGs that were susceptible to ASAP1 depletion, we conducted Metascape Pathway and Process Enrichment Analysis integrating the gene ontology sources, including GO Biological Process, KEGG pathway,

Reactome Gene Sets, Canonical Pathways and CORUM ¹⁶⁷. Top 20 clusters were defined with their representative enriched terms (Figure 6A, left; Additional file 8: Table S5), including cytokine signaling pathways (cytokine signaling in immune system, response to interleukin-1, TNF-signaling pathway and regulation of inflammatory response), metabolic processes (regulation of lipid metabolic process and regulation of sulfur metabolic process), apoptosis signaling pathways (regulation of apoptosis signaling pathway and positive regulation of cell death), MAPK pathways (regulation of p38 MAPK cascade and MAPK signaling pathway), cell cycle arrest and P53 downstream pathway. Furthermore, network enrichment captured the interactions between the 20 clusters, as visualized using Cytoscape (Figure 6A, right). Strikingly, among the 20 clusters, the cytokine signaling in immune system, regulation of lipid metabolic process and regulation of apoptotic signaling pathway were most significantly enriched. Protein-protein interaction clustering algorithm identified neighborhoods within the networks where the ASAP1-regulated genes were densely connected, such as ANXA1, C3, CXCL1, CXCL2 and CXCL8 node (involved in immune response), IMPDH1, PSMC4 and RAN node (involved in nucleotide and protein metabolism), and APEX1, MCM6 and RBL2 node (involved in cell cycle G1/S phase transition) (Figure 6B). These results revealed the novel and essential biological functions of ASAP1 in multiple molecular pathways.

Around 45% of ASAP1-regulated genes (78/174) were involved in cytokine signaling pathways (Additional file 9: Table S6), being interactive in cytokine signaling in immune system, response to interleukin-1, TNF-signaling pathway and regulation of inflammatory response. In regulation of apoptosis signaling and cell death pathways, 33 genes were modulated by ASAP1 depletion. Unsupervised hierarchical heatmap classified the 21 positive and 20 negative regulators in cytokine signaling pathways, 5 positive and 10 negative regulators in lipid metabolism pathway, and 8 positive and 9 negative regulators in apoptosis signaling pathways (Figure 6C), in the BT549, Hs578T and SUM149PT TNBC cell lines. As cytokine signaling pathways, e.g. TNF-signaling pathway, mediate extrinsic/intrinsic apoptosis ²⁵⁴, crosstalk might exist in the ASAP1-regulated cytokine and apoptosis signaling pathways. Indeed, among 33 ASAP1-regulated apoptosis genes, 23 genes (~70%) were interactive in cytokine signaling pathways (Additional file 9: Table S6), further stressing the implication of ASAP1 as a driver gene in cell survival and growth. Crosstalk was also observed between ASAP1-regulated genes in lipid metabolic process (17/31, ~50%) and cytokine signaling (Additional file 9: Table S6). To explore the association between these ASAP1-regulated cytokine, lipid metabolism and apoptosis genes and the survival of patients with TNBC, we performed Kaplan-Meier (KM) survival analysis using KM plotter ²⁴⁷. The results exhibited that, based on the mean expression of the selected genes in TNBC tumors, a low expression level of the negative regulators, which were downregulated under ASAP1 depletion, predicted longer relapse-free survival of TNBC patients with statistical significance (logrank $p = 0.00015$, HR = 2.76) (Figure 6D).

In contrast, low expression of positive regulators, which were upregulated by ASAP1 depletion, implied significantly worse prognosis (logrank $p = 0.0092$, HR = 0.47).

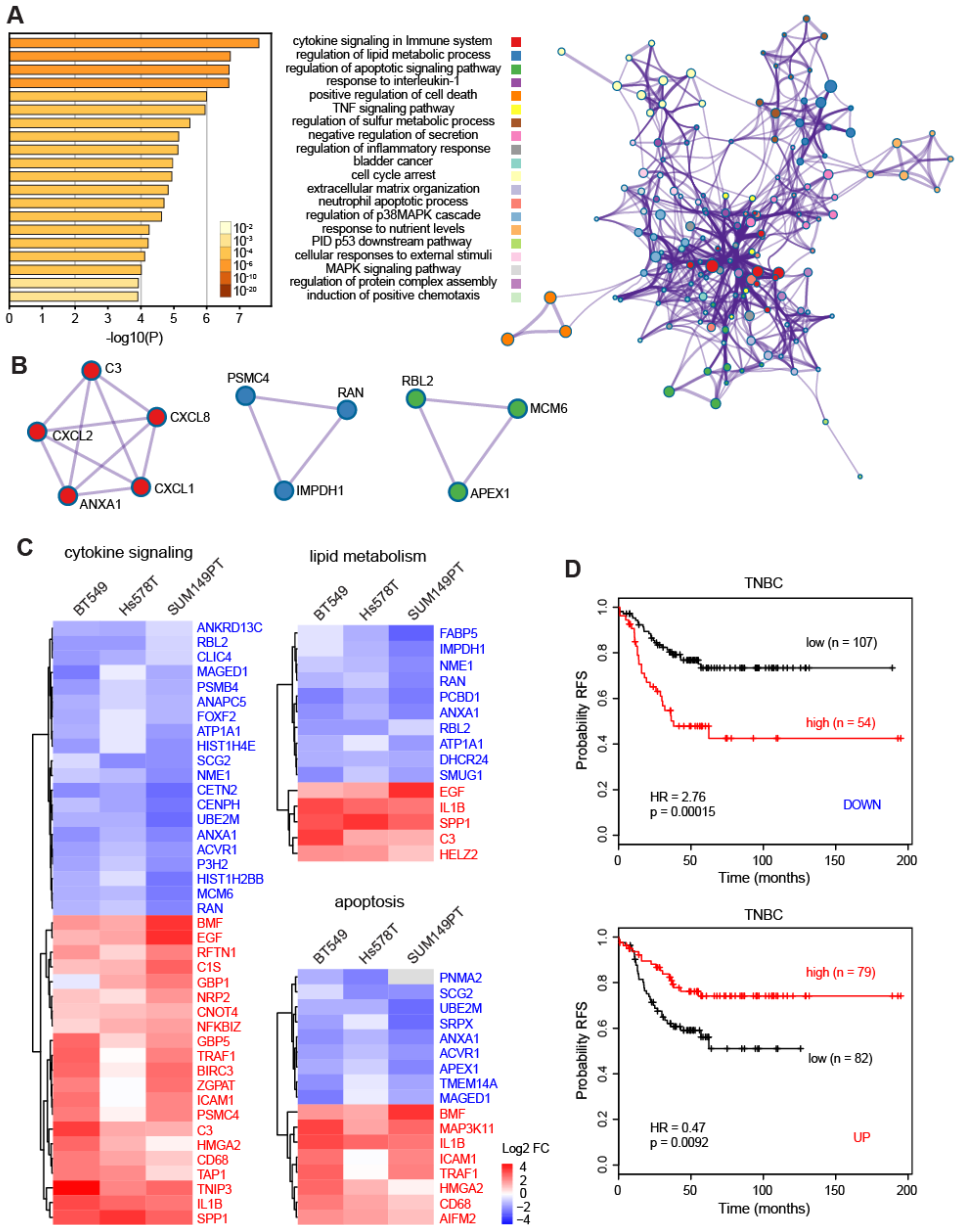


Figure 6. Metascape functional enrichment analysis and TNBC clinical relevance of ASAP1-regulated DEGs. (A) Top 20 clusters with their representative enriched term across input of 174 ASAP1-regulated DEGs. Left panel, heatmap of the 20 enriched terms. One term per cluster, colored by p-values. $\log_{10}(P)$ is the p-value in log base 10. Right panel, network of the 20 enriched terms, colored by cluster ID, where nodes that share the same cluster ID are typically close to each other. **(B)** Representative Molecular Complex Detection (MCODE) network nodes, showing the ASAP1-regulated DEGs densely connected. **(C)** Log₂ FC clustering of DEGs involved in

cytokine signaling, lipid metabolism and apoptosis pathways. Blue, negative regulators; red, positive regulators. (D) Relapse-free survival (RFS) KM curves of the DEGs from panel C in patients with TNBC. Mean expression of positive DEGs (DOWN) or negative DEGs (UP) was used.

Collectively, our data suggested that amplified ASAP1 is a key driver in TNBC progression by negatively regulating cell death pathways. The ASAP1-regulated genes in cytokine, lipid metabolism and apoptosis signaling pathways were clinically relevant to TNBC relapse-free survival.

Discussion

TNBC is characterized by its inter-tumoral heterogeneity. Based on gene expression signatures, TNBC has been further classified into more than six molecular subtypes⁸. Yet, no effective molecular targeted therapies are currently available in the clinic for this type of breast cancer. Although TNBC demonstrates substantial genetic alterations²⁵⁵, only two genes, *TP53* and *PIK3CA*, have been found with mutation frequency in ~10% of TNBC patient tumors¹⁰⁶, indicating other driver mutations involved in TNBC progression. While amplification frequently occurs in cancer genomes, amplified genes are not always overexpressed²⁵⁶. A recent study has applied integrative analysis combining gene expression, miRNA and copy number variation genomic profiles for TNBC patients (n=137) from TCGA to reclassify TNBC inter-tumoral heterogeneity²⁵⁷. As overexpression is a requisite for amplified genes to function as drivers in cancer, we attempted to identify TNBC candidate driver genes by integrating DNA copy number change and mRNA expression omics data across 222 TNBC cases (TCGA dataset n=118 and Metabric n=104). Using recurrent event calling algorithm ADMIRE analysis and transcript expression quantification, we consequently identified 148 genes with frequent focal CNGs and concurrent high expression in the cohort of TNBC tumors. Among these genes several are well-known oncogenes with involvement in breast cancer, e.g. *MYC*, *EGFR*, *CCNE1* and *FGFR1*, consistent to other studies^{19, 106, 258}. We also identified many novel candidates, such as *TMEM67*, *ANKH*, *BNIP1*, *CCT5*, *ASAP1* and *IRF2BP2*. KEGG pathways enrichment displayed the implication of the genes mainly in cancer-related or oncogenic signaling pathways. Our integrated genomic analysis reveals frequent CNGs and amplification as driver mutations in the TNBC genome. This large group of 148 candidate genes, displaying positive correlation in recurrent DNA CNGs and high RNA expression levels in the TNBC genome, may represent potential drivers during the course of TNBC progression.

Our current siRNA-based proliferation screen validated several candidate genes promoting TNBC cell proliferative phenotype, including the known oncogenes *MYC* and *EGFR* and the novel candidates *ASAP1*, *IRF2BP2*, *CCT5* and *DRD1*, indicating the implication of amplification-dependent drivers in TNBC proliferation. These genes (except for *DRD1*) acquired CNG/amplification and high expression in breast tumors. In particular,

amplification of MYC and ASAP1 is highly frequent in TNBC (35% and 30.3%, respectively) compared to non-TNBC tumors (25.5% and 22.6%, respectively). The amplification-based MYC oncogene has been found in various solid tumors, including kidney and colorectal cancers and breast cancer subtypes, including TNBC ^{47, 259}, indicating MYC amplification as a frequent driver mutation in cancer. A recent study has revealed that MYC alterations are mutually exclusive with PIK3CA, PTEN, APC, or BRAF alterations ²⁶⁰, suggesting MYC amplification as a distinct driver mutation in the cancer genome. The novel candidate, ASAP1, has also been reported to be frequently amplified, accompanied by enhanced expression, in different types of cancers, including pancreatic ductal adenocarcinoma, prostate cancer and melanoma ^{261, 262}, exceptionally in primary breast cancer where overexpression of ASAP1 was described to be independent of MYC amplification ²⁶³. These early results, though not reported for breast cancer, underline the impact of ASAP1 amplification over the cancer genome. Here, our results initially interpret that, similar to other cancer types, the aggressive breast cancer subtype TNBC acquires driver mutations, such as amplification-dependent overexpression of MYC and ASAP1, to progress, in spite of genetic heterogeneity. Of significance for ASAP1, we showed that knockdown of ASAP1 inhibits cell proliferation in different TNBC cell lines and high expression of ASAP1 is associated with poor metastatic relapse-free survival of patients with TNBC but not ER+ breast cancer, compelling the role of ASAP1 in TNBC progression, promoting not only proliferation but also metastasis.

In this study, we demonstrated for the first time the effect of ASAP1 on transcriptomic regulation in TNBC cells. ASAP1 (also named DDEF1 or AMAP1) was identified on the basis of Arf activity as a phospholipid-dependent Arf GTPase-activating protein and was found to bind to and be phosphorylated by Src family proteins and focal adhesion kinase (FAK) and to associate with focal adhesions ^{264, 265}. ASAP1 has been shown to promote cell proliferation and invasion in different cancer cells, including lung, colorectal, prostate and breast cancer cells ^{244, 261, 266}. High ASAP1 expression level was found in and was required for invadopodia formation in invasive MDA-MB-231 TNBC breast cancer cells, and interfering ASAP1-mediated protein complex inhibited metastasis of MDA-MB-231 derived xenografts ²⁶³. Overexpression of ASAP1 has been reported to be associated with poor metastasis-free survival in prostate, colorectal cancer and ovarian cancer and malignant phenotypes of primary breast cancers ^{244, 263, 267}. We showed that depletion of ASAP1 in different TNBC cells led to reprogramming of gene expression mainly in cytokine and apoptosis interactive signaling pathways, by upregulating positive regulators and downregulating negative regulators of the pathways. For instance, silencing ASAP1 downregulated the components in the identified mitotic cell cycle G1/S phase transition network node, including the anti-apoptotic APEX1 that is abnormally expressed in numerous human solid tumors and positively correlated with cancer progression ²⁶⁸, the proliferation marker MCM6 that is predictive for poor prognosis in breast cancer ²⁶⁹, and

the direct AKT target RBL2²⁷⁰. In addition, expression of genes involved in lipid metabolic process was also vulnerable to ASAP1 depletion, suggesting the novel role of ASAP1 in metabolism-related tumorigenesis, as lipid metabolism has been linked to cancer development by causing abnormal expression of various genes and dysregulating cytokines and signaling pathways²⁷¹. Most importantly, numerous ASAP1-regulated genes, particularly those that were downregulated when ASAP1 was targeted, displayed significant relevance to relapse-free survival of TNBC patients, indicating ASAP1 as an upstream regulator in driving TNBC progression.

Deconvolution of genetic alterations in cancer genome, such as focal CNAs, has provided an excellent possibility to classify new cancer subtypes and identify novel therapeutic targets for naïve resistant cancers^{235, 236, 257}. Our work elucidated extensive amplification-dependent gene expression alterations in TNBC, revealing ASAP1 as a potential TNBC driver functioning upstream of cytokine and apoptosis genes in promoting proliferation and survival. ASAP1 emerges as a potential diagnostic marker as well as therapeutic target for cancer, as ASAP1 has been found to be implicated in multiple oncogenic processes in various cancers^{244, 261, 267}. Our results suggest that targeting the upstream regulator ASAP1 and its downstream target genes may provide actionable therapeutic strategies for overcoming the intractable TNBC disease, as well as other resistant cancer types overexpressing ASAP1.

Acknowledgments

JH was financially supported by the China Scholarship Council. We thank Marije Niemeijer for the help with whole transcriptome sequencing analyses.

Funding

This work was supported by the ERC Advanced grant Triple-BC (grant no. 322737).

Authors' contributions

JH, YZ and BvdW conceived and designed the experiments. YZ and BvdW supervised the research. JH, RPM and LvdB performed the experiments. SC performed ADMIRE analyses. LW, JWMM and JAF co-supervised the research. JH, YZ and BvdW wrote the manuscript. All authors read, reviewed and approved the final manuscript.

Additional files: Supplementary data

Additional file 1. Table S1. 148 candidate driver genes for TNBC.

ADAM32	AXIN1	CAMK2B	DBNL	FBXL14	IRF2BP2	MYRFL	PLEKHF1	RASA3	TFDP1
ADAM9	BACE2	CARS	DCUN1D2	FBXW11	KCNMB4	NCOR2	PLXNC1	RBM12B	TGFB3
ADCY4	BAG4	CCNE1	DDAH1	FGF18	KIAA1217	NPM1	POLD2	RIPK3	TIAL1
ADIPOR2	BAI2	CCT2	DDHD2	FGFR1	KIAA1429	NRIP1	POLM	RRP7A	TM2D2
ADPRHL1	BCL11A	CCT5	DHRS1	FLJ12443	LANCL2	NTRK3	POP4	RTN4IP1	TMEM247
ADSSL1	BNIP1	CDC73	DRD1	GAB1	LCN7	OGG1	PPP1R9A	SACM1L	TMEM67
AIM1	BRD9	CEP170B	DUSP1	GMPR2	LDLRAD4	OLFML2B	PRKWKN1	SF3A1	TMEM8A
ANKH	BRF1	CFH	EGFR	GPR128	LHFP	OTULIN	PROZ	SFXN1	TRIO
ANKRD10	BRPF1	CLPTM1L	EPHA3	GRK5	LMCD1	PANK3	PTK2	SGSM2	TRIP13
ARFGEF3	BTBD6	CNOT2	ERC1	GUCY1A3	LRRC6	PAPOLG	PUS10	SIVA	TLL3
ARHGEF7	BTG3	CREBRF	F10	HRH2	LTB4R2	PCK2	QRSL1	SPDL1	USP25
ASAP1	C14orf79	CTIF	F7	HTPAP	MET	PDGFRA	RAB20	STK10	VOPP1
ATF6	C19ORF2	CTNNB1	FAM105A	INF2	MRPL28	PEF1	RAD18	TADA3L	WHSC1L1
ATP11A	C6orf203	CUL4A	FAM193A	ING1	MSX2	PHGDH	RAD54B	TARBP1	
ATP4B	CACNA2D	CXADR	FANCD2	IRAK2	MYC	PLEKHA2	RARS	TENS1	

Additional file 3. Table S2. Primary hits of siRNA-mediated loss-of-function screen.

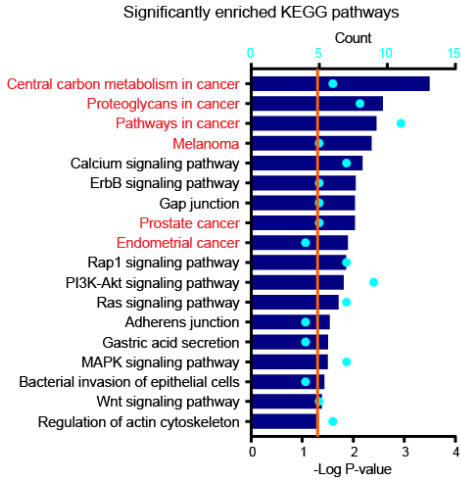
BT549						SUM149PT		
Genes	% control	STDEV	Genes	% control	STDEV	Genes	% control	STDEV
SPDL1	15.78547	0.028709	GMPR2	49.54181	0.119077	SF3A1	20.80776	0.02984
F7	20.16426	0.08556	DDHD2	51.09423	0.045467	TLL3	28.32151	0.085348
LHFP	22.43687	0.060953	ANKH	51.3599	0.009051	LHFP	29.34977	0.099702
TLL3	23.45475	0.122612	F10	51.43992	0.059609	CCT2	34.78913	0.101753
SF3A1	26.83166	0.112501	TM2D2	51.55195	0.104935	OGG1	40.60104	0.09454
SIVA	28.4481	0.023476	CCT2	51.94246	0.068448	SIVA	40.79477	0.049073
HRH2	32.91971	0.065549	INF2	52.07369	0.20202	CARS	41.26568	0.011031
FGFR1	34.08162	0.100692	TMEM8A	52.0865	0.049144	SPDL1	45.89733	0.050205
CTIF	34.10723	0.19601	CCT5	53.11398	0.055013	BRF1	46.21027	0.253498
MYC	35.06749	0.00594	LCN7	53.35084	0.007778	EGFR	46.7855	0.001131
CARS	36.17179	0.170483	RRP7A	53.71574	0.07962	HRH2	46.9852	0.221819
OGG1	36.82797	0.00792	RASA3	53.89179	0.017183	BNIP1	49.50071	0.113915
BRF1	37.37852	0.030688	ASAP1	54.25989	0.073115	CCT5	51.82249	0.071701
TMEM247	40.93148	0.05077	ANKRD10	55.46341	0.045538	RRP7A	52.29043	0.135835
POLM	41.42441	0.069155	LTB4R2	55.87632	0.110804	CTIF	52.41859	0.021496
CNOT2	43.43136	0.067104	IRF2BP2	56.17721	0.024112	FBXW11	53.07727	0.056639
DRD1	44.48124	0.074034	BNIP1	57.83205	0.019658	USP25	56.31704	0.055861
TADA3L	44.7085	0.066223	ERC1	58.58106	0.104935	PLEKHF1	56.51971	0.124734
BRPF1	44.81093	0.118087	SFXN1	58.86593	0.039527	BACE2	57.50624	0.108682
CDC73	45.49591	0.123037	TMEM67	59.1252	0.015981	ADPRHL1	58.4898	0.07064
PLEKHF1	49.42338	0.130037						

Additional file 4. Table S3. BC cell line panel.

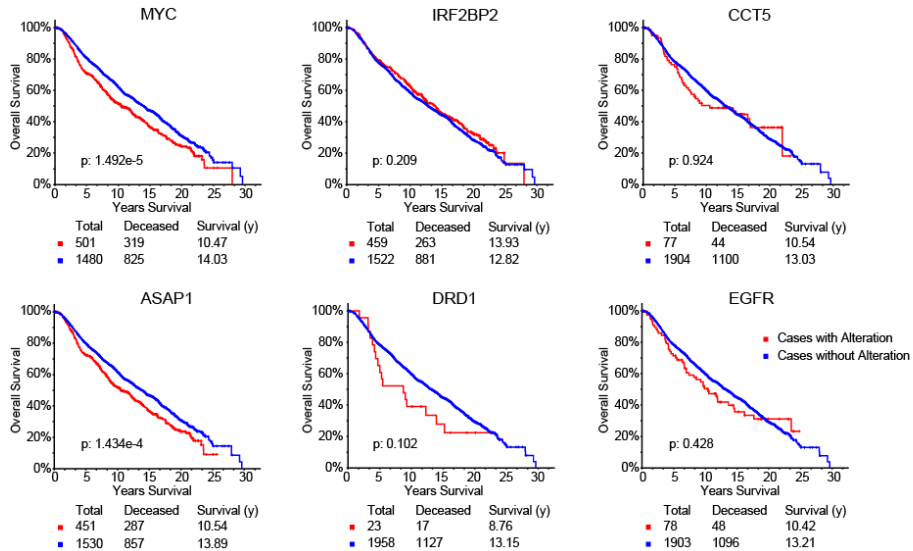
Cell line	Subtype	Cell line	Subtype	Cell line	Subtype
BT20	TNBC	SUM102PT	TNBC	MDAMB134VI	non_TNBC
BT549	TNBC	SUM1315MO2	TNBC	MDAMB175VII	non_TNBC
DU4475	TNBC	SUM149PT	TNBC	MDAMB330	non_TNBC
HCC1143	TNBC	SUM159PT	TNBC	MDAMB361	non_TNBC
HCC1187	TNBC	SUM185PE	TNBC	MDAMB415	non_TNBC
HCC1395	TNBC	SUM229PE	TNBC	MPE600	non_TNBC
HCC1599	TNBC	SUM52PE	TNBC	OCUBF	non_TNBC
HCC1806	TNBC	BT474	non_TNBC	SKBR3	non_TNBC
HCC1937	TNBC	BT483	non_TNBC	SKBR5	non_TNBC
HCC38	TNBC	CAMA1	non_TNBC	SUM190PT	non_TNBC
HCC70	TNBC	EVSAT	non_TNBC	SUM225CWN	non_TNBC
Hs578T	TNBC	HCC1419	non_TNBC	SUM44PE	non_TNBC
MDAMB157	TNBC	HCC1500	non_TNBC	T47D	non_TNBC
MDAMB231	TNBC	HCC1569	non_TNBC	UACC893	non_TNBC
MDAMB435s	TNBC	HCC1954	non_TNBC	ZR751	non_TNBC
MDAMB436	TNBC	HCC202	non_TNBC	ZR7530	non_TNBC
MDAMB453	TNBC	HCC2218	non_TNBC		
MDAMB468	TNBC	MCF7	non_TNBC		



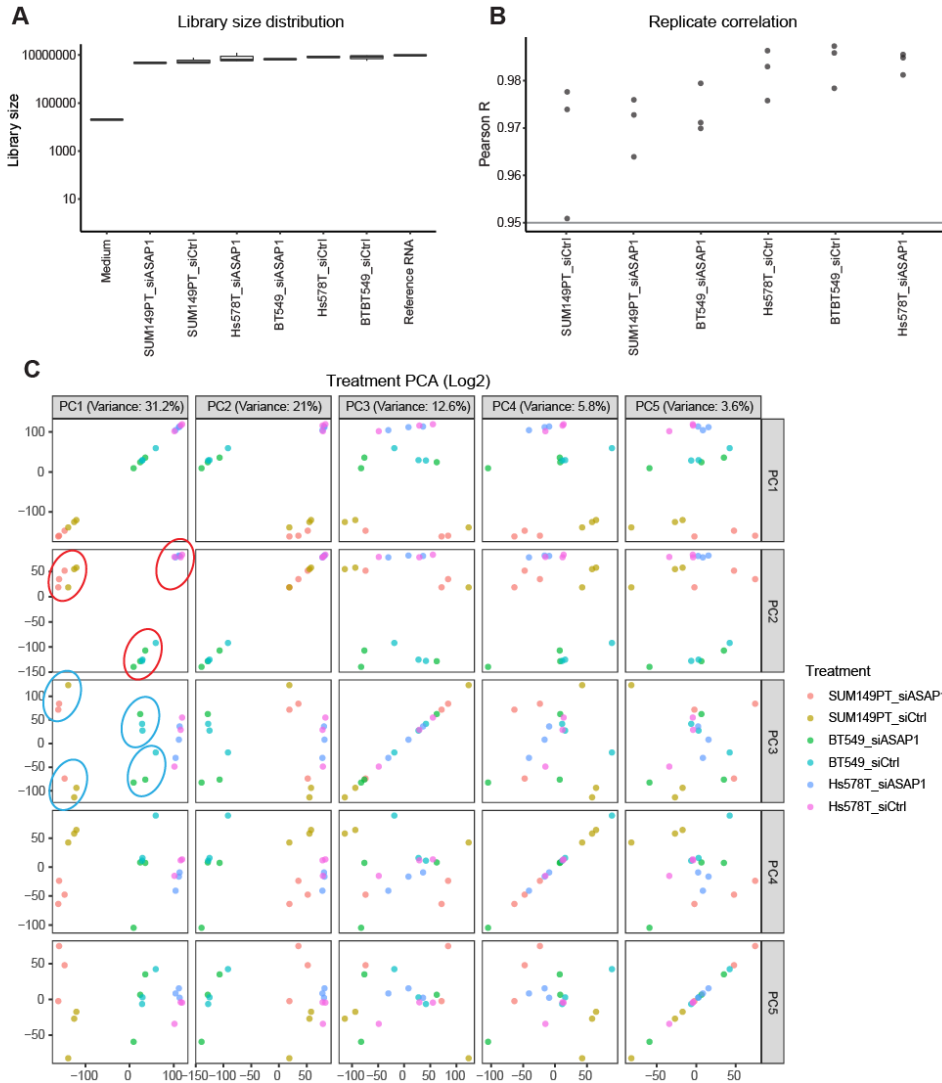
78 cytokine signaling related hits		31 lipid metabolism related hits	33 apoptosis related hits
ACVR1	IRAK2	ACADVL	ACVR1
ADA	KIF3B	ANXA1	ADA
ADAM19	LY6E	ATP1A1	AIFM2
ANAPC5	MAGED1	C3	ANXA1
ANKRD13C	MCM6	FABP5	APEX1
ANXA1	MMP1	IL1B	BEX3
ARL2BP	MMP3	PDK3	BMF
ATP1A1	NFKBIZ	RAN	CD68
BIRC3	NME1	RBL2	COL16A1
BMF	NRP2	SNCA	E2F3
C1S	P3H2	SREBF2	HMGA2
C3	PDK3	PDP2	ICAM1
CABLES1	PLPP3	HELZ2	IL1B
CD68	PNKD	SIK1	IL6
CENPH	PSMB4	WASHC1	INHBA
CETN2	PSMC4	ACAT1	MAGED1
CLIC4	PTPRB	ADA	MAP3K11
CNOT4	RAN	DHCR24	MMP3
CTSD	RBL2	EGF	PNMA2
CXCL1	RFTN1	IMPDH1	SCG2
CXCL2	RPLP0	NME1	SERPINE1
CXCL8	SCG2	PCBD1	SIK1
DUSP10	SERPINE1	EBP	SNCA
DUSP4	SLC7A11	SMUG1	SOS2
E2F3	SNCA	CHST14	SQSTM1
EGF	SOS2	SPP1	SRPX
EMB	SPP1	EBPL	TGFBR1
FHL1	SQSTM1	SLC7A11	TMBIM6
FOXF2	SREBF2	PNKD	TMEM14A
GBP1	TAP1	PLPP3	TRAF1
GBP5	TGFBR1	PYURF	TXNDC12
HIST1H2AI	TMBIM6		UBE2M
HIST1H2BB	TNIP3		YBX3
HIST1H4E	TRAF1		
HMGA2	UBE2M		
ICAM1	VEGFA		
IL1B	WASHC1		
IL6	YBX3		
INHBA	ZGPAT		



Additional file 2. Figure S1. KEGG pathway enrichment analysis of 148 candidate driver genes. Orange line indicated where P-value = 0.05, whereas cyan dots indicated the number of mapped genes in each pathway. Pathways involved in cancer progression were highlighted in red.



Additional file 5. Figure S2. Association of CNA-driven candidate hits, including oncogene MYC and novel driver gene ASAP1, with overall survival of 2173 breast cancer patients. Kaplan Meier plot was generated in cBioPortal using dataset "METABRIC, Nature 2012 & Nat Commun 2016".



Additional file 6. Figure S3. Quality control transcriptomic TemO-Seq analysis. (A) Sequencing library size distribution across treatments. **(B)** Sequencing reproducibility. Pearson correlation coefficient r was calculated among each replicate against triplicate mean per treatment. **(C)** Principle component analysis (PCA) across treatments using Log2 read counts. Red circle, cell line clustering; blue circle, treatment clustering.

Chapter 6

Discussion and future perspectives

Worldwide, breast cancer remains the leading cause of female cancer-related death¹. TNBC, characteristic of the absent expression of ER, PR and HER2 amplification, represents the most aggressive form of all breast cancer subtypes, is highly heterogeneous and associated with worse prognosis^{186, 187}. Despite the initial increased response to the standard-of-care chemotherapy, TNBC often exhibits intrinsic or acquired drug resistance, and subsequently, recurs in local and distal organs. Targeted therapies have long been pursued for the treatment of TNBC, but rarely demonstrate satisfactory clinical outcomes. Therefore, improved understanding of the intricate biological basis underlying TNBC insensitivity to targeted agents and defining new therapeutic opportunities are of the utmost importance. The work presented in this thesis was aimed at understanding the molecular mechanisms of TNBC drug resistance, discovering TNBC-specific kinase signaling transduction dependencies and identifying novel drug targets and effective therapies for TNBC. The results from the chapters were summarized and discussed in a broader context and future perspectives were also provided.

1. FRET imaging in cancer drug discovery

With the advent of a vast number of fluorescent proteins and advanced microscopy facilities, fluorescence optical imaging has been widely employed in preclinical cancer drug discovery. Fluorescence-based functional imaging approaches have been extending our understanding of cancer biology and drug efficacy, by providing high-throughput phenotypic readouts, including changes in morphology, cell proliferation, invasion, migration and angiogenesis^{99, 272}. In **Chapter 2** I exploited a FRET (fluorescence resonance energy transfer)-based high throughput imaging approach to investigate the dynamics of ERK and AKT kinase activity in response to a collection of kinase inhibitors (KIs) in TNBC cell lines. FRET, also known as Förster resonance energy transfer, refers to the nonradiative transfer of excited state energy between colocalized donor and acceptor fluorophores²⁷³⁻²⁷⁵. When combined with genetically encoded kinase reporters, FRET microscopy enables the direct visualization of kinase activity in highly spatiotemporal resolution in living cells¹¹⁹.

ERK and AKT are two key signaling elements of the canonical Ras/MAPK and PI3K/AKT/mTOR pathways, respectively. Activation of PI3K/AKT/mTOR pathway is common in TNBC^{41, 112, 134}, due to the recurrent copy number loss of negative regulators (e.g., PTEN, INPP4B) and activating mutation of PIK3CA¹⁹. Analogous to PTEN loss, Ras/MAPK pathway is often activated by the loss of NF1 and DUSP4, despite the scarcity of activating mutations in TNBC. In **Chapter 2**, the MEKi-resistant and AKTi-resistant TNBC cell models were transfected to stably express FRET-based biosensors specifically for ERK and AKT activity, allowing for high-throughput FRET imaging. Upon exposure to KI library, real-time ERK and AKT activity dynamics were recorded and quantified, and subsequently, the key parameters were correlated with proliferative response. This study has associated

ERK and AKT kinase activity with the anti-tumor effects of kinase drugs and revealed differential kinase dependencies of treatment-refractory TNBC cells. The work has not only advanced the live cell high-content imaging-based quantification of kinase activity profiles in TNBC, but also discovered possible off-target effects of clinical kinase drugs.

Considering the heterogeneous nature of this disease and the intricate pathway interconnections, potential use of our FRET imaging-based approach has yet to be made by incorporating multiple kinase biosensors in various TNBC cell lines representative for different molecular subtypes. A simultaneous application in non-TNBC cells and normal mammary cells could also aid in finding TNBC-specific kinase signaling addictions and discovering undesired adverse effects. Besides ERK and AKT sensors, a large amount of other FRET probes (kinases, GTPases, phosphoinositides, Ca²⁺ and metabolites) have also been developed and used in multiple biological imaging studies²⁷⁶⁻²⁷⁸. Recently, Kuchenov and colleagues have described a high-content imaging platform using 40 FRET biosensors to profile cancer-relevant signaling networks²⁷⁹. Despite that the authors announced the potential of the platform to image up to 384 FRET sensors in a single experiment, how the complex signaling crosstalk is related to the various biological processes and eventually influence the cancer phenotypes is yet to be addressed. Our study in **Chapter 2** demonstrated the feasibility of quantifying real-time kinase activity in TNBC cells in response to clinical kinase drugs and correlating with cell proliferation, a hallmark of cancer. Our work has revealed the differential kinase dependencies in MEKi- and AKTi-resistant TNBC cells, thus providing new opportunities to explore effective therapeutic kinase targets in treatment-refractory cancer cells, as well as assess the drug efficacy and possible off-target effects of clinically used drugs.

It is obvious that a lacking of tumor microenvironment has limited the translation of the findings derived from 2D cell culture into the clinic. This disadvantage can be compensated by utilizing the advanced and clinically relevant organoids and PDXs systems. As fluorescence imaging profoundly relies on the detection of emitted light, the absorbance and scattering by various tissues can constrain the depth in which the light penetrates. Another downside of fluorescence imaging is that the intrinsic fluorescence of biomolecules, and in some cases the kinase drugs, increases background signals. Another major application of FRET is fluorescence lifetime imaging microscopy (FLIM), which is suitable for the analysis of intracellular environment, independent of intensity-based ratiometric FRET calculation. In contrast to bulk FRET analyses where signals from FRET molecules in varied conformational states are captures and averaged, single-molecule FRET (smFRET) measurement allows for elucidating the structural heterogeneity of FRET in individual signaling molecules²⁸⁰. Nonetheless, along with the advances in optical microscopy, well-designed FRET probes and improved image analysis algorithms, FRET imaging has proved imperative and valuable in studying cancer biology and drug efficacy.

2. Exploring novel therapies for TNBC via high-throughput screen

High-throughput compound or gene screening plays an essential role in identifying novel therapeutic targets and combination treatment in cancer therapy. Protein kinases represent attractive drug targets due to their involvement in various cellular functions. **Chapter 2** utilized FRET imaging technology to screen a well-established inhibitor library containing about 400 kinase drugs in TNBC cells. The library spans 14 signaling pathways by targeting 118 kinases. Integrated proliferative response profiling and ERK- and AKT-based kinase activity dynamics analysis uncovered the differential kinase signaling dependencies of treatment-resistant TNBC cells. Specifically, MEKi-resistant cells were responsive to inhibitors against PI3K pathway but refractory to EGFR-targeted inhibitors, whereas AKTi-resistant cells were sensitive to EGFR/MAPK pathway blockade but showed resistance against mTOR inhibitors. These findings suggest that the molecularly heterogeneous TNBC may leverage alternate surviving pathways to by-pass kinase-targeted inhibition, thereby conferring resistance. However, the screening only partially explained the regulatory effects of the kinome on TNBC cell proliferation as the KIs target less than one third protein kinases (118/518). Moreover, less selective KIs could increase the likelihood of false discovery.

In contrast, genetic perturbation permits high-throughput screening in the desired set of genes, such as the entire genome or specifically the kinome. Suppression of gene expression can be achieved either by RNAi (siRNA and shRNA), or by CRISPR/Cas9 technology. Recently, an *in vivo* study has reported 40 novel modulators of breast cancer response to paclitaxel by performing genome-wide RNAi²⁸¹. A gene signature was derived from the screen hits with the potential to predict patient outcomes. By carrying out kinome-scale siRNA screen, **Chapter 3** identified specific vulnerable kinase targets in EGFRi- and mTORi-resistant TNBC cells. Pharmacological inhibition of these targets greatly suppressed TNBC cell proliferation in different resistant scenarios, highlighting the potential of targeting these kinase vulnerabilities to combat the hard-to-treat disease. Moreover, a kinome-wide siRNA screen has been performed in combination with lapatinib in **Chapter 3** to study the synthetic lethality interactions with EGFR-targeted inhibition and discover potential therapies to overcome EGFRi-resistance. Unlike compound screen, siRNA screening provides a high specificity for targeting the protein kinases in question, with the potential to look into the kinase signaling network in the kinome scale. This work has led to the identification of FYN kinase as a negative regulator of EGFR/PI3K/AKT pathway in EGFRi-resistant TNBC cells. Thus, dual targeting of EGFR and FYN could lead to cell death in TNBC cells representing the intact pathway. In addition, targeting FYN also enhanced the anti-proliferative effects of PI3Ki and AKTi. This is in line with the finding in **Chapter 2** that EGFRi/MEKi-resistant cells were responsive to PI3K/AKT inhibition as the resistant cells were more likely to depend on elevated PI3K pathway for proliferation in

the presence of FYN. However, whether pharmacological inhibition of FYN could synergize with EGFR inhibitors has yet to be confirmed. Supportively, several FYN inhibitors have been developed, albeit less selective.

Using high-throughput KI screening, **Chapter 4** has discovered a novel combination therapy (i.e., AEE788 + rapamycin) to overcome mTORi-resistance in TNBCs. Various types of cancer arise owing to dysfunction of mTOR signaling, and can confer higher susceptibility to mTOR inhibitors. Despite rapalogs (rapamycin and its analogs) have proven effective in a range of preclinical studies, clinical success is restricted to only a few rare cancers. It was reported that rapalogs are cytostatic, thus unlikely to cause tumor regression. When used as monotherapy, rapalogs exhibited modest anti-tumor activity due in part to incomplete mTOR inhibition. Other mechanisms underlying this insensitivity involve redundant signal transduction and feedback loops. Rapalog-mediated mTORC1 inhibition is thereby not sufficient to induce comprehensive pathway inactivation, necessitating the development of combination therapy in this scenario. The AEE788 + rapamycin combination identified in **Chapter 4** represents a novel therapeutic strategy to combat TNBC. In this study, cheminformatics-based target prediction and validation using siRNA have revealed putative targets of AEE788, which play key roles in determining rapalog efficacy. The combination, by targeting multiple kinases, not only sustains inhibited MAPK activity, but also effectively suppresses mTOR signaling, thereby eliciting synergistic anti-proliferative effects in TNBC. In addition, the findings are complementary to the presently published target spectrum of the kinase drug AEE788. The synergistic effects of AEE788-everolimus combination have been reported in prostate, germ and renal tumor cell lines^{198, 200, 201}. Specifically, by exploiting the integrated compound screen, target prediction and validation approach, I discovered the potential combination therapy for TNBC, and studied the mechanisms of action of the synergy in the highly heterogeneous TNBC. Provided the reported toxicity of AEE788 in clinical trials^{282, 283}, reduced doses of both drugs in the combination might decrease adverse effects while generating synergistic anti-tumor effect. Nevertheless, future studies assessing the effects in in vivo models are warranted for potential translation of the results in the clinic.

3. Bioinformatics-based therapeutic target identification

Genetic alterations are thought to be favored during the initiation, development and progression of cancer in an evolutionary fashion^{106, 284, 285}. Over 80% TNBCs exhibits TP53 mutation¹⁹, being a major reason for causing gene instability in this disease. Insightful analysis of genomic sequencing data in breast cancer exploiting bioinformatics holds the promise for the identification of novel therapeutic targets^{152, 286, 287}. For example, two independent bioinformatics-based studies have demonstrated that PIM kinase regulated chemotherapy response in TNBC and can be explored as novel targeted therapy^{288, 289}. In

Chapter 5, ADMIRE analysis of copy number and gene expression profiles was performed across a set of triple-negative tumors. This work has led to the discovery of several novel TNBC driver genes, besides the known oncogene EGFR and MYC. Of the identified driver genes, I functionally validated the most promising driver gene ASAP1 (an Arf GTPase-activating protein) and revealed its biological role in TNBC progression through transcriptome-wide bioinformatics study. Of relevance, high level of ASAP1 expression correlates with poor prognosis in patients with TNBC. Several studies have also reported the role of ASAP1 in breast cancer invasion and metastasis^{263, 290-292}. Studies by Onodera and colleagues showed that ASAP1 was localized at invadopodia together with cortactin and paxillin to form a trimeric protein complex, which accelerated extracellular matrix degradation and subsequently promoted tumor cell motility and invasion²⁶³. Consistently, among the most significantly enriched GO terms derived from DEGs upon ASAP1 depletion, as shown in **Chapter 5**, are extracellular matrix organization and regulation of protein complex assembly. With a couple of small molecule modulators of GTPase-activating proteins (including ASAP1) being developed^{293, 294}, the regulatory role of ASAP1 in tumor invasion and migration can be assessed in more relevant 3D systems (such as tumor organoids and PDXs), and thus assisting in the translation of the potential driver gene ASAP1 into a clinical therapeutic target.

4. Future perspectives

A major concern in this thesis is to which extent the findings can be translated into the clinic. Monolayer cell culture has been the main cancer model for conducting the research. Although several studies have argued that a sufficiently large panel of breast cancer cell lines represents the genomic and proteomic landscape of breast tumors and provides a reasonable model for breast cancer study^{91, 284, 295}, the results derived from 2D culture systems can be variable when tested in 3D and in vivo models, which more realistically mimic the cell-cell communication and microenvironment^{93, 99, 296, 297}. By utilizing state-of-art CRISPR/Cas gene editing technology, genome-wide integration of fluorescent proteins into PDX models allows us to monitor the dynamics of gene expression in living TNBC cells affected by the identified novel therapies. The continuing efforts in enlarging the biobank of breast tumor organoid and well-established PDX mouse models both provide an excellent possibility to assess the findings of this thesis for potential clinical translation. Another concern is that the evaluation of the anti-cancer effect of the proposed therapeutic targeting strategies has been limited to proliferation assays. Multi-faceted functionality studies are merited in a context-dependent manner. Application of our established FRET imaging approach in 3D culture of PDX-derived TNBC cells could better dissect the tumor heterogeneity in both highly temporal and spatial resolution. In addition, single-cell sequencing has proved to be an imperative tool to study the transcriptional diversity and variability in therapeutic response within a range of cancer types, including

TNBC. More importantly, future assessment of the novel therapies discovered in this thesis using organoids and PDXs would prove invaluable in advancing precision medicine in TNBC.

5. Conclusions

Altogether, the aim of the studies presented in this thesis was to systematically identify gene/kinase susceptibilities of refractory TNBC cells, and reveal novel potent targeted therapies for TNBC as monotherapy or in combination with approved kinase drugs. The work has identified important kinase signaling dependencies of TNBC cell proliferation (**Chapter 2**) and discovered novel multi-kinase targeting strategy to overcome mTORi resistance (**Chapter 4**) using compound library screen, found key regulators of TNBC resistance against EGFR-targeted inhibitors (**Chapter 3**), and identified and validated novel driver genes via integrated computational algorithms and bioinformatics approach (**Chapter 5**). This work provides novel insights into the molecular basis of TNBC response to clinical kinase drugs and provokes potential therapeutic targeting strategies for the incurable TNBC.

References

1. Bray, F. et al. Global cancer statistics 2018: GLOBOCAN estimates of incidence and mortality worldwide for 36 cancers in 185 countries. *CA Cancer J Clin* **68**, 394-424 (2018).
2. Perou, C.M. et al. Molecular portraits of human breast tumours. *Nature* **406**, 747-752 (2000).
3. Waks, A.G. & Winer, E.P. Breast Cancer Treatment: A Review. *JAMA* **321**, 288-300 (2019).
4. Foulkes, W.D., Smith, I.E. & Reis-Filho, J.S. Triple-negative breast cancer. *N Engl J Med* **363**, 1938-1948 (2010).
5. Prat, A. et al. Clinical implications of the intrinsic molecular subtypes of breast cancer. *Breast* **24 Suppl 2**, S26-35 (2015).
6. Cleator, S., Heller, W. & Coombes, R.C. Triple-negative breast cancer: therapeutic options. *Lancet Oncol* **8**, 235-244 (2007).
7. Dietze, E.C., Sistrunk, C., Miranda-Carboni, G., O'Regan, R. & Seewaldt, V.L. Triple-negative breast cancer in African-American women: disparities versus biology. *Nat Rev Cancer* **15**, 248-254 (2015).
8. Lehmann, B.D. et al. Identification of human triple-negative breast cancer subtypes and preclinical models for selection of targeted therapies. *J Clin Invest* **121**, 2750-2767 (2011).
9. Masuda, H. et al. Differential response to neoadjuvant chemotherapy among 7 triple-negative breast cancer molecular subtypes. *Clin Cancer Res* **19**, 5533-5540 (2013).
10. Ring, B.Z. et al. Generation of an algorithm based on minimal gene sets to clinically subtype triple negative breast cancer patients. *BMC Cancer* **16**, 143 (2016).
11. Lehmann, B.D. et al. Refinement of Triple-Negative Breast Cancer Molecular Subtypes: Implications for Neoadjuvant Chemotherapy Selection. *Plos One* **11** (2016).
12. Burstein, M.D. et al. Comprehensive genomic analysis identifies novel subtypes and targets of triple-negative breast cancer. *Clin Cancer Res* **21**, 1688-1698 (2015).
13. von Minckwitz, G. et al. Definition and impact of pathologic complete response on prognosis after neoadjuvant chemotherapy in various intrinsic breast cancer subtypes. *J Clin Oncol* **30**, 1796-1804 (2012).
14. Liedtke, C. et al. Response to neoadjuvant therapy and long-term survival in patients with triple-negative breast cancer. *J Clin Oncol* **26**, 1275-1281 (2008).
15. Carey, L.A. et al. The triple negative paradox: primary tumor chemosensitivity of breast cancer subtypes. *Clin Cancer Res* **13**, 2329-2334 (2007).
16. Bonotto, M. et al. Measures of outcome in metastatic breast cancer: insights from a real-world scenario. *Oncologist* **19**, 608-615 (2014).
17. Conlin, A.K. & Seidman, A.D. Taxanes in breast cancer: an update. *Curr Oncol Rep* **9**, 22-30 (2007).
18. Litton, J.K. et al. Talazoparib in Patients with Advanced Breast Cancer and a Germline BRCA Mutation. *N Engl J Med* **379**, 753-763 (2018).
19. Cancer Genome Atlas, N. Comprehensive molecular portraits of human breast tumours. *Nature* **490**, 61-70 (2012).
20. Kalimutho, M. et al. Targeted Therapies for Triple-Negative Breast Cancer: Combating a Stubborn Disease. *Trends Pharmacol Sci* **36**, 822-846 (2015).
21. Lord, C.J., Tutt, A.N. & Ashworth, A. Synthetic lethality and cancer therapy: lessons learned from the development of PARP inhibitors. *Annu Rev Med* **66**, 455-470 (2015).
22. Hoy, S.M. Talazoparib: First Global Approval. *Drugs* **78**, 1939-1946 (2018).
23. Lips, E.H. et al. Triple-negative breast cancer: BRCAness and concordance of clinical features with BRCA1-mutation carriers. *Br J Cancer* **108**, 2172-2177 (2013).
24. Westover, D., Zugazagoitia, J., Cho, B.C., Lovly, C.M. & Paz-Ares, L. Mechanisms of acquired resistance to first- and second-generation EGFR tyrosine kinase inhibitors. *Ann Oncol* **29**, i10-i19 (2018).
25. Politi, K., Ayeni, D. & Lynch, T. The Next Wave of EGFR Tyrosine Kinase Inhibitors Enter the Clinic. *Cancer Cell* **27**, 751-753 (2015).
26. Corkery, B., Crown, J., Clynes, M. & O'Donovan, N. Epidermal growth factor receptor as a potential therapeutic target in triple-negative breast cancer. *Ann Oncol* **20**, 862-867 (2009).
27. Mertins, P. et al. Proteogenomics connects somatic mutations to signalling in breast cancer. *Nature* **534**, 55-62 (2016).
28. Carey, L.A. et al. TBCRC 001: randomized phase II study of cetuximab in combination with carboplatin in stage IV triple-negative breast cancer. *J Clin Oncol* **30**, 2615-2623 (2012).
29. Baselga, J. et al. Randomized phase II study of the anti-epidermal growth factor receptor monoclonal antibody cetuximab with cisplatin versus cisplatin alone in patients with metastatic triple-negative breast cancer. *J Clin Oncol* **31**, 2586-2592 (2013).

30. Sergina, N.V. et al. Escape from HER-family tyrosine kinase inhibitor therapy by the kinase-inactive HER3. *Nature* **445**, 437-441 (2007).
31. Nabholz, J.M. et al. Multicentric neoadjuvant pilot Phase II study of cetuximab combined with docetaxel in operable triple negative breast cancer. *Int J Cancer* **138**, 2274-2280 (2016).
32. Yardley, D.A. et al. Panitumumab, Gemcitabine, and Carboplatin as Treatment for Women With Metastatic Triple-Negative Breast Cancer: A Sarah Cannon Research Institute Phase II Trial. *Clin Breast Cancer* **16**, 349-355 (2016).
33. von Minckwitz, G. et al. Neoadjuvant chemotherapy and bevacizumab for HER2-negative breast cancer. *N Engl J Med* **366**, 299-309 (2012).
34. von Minckwitz, G. et al. Survival after neoadjuvant chemotherapy with or without bevacizumab or everolimus for HER2-negative primary breast cancer (GBG 44-GeparQuinto)dagger. *Ann Oncol* **25**, 2363-2372 (2014).
35. Earl, H.M. et al. Efficacy of neoadjuvant bevacizumab added to docetaxel followed by fluorouracil, epirubicin, and cyclophosphamide, for women with HER2-negative early breast cancer (ARTemis): an open-label, randomised, phase 3 trial. *Lancet Oncol* **16**, 656-666 (2015).
36. Ibrahim, Y.H. et al. PI3K inhibition impairs BRCA1/2 expression and sensitizes BRCA-proficient triple-negative breast cancer to PARP inhibition. *Cancer Discov* **2**, 1036-1047 (2012).
37. Martin, M. et al. A randomized adaptive phase II/III study of buparlisib, a pan-class I PI3K inhibitor, combined with paclitaxel for the treatment of HER2- advanced breast cancer (BELLE-4). *Ann Oncol* **28**, 313-320 (2017).
38. Kim, S.B. et al. Ipatasertib plus paclitaxel versus placebo plus paclitaxel as first-line therapy for metastatic triple-negative breast cancer (LOTUS): a multicentre, randomised, double-blind, placebo-controlled, phase 2 trial. *Lancet Oncol* **18**, 1360-1372 (2017).
39. Ueng, S.H. et al. Phosphorylated mTOR expression correlates with poor outcome in early-stage triple negative breast carcinomas. *Int J Clin Exp Pathol* **5**, 806-813 (2012).
40. Singh, J. et al. Phase 2 trial of everolimus and carboplatin combination in patients with triple negative metastatic breast cancer. *Breast Cancer Res* **16**, R32 (2014).
41. Basho, R.K. et al. Targeting the PI3K/AKT/mTOR Pathway for the Treatment of Mesenchymal Triple-Negative Breast Cancer: Evidence From a Phase 1 Trial of mTOR Inhibition in Combination With Liposomal Doxorubicin and Bevacizumab. *JAMA Oncol* **3**, 509-515 (2017).
42. Jovanovic, B. et al. A Randomized Phase II Neoadjuvant Study of Cisplatin, Paclitaxel With or Without Everolimus in Patients with Stage II/III Triple-Negative Breast Cancer (TNBC): Responses and Long-term Outcome Correlated with Increased Frequency of DNA Damage Response Gene Mutations, TNBC Subtype, AR Status, and Ki67. *Clin Cancer Res* **23**, 4035-4045 (2017).
43. Cochrane, D.R. et al. Role of the androgen receptor in breast cancer and preclinical analysis of enzalutamide. *Breast Cancer Res* **16**, R7 (2014).
44. Gucalp, A. et al. Phase II trial of bicalutamide in patients with androgen receptor-positive, estrogen receptor-negative metastatic Breast Cancer. *Clin Cancer Res* **19**, 5505-5512 (2013).
45. Traina, T.A. et al. Overall survival (OS) in patients (Pts) with diagnostic positive (Dx plus) breast cancer: Subgroup analysis from a phase 2 study of enzalutamide (ENZA), an androgen receptor (AR) inhibitor, in AR plus triple-negative breast cancer (TN BC) treated with 0-1 prior lines of therapy. *Journal of Clinical Oncology* **35** (2017).
46. Dai, M. et al. CDK4 regulates cancer stemness and is a novel therapeutic target for triple-negative breast cancer. *Sci Rep* **6**, 35383 (2016).
47. Horiuchi, D. et al. MYC pathway activation in triple-negative breast cancer is synthetic lethal with CDK inhibition. *J Exp Med* **209**, 679-696 (2012).
48. Budczies, J. et al. Classical pathology and mutational load of breast cancer - integration of two worlds. *J Pathol Clin Res* **1**, 225-238 (2015).
49. Vogelstein, B. et al. Cancer genome landscapes. *Science* **339**, 1546-1558 (2013).
50. Mittendorf, E.A. et al. PD-L1 expression in triple-negative breast cancer. *Cancer Immunol Res* **2**, 361-370 (2014).
51. Wimberly, H. et al. PD-L1 Expression Correlates with Tumor-Infiltrating Lymphocytes and Response to Neoadjuvant Chemotherapy in Breast Cancer. *Cancer Immunol Res* **3**, 326-332 (2015).
52. Sabatier, R. et al. Prognostic and predictive value of PDL1 expression in breast cancer. *Oncotarget* **6**, 5449-5464 (2015).
53. Schmid, P. et al. Atezolizumab and Nab-Paclitaxel in Advanced Triple-Negative Breast Cancer. *N Engl J Med* **379**, 2108-2121 (2018).

54. Bardia, A. et al. Efficacy and Safety of Anti-Trop-2 Antibody Drug Conjugate Sacituzumab Govitecan (IMMU-132) in Heavily Pretreated Patients With Metastatic Triple-Negative Breast Cancer. *J Clin Oncol* **35**, 2141-2148 (2017).
55. Kim, C. et al. Chemoresistance Evolution in Triple-Negative Breast Cancer Delineated by Single-Cell Sequencing. *Cell* **173**, 879-893 e813 (2018).
56. Longley, D.B. & Johnston, P.G. Molecular mechanisms of drug resistance. *J Pathol* **205**, 275-292 (2005).
57. Palasuberniam, P. et al. ABCG2 transporter inhibitor restores the sensitivity of triple negative breast cancer cells to aminolevulinic acid-mediated photodynamic therapy. *Sci Rep* **5**, 13298 (2015).
58. Duncan, J.S. et al. Dynamic reprogramming of the kinome in response to targeted MEK inhibition in triple-negative breast cancer. *Cell* **149**, 307-321 (2012).
59. Castel, P. et al. PDK1-SGK1 Signaling Sustains AKT-Independent mTORC1 Activation and Confers Resistance to PI3Kalpha Inhibition. *Cancer Cell* **30**, 229-242 (2016).
60. Lu, H. et al. PAK signalling drives acquired drug resistance to MAPK inhibitors in BRAF-mutant melanomas. *Nature* **550**, 133-136 (2017).
61. Wu, S. et al. MSK1-Mediated beta-Catenin Phosphorylation Confers Resistance to PI3K/mTOR Inhibitors in Glioblastoma. *Mol Cancer Ther* **15**, 1656-1668 (2016).
62. Tenbaum, S.P. et al. beta-catenin confers resistance to PI3K and AKT inhibitors and subverts FOXO3a to promote metastasis in colon cancer. *Nat Med* **18**, 892-901 (2012).
63. Arques, O. et al. Tankyrase Inhibition Blocks Wnt/beta-Catenin Pathway and Reverts Resistance to PI3K and AKT Inhibitors in the Treatment of Colorectal Cancer. *Clin Cancer Res* **22**, 644-656 (2016).
64. Nair, A. et al. Combinatorial inhibition of PTPN12-regulated receptors leads to a broadly effective therapeutic strategy in triple-negative breast cancer. *Nat Med* **24**, 505-511 (2018).
65. Sun, T. et al. Activation of multiple proto-oncogenic tyrosine kinases in breast cancer via loss of the PTPN12 phosphatase. *Cell* **144**, 703-718 (2011).
66. Miller, M.A. et al. Reduced Proteolytic Shedding of Receptor Tyrosine Kinases Is a Post-Translational Mechanism of Kinase Inhibitor Resistance. *Cancer Discov* **6**, 382-399 (2016).
67. Donnella, H.J. et al. Kinome rewiring reveals AURKA limits PI3K-pathway inhibitor efficacy in breast cancer. *Nat Chem Biol* **14**, 768-777 (2018).
68. Yoon, S.O. et al. Focal Adhesion- and IGF1R-Dependent Survival and Migratory Pathways Mediate Tumor Resistance to mTORC1/2 Inhibition. *Mol Cell* **67**, 512-527 e514 (2017).
69. Prat, A. et al. Predicting response and survival in chemotherapy-treated triple-negative breast cancer. *Br J Cancer* **111**, 1532-1541 (2014).
70. Rinnerthaler, G., Gampenrieder, S.P. & Greil, R. ASCO 2018 highlights: metastatic breast cancer. *Memo* **11**, 276-279 (2018).
71. Long, G.V. et al. Combined BRAF and MEK inhibition versus BRAF inhibition alone in melanoma. *N Engl J Med* **371**, 1877-1888 (2014).
72. Hoeflich, K.P. et al. In vivo antitumor activity of MEK and phosphatidylinositol 3-kinase inhibitors in basal-like breast cancer models. *Clin Cancer Res* **15**, 4649-4664 (2009).
73. Mirzoeva, O.K. et al. Basal subtype and MAPK/ERK kinase (MEK)-phosphoinositide 3-kinase feedback signaling determine susceptibility of breast cancer cells to MEK inhibition. *Cancer Res* **69**, 565-572 (2009).
74. Kurzrock, R. et al. Phase I dose-escalation of the oral MEK1/2 inhibitor GSK1120212 (GSK212) dosed in combination with the oral AKT inhibitor GSK2141795 (GSK795). *Journal of Clinical Oncology* **29** (2011).
75. Lee, A. & Djamgoz, M.B.A. Triple negative breast cancer: Emerging therapeutic modalities and novel combination therapies. *Cancer Treat Rev* **62**, 110-122 (2018).
76. Wong, J.P. et al. Dual Targeting of PDGFRalpha and FGFR1 Displays Synergistic Efficacy in Malignant Rhabdoid Tumors. *Cell Rep* **17**, 1265-1275 (2016).
77. Andreopoulou, E., Kelly, C.M. & McDaid, H.M. Therapeutic Advances and New Directions for Triple-Negative Breast Cancer. *Breast Care (Basel)* **12**, 21-28 (2017).
78. Esteva, F.J., Hubbard-Lucey, V.M., Tang, J. & Pusztai, L. Immunotherapy and targeted therapy combinations in metastatic breast cancer. *Lancet Oncol* **20**, e175-e186 (2019).
79. Schaer, D.A. et al. The CDK4/6 Inhibitor Abemaciclib Induces a T Cell Inflamed Tumor Microenvironment and Enhances the Efficacy of PD-L1 Checkpoint Blockade. *Cell Rep* **22**, 2978-2994 (2018).
80. Lee, M.J. et al. Sequential application of anticancer drugs enhances cell death by rewiring apoptotic signaling networks. *Cell* **149**, 780-794 (2012).
81. Motwani, M. et al. Augmentation of apoptosis and tumor regression by flavopiridol in the presence of CPT-11 in Hct116 colon cancer monolayers and xenografts. *Clin Cancer Res* **7**, 4209-4219 (2001).

82. McDonald, E.R., 3rd et al. Project DRIVE: A Compendium of Cancer Dependencies and Synthetic Lethal Relationships Uncovered by Large-Scale, Deep RNAi Screening. *Cell* **170**, 577-592 e510 (2017).
83. Petrocca, F. et al. A genome-wide siRNA screen identifies proteasome addiction as a vulnerability of basal-like triple-negative breast cancer cells. *Cancer Cell* **24**, 182-196 (2013).
84. Campbell, J. et al. Large-Scale Profiling of Kinase Dependencies in Cancer Cell Lines. *Cell Rep* **14**, 2490-2501 (2016).
85. Tsherniak, A. et al. Defining a Cancer Dependency Map. *Cell* **170**, 564-576 e516 (2017).
86. Holbeck, S.L. et al. The National Cancer Institute ALMANAC: A Comprehensive Screening Resource for the Detection of Anticancer Drug Pairs with Enhanced Therapeutic Activity. *Cancer Res* **77**, 3564-3576 (2017).
87. Hochgrafe, F. et al. Tyrosine phosphorylation profiling reveals the signaling network characteristics of Basal breast cancer cells. *Cancer Res* **70**, 9391-9401 (2010).
88. Sanchez-Vega, F. et al. Oncogenic Signaling Pathways in The Cancer Genome Atlas. *Cell* **173**, 321-337 e310 (2018).
89. Patel, N. et al. Integrated genomics and functional validation identifies malignant cell specific dependencies in triple negative breast cancer. *Nat Commun* **9**, 1044 (2018).
90. Kawazu, M. et al. Integrative analysis of genomic alterations in triple-negative breast cancer in association with homologous recombination deficiency. *PLoS Genet* **13**, e1006853 (2017).
91. Marcotte, R. et al. Functional Genomic Landscape of Human Breast Cancer Drivers, Vulnerabilities, and Resistance. *Cell* **164**, 293-309 (2016).
92. Boehm, J.S. & Golub, T.R. An ecosystem of cancer cell line factories to support a cancer dependency map. *Nat Rev Genet* **16**, 373-374 (2015).
93. Drost, J. & Clevers, H. Organoids in cancer research. *Nat Rev Cancer* **18**, 407-418 (2018).
94. Wang, T. et al. Gene Essentiality Profiling Reveals Gene Networks and Synthetic Lethal Interactions with Oncogenic Ras. *Cell* **168**, 890-903 e815 (2017).
95. Tian, X. et al. CRISPR/Cas9 - An evolving biological tool kit for cancer biology and oncology. *NPJ Precis Oncol* **3**, 8 (2019).
96. Munoz, D.M. et al. CRISPR Screens Provide a Comprehensive Assessment of Cancer Vulnerabilities but Generate False-Positive Hits for Highly Amplified Genomic Regions. *Cancer Discov* **6**, 900-913 (2016).
97. Tzelepis, K. et al. A CRISPR Dropout Screen Identifies Genetic Vulnerabilities and Therapeutic Targets in Acute Myeloid Leukemia. *Cell Rep* **17**, 1193-1205 (2016).
98. Yu, C. et al. High-throughput identification of genotype-specific cancer vulnerabilities in mixtures of barcoded tumor cell lines. *Nat Biotechnol* **34**, 419-423 (2016).
99. Conway, J.R., Carragher, N.O. & Timpson, P. Developments in preclinical cancer imaging: innovating the discovery of therapeutics. *Nat Rev Cancer* **14**, 314-328 (2014).
100. Lemmon, M.A. & Schlessinger, J. Cell signaling by receptor tyrosine kinases. *Cell* **141**, 1117-1134 (2010).
101. Logue, J.S. & Morrison, D.K. Complexity in the signaling network: insights from the use of targeted inhibitors in cancer therapy. *Genes Dev* **26**, 641-650 (2012).
102. Yarden, Y. & Slivkowsky, M.X. Untangling the ErbB signalling network. *Nat Rev Mol Cell Biol* **2**, 127-137 (2001).
103. Fleuren, E.D., Zhang, L., Wu, J. & Daly, R.J. The kinome 'at large' in cancer. *Nat Rev Cancer* **16**, 83-98 (2016).
104. Siegel, R.L., Miller, K.D. & Jemal, A. Cancer statistics, 2018. *CA Cancer J Clin* **68**, 7-30 (2018).
105. Dent, R. et al. Triple-negative breast cancer: Clinical features and patterns of recurrence. *Clin Cancer Res* **13**, 4429-4434 (2007).
106. Shah, S.P. et al. The clonal and mutational evolution spectrum of primary triple-negative breast cancers. *Nature* **486**, 395-399 (2012).
107. Bianchini, G., Balko, J.M., Mayer, I.A., Sanders, M.E. & Gianni, L. Triple-negative breast cancer: challenges and opportunities of a heterogeneous disease. *Nat Rev Clin Oncol* **13**, 674-690 (2016).
108. Ryall, K.A. et al. An integrated bioinformatics analysis to dissect kinase dependency in triple negative breast cancer. *BMC Genomics* **16 Suppl 12**, S2 (2015).
109. Zawistowski, J.S. et al. Enhancer Remodeling during Adaptive Bypass to MEK Inhibition Is Attenuated by Pharmacologic Targeting of the P-TEFb Complex. *Cancer Discov* **7**, 302-321 (2017).
110. Saura, C. et al. Phase Ib study of Buparlisib plus Trastuzumab in patients with HER2-positive advanced or metastatic breast cancer that has progressed on Trastuzumab-based therapy. *Clin Cancer Res* **20**, 1935-1945 (2014).
111. Ferguson, F.M. & Gray, N.S. Kinase inhibitors: the road ahead. *Nat Rev Drug Discov* **17**, 353-377 (2018).

112. Bahrami, A. et al. The Therapeutic Potential of PI3K/Akt/mTOR Inhibitors in Breast Cancer: Rational and Progress. *J Cell Biochem* **119**, 213-222 (2018).
113. Wei, W. et al. Single-Cell Phosphoproteomics Resolves Adaptive Signaling Dynamics and Informs Targeted Combination Therapy in Glioblastoma. *Cancer Cell* **29**, 563-573 (2016).
114. Holohan, C., Van Schaeybroeck, S., Longley, D.B. & Johnston, P.G. Cancer drug resistance: an evolving paradigm. *Nat Rev Cancer* **13**, 714-726 (2013).
115. Chandarlapaty, S. Negative feedback and adaptive resistance to the targeted therapy of cancer. *Cancer Discov* **2**, 311-319 (2012).
116. Fruhwirth, G.O. et al. How Forster resonance energy transfer imaging improves the understanding of protein interaction networks in cancer biology. *Chemphyschem* **12**, 442-461 (2011).
117. Fujita, Y., Komatsu, N., Matsuda, M. & Aoki, K. Fluorescence resonance energy transfer based quantitative analysis of feedforward and feedback loops in epidermal growth factor receptor signaling and the sensitivity to molecular targeting drugs. *FEBS J* **281**, 3177-3192 (2014).
118. Aoki, K., Komatsu, N., Hirata, E., Kamioka, Y. & Matsuda, M. Stable expression of FRET biosensors: a new light in cancer research. *Cancer Sci* **103**, 614-619 (2012).
119. Zhang, J. & Allen, M.D. FRET-based biosensors for protein kinases: illuminating the kinome. *Mol Biosyst* **3**, 759-765 (2007).
120. Zhang, J., Ma, Y., Taylor, S.S. & Tsien, R.Y. Genetically encoded reporters of protein kinase A activity reveal impact of substrate tethering. *Proc Natl Acad Sci U S A* **98**, 14997-15002 (2001).
121. Terai, K. & Matsuda, M. Ras binding opens c-Raf to expose the docking site for mitogen-activated protein kinase kinase. *EMBO Rep* **6**, 251-255 (2005).
122. Regot, S., Hughey, J.J., Bajar, B.T., Carrasco, S. & Covert, M.W. High-sensitivity measurements of multiple kinase activities in live single cells. *Cell* **157**, 1724-1734 (2014).
123. Komatsu, N. et al. Development of an optimized backbone of FRET biosensors for kinases and GTPases. *Mol Biol Cell* **22**, 4647-4656 (2011).
124. Miura, H., Matsuda, M. & Aoki, K. Development of a FRET biosensor with high specificity for Akt. *Cell Struct Funct* **39**, 9-20 (2014).
125. Zhang, Y. et al. Elevated insulin-like growth factor 1 receptor signaling induces antiestrogen resistance through the MAPK/ERK and PI3K/Akt signaling routes. *Breast Cancer Res* **13**, R52 (2011).
126. Wang, R. et al. Regulation of Cdc25C by ERK-MAP kinases during the G2/M transition. *Cell* **128**, 1119-1132 (2007).
127. Harvey, C.D. et al. A genetically encoded fluorescent sensor of ERK activity. *Proc Natl Acad Sci U S A* **105**, 19264-19269 (2008).
128. Kunkel, M.T., Ni, Q., Tsien, R.Y., Zhang, J. & Newton, A.C. Spatio-temporal dynamics of protein kinase B/Akt signaling revealed by a genetically encoded fluorescent reporter. *J Biol Chem* **280**, 5581-5587 (2005).
129. Repetto, M.V. et al. CDK and MAPK Synergistically Regulate Signaling Dynamics via a Shared Multi-site Phosphorylation Region on the Scaffold Protein Ste5. *Mol Cell* **69**, 938-952 e936 (2018).
130. Shukla, S. & Gupta, S. Apigenin-induced cell cycle arrest is mediated by modulation of MAPK, PI3K-Akt, and loss of cyclin D1 associated retinoblastoma dephosphorylation in human prostate cancer cells. *Cell Cycle* **6**, 1102-1114 (2007).
131. Ochodnicka-Mackovicova, K. et al. NF-kappaB and AKT signaling prevent DNA damage in transformed pre-B cells by suppressing RAG1/2 expression and activity. *Blood* **126**, 1324-1335 (2015).
132. Lahair, M.M., Howe, C.J., Rodriguez-Mora, O., McCubrey, J.A. & Franklin, R.A. Molecular pathways leading to oxidative stress-induced phosphorylation of Akt. *Antioxid Redox Signal* **8**, 1749-1756 (2006).
133. Mendoza, M.C., Er, E.E. & Blenis, J. The Ras-ERK and PI3K-mTOR pathways: cross-talk and compensation. *Trends Biochem Sci* **36**, 320-328 (2011).
134. Costa, R.L.B., Han, H.S. & Gradishar, W.J. Targeting the PI3K/AKT/mTOR pathway in triple-negative breast cancer: a review. *Breast Cancer Res Treat* **169**, 397-406 (2018).
135. Gross, S., Rahal, R., Stransky, N., Lengauer, C. & Hoeflich, K.P. Targeting cancer with kinase inhibitors. *J Clin Invest* **125**, 1780-1789 (2015).
136. Xu, H., Eirew, P., Mullaly, S.C. & Aparicio, S. The omics of triple-negative breast cancers. *Clin Chem* **60**, 122-133 (2014).
137. Sanchez-Vega, F. et al. Oncogenic Signaling Pathways in The Cancer Genome Atlas. *Cell* **173**, 321-+ (2018).
138. Wallace, M.D. et al. Comparative oncogenomics implicates the neurofibromin 1 gene (NF1) as a breast cancer driver. *Genetics* **192**, 385-396 (2012).

139. Balko, J.M. et al. Profiling of residual breast cancers after neoadjuvant chemotherapy identifies DUSP4 deficiency as a mechanism of drug resistance. *Nat Med* **18**, 1052-1059 (2012).
140. Gewinner, C. et al. Evidence that inositol polyphosphate 4-phosphatase type II is a tumor suppressor that inhibits PI3K signaling. *Cancer Cell* **16**, 115-125 (2009).
141. Li, Y.H. et al. The Human Kinome Targeted by FDA Approved Multi-Target Drugs and Combination Products: A Comparative Study from the Drug-Target Interaction Network Perspective. *Plos One* **11** (2016).
142. Kothari, V. et al. Outlier kinase expression by RNA sequencing as targets for precision therapy. *Cancer Discov* **3**, 280-293 (2013).
143. Dermit, M., Dokal, A. & Cutillas, P.R. Approaches to identify kinase dependencies in cancer signalling networks. *FEBS Lett* **591**, 2577-2592 (2017).
144. Sun, M. et al. AKT1/PKBalpha kinase is frequently elevated in human cancers and its constitutive activation is required for oncogenic transformation in NIH3T3 cells. *Am J Pathol* **159**, 431-437 (2001).
145. Kilpinen, S., Ojala, K. & Kallioniemi, O. Analysis of kinase gene expression patterns across 5681 human tissue samples reveals functional genomic taxonomy of the kinome. *Plos One* **5**, e15068 (2010).
146. Bhullar, K.S. et al. Kinase-targeted cancer therapies: progress, challenges and future directions. *Mol Cancer* **17**, 48 (2018).
147. Garcia-Aranda, M. & Redondo, M. Protein Kinase Targets in Breast Cancer. *Int J Mol Sci* **18** (2017).
148. Wee, P. & Wang, Z. Epidermal Growth Factor Receptor Cell Proliferation Signaling Pathways. *Cancers (Basel)* **9** (2017).
149. Scaltriti, M. & Baselga, J. The epidermal growth factor receptor pathway: a model for targeted therapy. *Clin Cancer Res* **12**, 5268-5272 (2006).
150. Nakai, K., Hung, M.C. & Yamaguchi, H. A perspective on anti-EGFR therapies targeting triple-negative breast cancer. *Am J Cancer Res* **6**, 1609-1623 (2016).
151. Sigismund, S., Avanzato, D. & Lanzetti, L. Emerging functions of the EGFR in cancer. *Mol Oncol* **12**, 3-20 (2018).
152. Bailey, M.H. et al. Comprehensive Characterization of Cancer Driver Genes and Mutations. *Cell* **174**, 1034-1035 (2018).
153. Seshacharyulu, P. et al. Targeting the EGFR signaling pathway in cancer therapy. *Expert Opin Ther Targets* **16**, 15-31 (2012).
154. Asami, K. & Atagi, S. Epidermal growth factor receptor tyrosine kinase inhibitors for non-small cell lung cancer. *World J Clin Oncol* **5**, 646-659 (2014).
155. Lee, H.J. et al. Prognostic and predictive values of EGFR overexpression and EGFR copy number alteration in HER2-positive breast cancer. *Br J Cancer* **112**, 103-111 (2015).
156. Hashimoto, K. et al. Activated PI3K/AKT and MAPK pathways are potential good prognostic markers in node-positive, triple-negative breast cancer. *Ann Oncol* **25**, 1973-1979 (2014).
157. Bedard, P.L. et al. A phase Ib dose-escalation study of the oral pan-PI3K inhibitor buparlisib (BKM120) in combination with the oral MEK1/2 inhibitor trametinib (GSK1120212) in patients with selected advanced solid tumors. *Clin Cancer Res* **21**, 730-738 (2015).
158. Butti, R. et al. Receptor tyrosine kinases (RTKs) in breast cancer: signaling, therapeutic implications and challenges. *Mol Cancer* **17**, 34 (2018).
159. Lima, Z.S. et al. Recent advances of therapeutic targets based on the molecular signature in breast cancer: genetic mutations and implications for current treatment paradigms. *J Hematol Oncol* **12**, 38 (2019).
160. Garrido-Castro, A.C., Lin, N.U. & Polyak, K. Insights into Molecular Classifications of Triple-Negative Breast Cancer: Improving Patient Selection for Treatment. *Cancer Discov* **9**, 176-198 (2019).
161. Manning, G., Whyte, D.B., Martinez, R., Hunter, T. & Sudarsanam, S. The protein kinase complement of the human genome. *Science* **298**, 1912-1934 (2002).
162. Fabbro, D., Cowan-Jacob, S.W. & Moebitz, H. Ten things you should know about protein kinases: IUPHAR Review 14. *Br J Pharmacol* **172**, 2675-2700 (2015).
163. McLaughlin, R.P. et al. A kinase inhibitor screen identifies a dual cdc7/CDK9 inhibitor to sensitize triple-negative breast cancer to EGFR-targeted therapy. *Breast Cancer Res* **21**, 77 (2019).
164. Cabodi, S. et al. A PKC-eta/Fyn-dependent pathway leading to keratinocyte growth arrest and differentiation. *Mol Cell* **6**, 1121-1129 (2000).
165. Koedoot, E. et al. Uncovering the signaling landscape controlling breast cancer cell migration identifies novel metastasis driver genes. *Nat Commun* **10**, 2983 (2019).
166. Zhang, Y. et al. IGF1R signaling drives antiestrogen resistance through PAK2/PIX activation in luminal breast cancer. *Oncogene* **37**, 1869-1884 (2018).

167. Zhou, Y. et al. Metascape provides a biologist-oriented resource for the analysis of systems-level datasets. *Nat Commun* **10**, 1523 (2019).
168. Rakha, E.A. et al. Prognostic markers in triple-negative breast cancer. *Cancer* **109**, 25-32 (2007).
169. Park, H.S. et al. High EGFR gene copy number predicts poor outcome in triple-negative breast cancer. *Mod Pathol* **27**, 1212-1222 (2014).
170. Baselga, J. et al. Phase II multicenter study of the anti-epidermal growth factor receptor monoclonal antibody cetuximab in combination with platinum-based chemotherapy in patients with platinum-refractory metastatic and/or recurrent squamous cell carcinoma of the head and neck. *J Clin Oncol* **23**, 5568-5577 (2005).
171. Dickler, M.N., Cobleigh, M.A., Miller, K.D., Klein, P.M. & Winer, E.P. Efficacy and safety of erlotinib in patients with locally advanced or metastatic breast cancer. *Breast Cancer Res Treat* **115**, 115-121 (2009).
172. Rana, P. & Sridhar, S.S. Efficacy and tolerability of lapatinib in the management of breast cancer. *Breast Cancer (Auckl)* **6**, 67-77 (2012).
173. Downward, J., Parker, P. & Waterfield, M.D. Autophosphorylation sites on the epidermal growth factor receptor. *Nature* **311**, 483-485 (1984).
174. Daub, H., Specht, K. & Ullrich, A. Strategies to overcome resistance to targeted protein kinase inhibitors. *Nature Reviews Drug Discovery* **3**, 1001-1010 (2004).
175. Bar, J. & Onn, A. Overcoming molecular mechanisms of resistance to first-generation epidermal growth factor receptor tyrosine kinase inhibitors. *Clin Lung Cancer* **13**, 267-279 (2012).
176. Eng, J. et al. Impact of Concurrent PIK3CA Mutations on Response to EGFR Tyrosine Kinase Inhibition in EGFR-Mutant Lung Cancers and on Prognosis in Oncogene-Driven Lung Adenocarcinomas. *J Thorac Oncol* **10**, 1713-1719 (2015).
177. Eichhorn, P.J. et al. Phosphatidylinositol 3-kinase hyperactivation results in lapatinib resistance that is reversed by the mTOR/phosphatidylinositol 3-kinase inhibitor NVP-BE2235. *Cancer Res* **68**, 9221-9230 (2008).
178. Sos, M.L. et al. PTEN loss contributes to erlotinib resistance in EGFR-mutant lung cancer by activation of Akt and EGFR. *Cancer Res* **69**, 3256-3261 (2009).
179. Espada, J. & Martin-Perez, J. An Update on Src Family of Nonreceptor Tyrosine Kinases Biology. *Int Rev Cell Mol Biol* **331**, 83-122 (2017).
180. Zhang, S. & Yu, D. Targeting Src family kinases in anti-cancer therapies: turning promise into triumph. *Trends Pharmacol Sci* **33**, 122-128 (2012).
181. Posadas, E.M. et al. FYN is overexpressed in human prostate cancer. *BJU Int* **103**, 171-177 (2009).
182. Saito, Y.D., Jensen, A.R., Salgia, R. & Posadas, E.M. Fyn: a novel molecular target in cancer. *Cancer* **116**, 1629-1637 (2010).
183. Sorensen, K.D., Borre, M., Orntoft, T.F., Dyrskjot, L. & Topping, N. Chromosomal deletion, promoter hypermethylation and downregulation of FYN in prostate cancer. *Int J Cancer* **122**, 509-519 (2008).
184. Lee, G.H. et al. FYN promotes mesenchymal phenotypes of basal type breast cancer cells through STAT5/NOTCH2 signaling node. *Oncogene* **37**, 1857-1868 (2018).
185. Rexer, B.N. et al. Phosphoproteomic mass spectrometry profiling links Src family kinases to escape from HER2 tyrosine kinase inhibition. *Oncogene* **30**, 4163-4174 (2011).
186. Podo, F. et al. Triple-negative breast cancer: present challenges and new perspectives. *Mol Oncol* **4**, 209-229 (2010).
187. Gluz, O. et al. Triple-negative breast cancer--current status and future directions. *Ann Oncol* **20**, 1913-1927 (2009).
188. Jhan, J.R. & Andrechek, E.R. Triple-negative breast cancer and the potential for targeted therapy. *Pharmacogenomics* **18**, 1595-1609 (2017).
189. Saxton, R.A. & Sabatini, D.M. mTOR Signaling in Growth, Metabolism, and Disease. *Cell* **168**, 960-976 (2017).
190. Conciatori, F. et al. mTOR Cross-Talk in Cancer and Potential for Combination Therapy. *Cancers (Basel)* **10** (2018).
191. Walsh, S. et al. mTOR in breast cancer: differential expression in triple-negative and non-triple-negative tumors. *Breast* **21**, 178-182 (2012).
192. Carracedo, A. et al. Inhibition of mTORC1 leads to MAPK pathway activation through a PI3K-dependent feedback loop in human cancer. *Journal of Clinical Investigation* **118**, 3065-3074 (2008).
193. Yu, Y.H. et al. Phosphoproteomic Analysis Identifies Grb10 as an mTORC1 Substrate That Negatively Regulates Insulin Signaling. *Science* **332**, 1322-1326 (2011).

194. Faes, S., Demartines, N. & Dormond, O. Resistance to mTORC1 Inhibitors in Cancer Therapy: From Kinase Mutations to Intratumoral Heterogeneity of Kinase Activity. *Oxid Med Cell Longev* **2017**, 1726078 (2017).
195. Chalakur-Ramireddy, N.K.R. & Pakala, S.B. Combined drug therapeutic strategies for the effective treatment of Triple Negative Breast Cancer. *Biosci Rep* **38** (2018).
196. Ma, X.D., Lv, X.Q. & Zhang, J.K. Exploiting polypharmacology for improving therapeutic outcome of kinase inhibitors (KIs): An update of recent medicinal chemistry efforts. *European Journal of Medicinal Chemistry* **143**, 449-463 (2018).
197. Sticz, T. et al. The Effects of Different mTOR Inhibitors in EGFR Inhibitor Resistant Colon Carcinoma Cells. *Pathol Oncol Res* (2018).
198. Schaffrath, J. et al. Efficacy of targeted drugs in germ cell cancer cell lines with differential cisplatin sensitivity. *Plos One* **12** (2017).
199. Liu, T. et al. Combinatorial effects of lapatinib and rapamycin in triple-negative breast cancer cells. *Mol Cancer Ther* **10**, 1460-1469 (2011).
200. Wedel, S. et al. Combined targeting of the VEGFr/EGFr and the mammalian target of rapamycin (mTOR) signaling pathway delays cell cycle progression and alters adhesion behavior of prostate carcinoma cells. *Cancer Lett* **301**, 17-28 (2011).
201. Juengel, E. et al. Combining the receptor tyrosine kinase inhibitor AEE788 and the mammalian target of rapamycin (mTOR) inhibitor RAD001 strongly inhibits adhesion and growth of renal cell carcinoma cells. *BMC Cancer* **9**, 161 (2009).
202. Ballou, L.M. & Lin, R.Z. Rapamycin and mTOR kinase inhibitors. *J Chem Biol* **1**, 27-36 (2008).
203. Chiang, G.G. & Abraham, R.T. Phosphorylation of mammalian target of rapamycin (mTOR) at ser-2448 is mediated by p70S6 kinase. *J Biol Chem* **280**, 25485-25490 (2005).
204. Musa, J. et al. Eukaryotic initiation factor 4E-binding protein 1 (4E-BP1): a master regulator of mRNA translation involved in tumorigenesis. *Oncogene* **35**, 4675-4688 (2016).
205. Feun, L. et al. Arginine deprivation as a targeted therapy for cancer. *Curr Pharm Des* **14**, 1049-1057 (2008).
206. Gingras, A.C. et al. Regulation of 4E-BP1 phosphorylation: a novel two-step mechanism. *Genes Dev* **13**, 1422-1437 (1999).
207. Galluzzi, L., Buque, A., Kepp, O., Zitvogel, L. & Kroemer, G. Immunogenic cell death in cancer and infectious disease. *Nat Rev Immunol* **17**, 97-111 (2017).
208. Kepp, O. et al. Consensus guidelines for the detection of immunogenic cell death. *Oncoimmunology* **3**, e955691 (2014).
209. Rufo, N., Garg, A.D. & Agostinis, P. The Unfolded Protein Response in Immunogenic Cell Death and Cancer Immunotherapy. *Trends Cancer* **3**, 643-658 (2017).
210. Kepp, O. et al. eIF2alpha phosphorylation as a biomarker of immunogenic cell death. *Semin Cancer Biol* **33**, 86-92 (2015).
211. Schenone, M., Dancik, V., Wagner, B.K. & Clemons, P.A. Target identification and mechanism of action in chemical biology and drug discovery. *Nat Chem Biol* **9**, 232-240 (2013).
212. Papadatos, G., Gaulton, A., Hersey, A. & Overington, J.P. Activity, assay and target data curation and quality in the ChEMBL database. *J Comput Aided Mol Des* **29**, 885-896 (2015).
213. Traxler, P. et al. AEE788: a dual family epidermal growth factor receptor/ErbB2 and vascular endothelial growth factor receptor tyrosine kinase inhibitor with antitumor and antiangiogenic activity. *Cancer Res* **64**, 4931-4941 (2004).
214. Jiang, B.H. & Liu, L.Z. Role of mTOR in anticancer drug resistance: perspectives for improved drug treatment. *Drug Resist Updat* **11**, 63-76 (2008).
215. Hare, S.H. & Harvey, A.J. mTOR function and therapeutic targeting in breast cancer. *Am J Cancer Res* **7**, 383-404 (2017).
216. Ilagan, E. & Manning, B.D. Emerging role of mTOR in the response to cancer therapeutics. *Trends Cancer* **2**, 241-251 (2016).
217. Efeyan, A. & Sabatini, D.M. mTOR and cancer: many loops in one pathway. *Curr Opin Cell Biol* **22**, 169-176 (2010).
218. She, Q.B. et al. Integrated molecular pathway analysis informs a synergistic combination therapy targeting PTEN/PI3K and EGFR pathways for basal-like breast cancer. *BMC Cancer* **16**, 587 (2016).
219. Willmarth, N.E. & Ethier, S.P. Autocrine and juxtacrine effects of amphiregulin on the proliferative, invasive, and migratory properties of normal and neoplastic human mammary epithelial cells. *J Biol Chem* **281**, 37728-37737 (2006).

220. Kappler, C.S. et al. Oncogenic signaling in amphiregulin and EGFR-expressing PTEN-null human breast cancer. *Mol Oncol* **9**, 527-543 (2015).
221. Klaefer, S. et al. The target landscape of clinical kinase drugs. *Science* **358** (2017).
222. Traxler, P. et al. AEE788: A dual family epidermal growth factor receptor/ErbB2 and vascular endothelial growth factor receptor tyrosine kinase inhibitor with antitumor and antiangiogenic activity. *Cancer Res* **64**, 4931-4941 (2004).
223. Fujishita, T., Kojima, Y., Kajino-Sakamoto, R., Taketo, M.M. & Aoki, M. Tumor microenvironment confers mTOR inhibitor resistance in invasive intestinal adenocarcinoma. *Oncogene* **36**, 6480-6489 (2017).
224. Madden, J.M. et al. Abrogating phosphorylation of eIF4B is required for EGFR and mTOR inhibitor synergy in triple-negative breast cancer. *Breast Cancer Res Treat* **147**, 283-293 (2014).
225. You, K.S., Yi, Y.W., Kwak, S.J. & Seong, Y.S. Inhibition of RPTOR overcomes resistance to EGFR inhibition in triple-negative breast cancer cells. *Int J Oncol* **52**, 828-840 (2018).
226. Advani, S.H. Targeting mTOR pathway: A new concept in cancer therapy. *Indian J Med Paediatr Oncol* **31**, 132-136 (2010).
227. Laphanuwat, P. et al. Cyclin D1 depletion interferes with oxidative balance and promotes cancer cell senescence. *J Cell Sci* **131** (2018).
228. Goudar, R.K. et al. Combination therapy of inhibitors of epidermal growth factor receptor/vascular endothelial growth factor receptor 2 (AEE788) and the mammalian target of rapamycin (RAD001) offers improved glioblastoma tumor growth inhibition. *Mol Cancer Ther* **4**, 101-112 (2005).
229. Cretella, D. et al. The anti-tumor efficacy of CDK4/6 inhibition is enhanced by the combination with PI3K/AKT/mTOR inhibitors through impairment of glucose metabolism in TNBC cells. *J Exp Clin Cancer Res* **37**, 72 (2018).
230. Yamamoto, T., Kanaya, N., Somlo, G. & Chen, S. Synergistic anti-cancer activity of CDK4/6 inhibitor palbociclib and dual mTOR kinase inhibitor MLN0128 in pRb-expressing ER-negative breast cancer. *Breast Cancer Res Treat* (2019).
231. Chen, L., Yang, G. & Dong, H. Everolimus Reverses Palbociclib Resistance in ER+ Human Breast Cancer Cells by Inhibiting Phosphatidylinositol 3-Kinase(PI3K)/Akt/Mammalian Target of Rapamycin (mTOR) Pathway. *Med Sci Monit* **25**, 77-86 (2019).
232. Curtis, C. et al. The genomic and transcriptomic architecture of 2,000 breast tumours reveals novel subgroups. *Nature* **486**, 346-352 (2012).
233. Shi, Y., Jin, J., Ji, W. & Guan, X. Therapeutic landscape in mutational triple negative breast cancer. *Mol Cancer* **17**, 99 (2018).
234. Stranger, B.E. et al. Relative impact of nucleotide and copy number variation on gene expression phenotypes. *Science* **315**, 848-853 (2007).
235. van Dyk, E., Hoogstraal, M., Ten Hoeve, J., Reinders, M.J. & Wessels, L.F. RUBIC identifies driver genes by detecting recurrent DNA copy number breaks. *Nat Commun* **7**, 12159 (2016).
236. Wang, K. et al. Genomic landscape of copy number aberrations enables the identification of oncogenic drivers in hepatocellular carcinoma. *Hepatology* **58**, 706-717 (2013).
237. Liang, L., Fang, J.Y. & Xu, J. Gastric cancer and gene copy number variation: emerging cancer drivers for targeted therapy. *Oncogene* **35**, 1475-1482 (2016).
238. Slamon, D.J. et al. Human breast cancer: correlation of relapse and survival with amplification of the HER-2/neu oncogene. *Science* **235**, 177-182 (1987).
239. Rimawi, M.F. et al. Multicenter phase II study of neoadjuvant lapatinib and trastuzumab with hormonal therapy and without chemotherapy in patients with human epidermal growth factor receptor 2-overexpressing breast cancer: TBCRC 006. *J Clin Oncol* **31**, 1726-1731 (2013).
240. Weisman, P.S. et al. Genetic alterations of triple negative breast cancer by targeted next-generation sequencing and correlation with tumor morphology. *Mod Pathol* **29**, 476-488 (2016).
241. Krepisch, A.C.V. et al. Genome-wide Profiling of Copy Number Alterations in Triple-negative Breast Cancer Identifies a Region at 19p13 Associated With Lymph Node Metastasis. *Eur J Cancer* **48**, S134-S134 (2012).
242. Jezequel, P. et al. bc-GenExMiner: an easy-to-use online platform for gene prognostic analyses in breast cancer. *Breast Cancer Res Treat* **131**, 765-775 (2012).
243. Gao, J. et al. Integrative analysis of complex cancer genomics and clinical profiles using the cBioPortal. *Sci Signal* **6**, pl1 (2013).
244. Muller, T. et al. ASAP1 promotes tumor cell motility and invasiveness, stimulates metastasis formation in vivo, and correlates with poor survival in colorectal cancer patients. *Oncogene* **29**, 2393-2403 (2010).

245. van Dyk, E., Reinders, M.J. & Wessels, L.F. A scale-space method for detecting recurrent DNA copy number changes with analytical false discovery rate control. *Nucleic Acids Res* **41**, e100 (2013).
246. Jandu, H. et al. Molecular characterization of irinotecan (SN-38) resistant human breast cancer cell lines. *BMC Cancer* **16**, 34 (2016).
247. Lanczky, A. et al. miRpower: a web-tool to validate survival-associated miRNAs utilizing expression data from 2178 breast cancer patients. *Breast Cancer Res Treat* **160**, 439-446 (2016).
248. Jolly, C. & Van Loo, P. Timing somatic events in the evolution of cancer. *Genome Biol* **19**, 95 (2018).
249. Pereira, B. et al. The somatic mutation profiles of 2,433 breast cancers refines their genomic and transcriptomic landscapes. *Nat Commun* **7**, 11479 (2016).
250. Chaignat, E. et al. Copy number variation modifies expression time courses. *Genome Res* **21**, 106-113 (2011).
251. Gamazon, E.R. & Stranger, B.E. The impact of human copy number variation on gene expression. *Brief Funct Genomics* **14**, 352-357 (2015).
252. Mazaki, Y. et al. An ADP-ribosylation factor GTPase-activating protein Git2-short/KIAA0148 is involved in subcellular localization of paxillin and actin cytoskeletal organization. *Mol Biol Cell* **12**, 645-662 (2001).
253. Zhang, T. et al. Lentiviral vector mediated-ASAP1 expression promotes epithelial to mesenchymal transition in ovarian cancer cells. *Oncol Lett* **15**, 4432-4438 (2018).
254. Wang, L., Du, F. & Wang, X. TNF-alpha induces two distinct caspase-8 activation pathways. *Cell* **133**, 693-703 (2008).
255. Metzger-Filho, O. et al. Dissecting the heterogeneity of triple-negative breast cancer. *J Clin Oncol* **30**, 1879-1887 (2012).
256. Santarius, T., Shipley, J., Brewer, D., Stratton, M.R. & Cooper, C.S. A census of amplified and overexpressed human cancer genes. *Nat Rev Cancer* **10**, 59-64 (2010).
257. Chiu, A.M., Mitra, M., Boymoushakian, L. & Collier, H.A. Integrative analysis of the inter-tumoral heterogeneity of triple-negative breast cancer. *Sci Rep* **8**, 11807 (2018).
258. Zhao, Z.M. et al. CCNE1 amplification is associated with poor prognosis in patients with triple negative breast cancer. *BMC Cancer* **19**, 96 (2019).
259. Fallah, Y., Brundage, J., Allegakoen, P. & Shajahan-Haq, A.N. MYC-Driven Pathways in Breast Cancer Subtypes. *Biomolecules* **7** (2017).
260. Schaub, F.X. et al. Pan-cancer Alterations of the MYC Oncogene and Its Proximal Network across the Cancer Genome Atlas. *Cell Syst* **6**, 282-300 e282 (2018).
261. Lin, D. et al. ASAP1, a gene at 8q24, is associated with prostate cancer metastasis. *Cancer Res* **68**, 4352-4359 (2008).
262. Ehlers, J.P., Worley, L., Onken, M.D. & Harbour, J.W. DDEF1 is located in an amplified region of chromosome 8q and is overexpressed in uveal melanoma. *Clin Cancer Res* **11**, 3609-3613 (2005).
263. Onodera, Y. et al. Expression of AMAP1, an ArfGAP, provides novel targets to inhibit breast cancer invasive activities. *EMBO J* **24**, 963-973 (2005).
264. Brown, M.T. et al. ASAP1, a phospholipid-dependent arf GTPase-activating protein that associates with and is phosphorylated by Src. *Mol Cell Biol* **18**, 7038-7051 (1998).
265. Liu, Y., Loijens, J.C., Martin, K.H., Karginov, A.V. & Parsons, J.T. The association of ASAP1, an ADP ribosylation factor-GTPase activating protein, with focal adhesion kinase contributes to the process of focal adhesion assembly. *Mol Biol Cell* **13**, 2147-2156 (2002).
266. Sabe, H. et al. The EGFR-GEP100-Arf6-AMAP1 signaling pathway specific to breast cancer invasion and metastasis. *Traffic* **10**, 982-993 (2009).
267. Hou, T. et al. Overexpression of ASAP1 is associated with poor prognosis in epithelial ovarian cancer. *Int J Clin Exp Pathol* **7**, 280-287 (2014).
268. Kim, M.H. et al. Colon cancer progression is driven by APEX1-mediated upregulation of Jagged. *J Clin Invest* (2013).
269. Kwok, H.F. et al. Prognostic significance of minichromosome maintenance proteins in breast cancer. *Am J Cancer Res* **5**, 52-71 (2015).
270. Ventura, E., Pentimalli, F. & Giordano, A. RBL2/p130: a direct AKT substrate and mediator of AKT inhibition-induced apoptosis. *Oncoscience* **5**, 278-280 (2018).
271. Long, J. et al. Lipid metabolism and carcinogenesis, cancer development. *Am J Cancer Res* **8**, 778-791 (2018).
272. O'Farrell, A.C., Shnyder, S.D., Marston, G., Coletta, P.L. & Gill, J.H. Non-invasive molecular imaging for preclinical cancer therapeutic development. *Br J Pharmacol* **169**, 719-735 (2013).

273. Sekar, R.B. & Periasamy, A. Fluorescence resonance energy transfer (FRET) microscopy imaging of live cell protein localizations. *J Cell Biol* **160**, 629-633 (2003).
274. Piston, D.W. & Kremers, G.J. Fluorescent protein FRET: the good, the bad and the ugly. *Trends Biochem Sci* **32**, 407-414 (2007).
275. Forster, T. *Zwischenmolekulare Energiewanderung Und Fluoreszenz. *Ann Phys-Berlin* **2**, 55-75 (1948).
276. Kiyokawa, E., Hara, S., Nakamura, T. & Matsuda, M. Fluorescence (Forster) resonance energy transfer imaging of oncogene activity in living cells. *Cancer Sci* **97**, 8-15 (2006).
277. Arai, Y. & Nagai, T. Extensive use of FRET in biological imaging. *Microscopy (Oxf)* **62**, 419-428 (2013).
278. Maryu, G. et al. Live-cell Imaging with Genetically Encoded Protein Kinase Activity Reporters. *Cell Struct Funct* **43**, 61-74 (2018).
279. Kuchenov, D. et al. High-Content Imaging Platform for Profiling Intracellular Signaling Network Activity in Living Cells. *Cell Chem Biol* **23**, 1550-1559 (2016).
280. Okamoto, K. & Sako, Y. Recent advances in FRET for the study of protein interactions and dynamics. *Curr Opin Struct Biol* **46**, 16-23 (2017).
281. Sultan, M. et al. 78PAN in vivo genome-wide RNAi screen identifies novel mediators of paclitaxel response in breast cancer. *Annals of Oncology* **30** (2019).
282. Reardon, D.A. et al. Pharmacokinetic drug interaction between AEE788 and RAD001 causing thrombocytopenia in patients with glioblastoma. *Cancer Chemother Pharmacol* **69**, 281-287 (2012).
283. Reardon, D.A. et al. Phase I study of AEE788, a novel multitarget inhibitor of ErbB- and VEGF-receptor-family tyrosine kinases, in recurrent glioblastoma patients. *Cancer Chemother Pharmacol* **69**, 1507-1518 (2012).
284. Iorio, F. et al. A Landscape of Pharmacogenomic Interactions in Cancer. *Cell* **166**, 740-754 (2016).
285. Krijgsman, O., Carvalho, B., Meijer, G.A., Steenberg, R.D. & Ylstra, B. Focal chromosomal copy number aberrations in cancer-Needles in a genome haystack. *Biochim Biophys Acta* **1843**, 2698-2704 (2014).
286. Basudan, A. et al. Frequent ESR1 and CDK Pathway Copy-Number Alterations in Metastatic Breast Cancer. *Mol Cancer Res* **17**, 457-468 (2019).
287. Ding, L. et al. Perspective on Oncogenic Processes at the End of the Beginning of Cancer Genomics. *Cell* **173**, 305-320 e310 (2018).
288. Horiuchi, D. et al. PIM1 kinase inhibition as a targeted therapy against triple-negative breast tumors with elevated MYC expression. *Nat Med* **22**, 1321-1329 (2016).
289. Braso-Maristany, F. et al. PIM1 kinase regulates cell death, tumor growth and chemotherapy response in triple-negative breast cancer. *Nat Med* **22**, 1303-1313 (2016).
290. Hashimoto, S. et al. Targeting AMAP1 and cortactin binding bearing an atypical src homology 3/proline interface for prevention of breast cancer invasion and metastasis. *Proc Natl Acad Sci U S A* **103**, 7036-7041 (2006).
291. Nam, J.M. et al. CIN85, a Cbl-interacting protein, is a component of AMAP1-mediated breast cancer invasion machinery. *EMBO J* **26**, 647-656 (2007).
292. Onodera, Y. et al. Rab5c promotes AMAP1-PRKD2 complex formation to enhance beta1 integrin recycling in EGF-induced cancer invasion. *J Cell Biol* **197**, 983-996 (2012).
293. Singh, M.K. et al. Structure-activity relationship studies of QS11, a small molecule Wnt synergistic agonist. *Bioorg Med Chem Lett* **25**, 4838-4842 (2015).
294. Zhang, Q. et al. Small-molecule synergist of the Wnt/beta-catenin signaling pathway. *Proc Natl Acad Sci U S A* **104**, 7444-7448 (2007).
295. Dai, X., Cheng, H., Bai, Z. & Li, J. Breast Cancer Cell Line Classification and Its Relevance with Breast Tumor Subtyping. *J Cancer* **8**, 3131-3141 (2017).
296. Dobrolecki, L.E. et al. Patient-derived xenograft (PDX) models in basic and translational breast cancer research. *Cancer Metastasis Rev* **35**, 547-573 (2016).
297. Park, M.K., Lee, C.H. & Lee, H. Mouse models of breast cancer in preclinical research. *Lab Anim Res* **34**, 160-165 (2018).

Summary

Uncovering vulnerabilities in triple-negative breast cancer

Triple-negative breast cancer (TNBC) constitutes a small subtype (~15%) of breast cancer, but causes the majority of breast cancer-related deaths. As defined by the absence of ER and PR expression and HER2 overexpression, TNBC is not curable by hormone receptor or HER2-targeted therapies. Furthermore, TNBC is highly heterogeneous and most aggressive. To date, cytotoxic chemotherapy remains the mainstay in the management of TNBC. Despite the initial response to the standard-of-care chemotherapy, TNBC often exhibits intrinsic or acquired drug resistance, and subsequently, recurs in local and distal organs. Targeted therapies have long been pursued for the treatment of TNBC, but rarely demonstrate satisfactory clinical outcomes. Therefore, improved understanding of the intricate biological basis underlying TNBC insensitivity to targeted agents and defining new therapeutic opportunities are of the utmost importance. The aim of the studies presented in this thesis was to systematically identify gene/kinase susceptibilities of refractory TNBC cells, and reveal novel potent targeted therapies for TNBC as monotherapy or in combination with approved kinase drugs.

Chapter 2 exploited a FRET (fluorescence resonance energy transfer)-based high throughput imaging approach to quantitatively monitor ERK and AKT dynamic activity in MEKi-resistant and AKTi-resistant TNBC cells in response to the 378 kinase inhibitors. By deriving a mathematical model to integrate proliferative response profiling and ERK- and AKT-based kinase activity dynamics analysis, I revealed unique kinase dependencies on RTK/MAPK and PI3K/AKT pathways that are distinctly targetable in the resistant TNBC cells. Specifically, MEKi-resistant cells were responsive to inhibitors against PI3K pathway but refractory to EGFR-targeted inhibitors, whereas AKTi-resistant cells were sensitive to EGFR/MAPK pathway blockade but showed resistance against mTOR inhibitors. The work provides new opportunities to explore effective therapeutic kinase targets in treatment-refractory cancer cells, as well as assess the drug efficacy and possible off-target effects of clinically used drugs.

By carrying out kinome-scale siRNA screen, **Chapter 3** identified specific vulnerable kinase targets in EGFRi- and mTORi-resistant TNBC cells. Pharmacological inhibition of these targets greatly suppressed TNBC cell proliferation in different resistant scenarios, highlighting the potential of targeting these kinase vulnerabilities to combat the hard-to-treat disease. Moreover, a kinome-wide siRNA screen was performed in EGFRi-resistant TNBC cells in combination with lapatinib treatment. The combination screen investigated the synthetic lethality interactions with EGFR-targeted inhibition. The results have demonstrated that, a Src family member FYN, conferred TNBC resistance against

EGFR kinase-targeted inhibition via negatively regulating EGFR/PI3K/AKT signaling. Targeting FYN released the activity of downstream PI3K and AKT signaling, rationalizing the co-targeting strategy to subvert drug resistance against inhibitors targeting EGFR/PI3K/AKT signaling axis in cancer cells with elevated EGFR expression, including TNBC.

In **Chapter 4**, a broad kinase inhibitor library screening was carried out across ~20 TNBC cell lines representative for six main TNBC subtypes. The research demonstrated a poor correlation of TNBC molecular subtypes with their proliferative responses to various kinase inhibitors. This study explored effective combined drug treatment to overcome TNBC resistance to mTOR inhibitors. The targets of the identified synergistic kinase inhibitors were predicted by cheminformatics-based survey and functionally validated by siRNA-mediated gene suppression. The AEE788 + rapamycin combination identified in this chapter represents a novel therapeutic strategy to combat TNBC. The putative targets of AEE788 have been revealed in determining rapalog combination efficacy. The combination, by targeting multiple kinases, not only sustains inhibited MAPK activity, but also effectively suppresses mTOR signaling, thereby eliciting synergistic anti-proliferative effects in TNBC. In addition, the findings are complementary to the presently published target spectrum of the kinase drug AEE788. **Chapter 4** revealed the synergistic effects of multi-kinase targeted inhibitor AEE788 on rapalogs treatment in TNBCs. Cheminformatics-guided target prediction and validation further pronounced the polypharmacology mechanisms underlying the synergy.

Genetic alterations are thought to be favored during the initiation, development and progression of cancer in an evolutionary fashion. Over 80% of TNBCs exhibits TP53 mutation, being a major reason for causing gene instability in this disease. Insightful analysis of genomic sequencing data in (triple negative) breast cancer exploiting bioinformatics holds the promise for the identification of novel therapeutic targets. **Chapter 5** has exploited the robust ADMIRE algorithm to analyze the copy number and gene expression profiles across a set of triple-negative tumors. The analysis prioritized 148 candidate genes driving TNBC cell growth and proliferation. siRNA-based functional screen further validated, besides known EGFR and MYC oncogenes, novel driver genes including ASAP1 which showed high amplification frequency and gene expression in TNBC cohorts. Of relevance, high level of ASAP1 expression correlates with poor prognosis in patients with TNBC. TempO-Seq-based targeted whole genome RNA sequencing analysis concluded that, the novel TNBC driver gene ASAP1, regulates various cytokine and apoptosis signaling components that are significantly associated with TNBC prognosis, supporting the potentiality of ASAP1 as a therapeutic target for the dismal disease.

In summary, the work presented in this thesis has identified important kinase signaling addictions of drug-resistant TNBC cells and key regulators conferring kinase inhibitor resistance, and discovered novel driver genes and combinatorial targeting strategies to subvert drug resistance. These studies provide new insights into the molecular basis underlying TNBC responses to clinical kinase drugs and provoke potential therapeutic targeting strategies for the incurable TNBC.

Samenvatting

Het blootleggen van kwetsbaarheden bij triple negatieve borstkanker

Triple negatieve borstkanker (“triple-negative breast cancer”, TNBC) vormt een klein subtype (~ 15%) van borstkanker, maar veroorzaakt de meeste sterfgevallen door borstkanker. Zoals gedefinieerd door de afwezigheid van oestrogeen receptor (ER) en progesteron receptor (PR) expressie en humane epidermale groeifactor receptor 2 (HER2) overexpressie, is TNBC niet te genezen door hormoonreceptor- of op HER2-gerichte therapieën. Bovendien is TNBC zeer heterogeen en agressief. Tot op heden blijft chemotherapie de standaard bij de behandeling van TNBC. Ondanks een goede eerste response op reguliere chemotherapie, vertoont TNBC vaak intrinsieke of verworven resistentie tegen deze geneesmiddelen en keert vervolgens terug in lokale en distale organen. Doelgerichte therapieën worden al lang bestudeerd voor de behandeling van TNBC, maar vertonen zelden bevredigende klinische resultaten. Daarom is het begrijpen van de ingewikkelde biologische basis die ten grondslag ligt aan TNBC ongevoeligheid voor gerichte middelen en het definiëren van nieuwe therapeutische mogelijkheden van het grootste belang. Het doel van de studies in dit proefschrift was om systematisch de gen en kinase afhankelijkheden van resistente TNBC cellen te identificeren en nieuwe effectieve doelgerichte therapieën voor TNBC te onthullen als monotherapie of in combinatie met goedgekeurde kinase remmende medicijnen.

Hoofdstuk 2 maakte gebruik van een op FRET (fluorescentie resonantie energieoverdracht) gebaseerde imaging techniek op grote schaal (“high-throughput”) om kwantitatief ERK en AKT dynamische activiteit te monitoren in MEK-remmer (MEKi) resistente en AKT-remmer (AKTi) resistente TNBC cellen na behandeling met 378 kinase remmers. Door een wiskundig model af te leiden om proliferatieve responses te profileren en ERK- en AKT-gebaseerde dynamische kinase-activiteitanalyse te integreren, onthulden wij unieke kinase afhankelijkheden van RTK / MAPK- en PI3K / AKT-routes die duidelijk kunnen worden aangegrepen in de resistente TNBC cellen. Zo reageerden MEKi-resistente cellen op remmers van de PI3K-pathway terwijl deze ongevoelig waren voor EGFR-gerichte remmers. In tegenstelling waren de AKTi-resistente cellen gevoelig voor EGFR / MAPK-sigitaaltransductie-blokkade, maar vertoonden deze resistentie tegen mTOR-remmers. Dit werk biedt nieuwe mogelijkheden om effectieve therapeutische kinasedoelen in resistente kankercellen te onderzoeken, evenals de werkzaamheid van geneesmiddelen en mogelijke niet-doelgerichte (“off-target”) effecten van klinisch gebruikte geneesmiddelen te beoordelen.

Door het uitvoeren van een siRNA-screening op schaal van het gehele kinase repertoire (kinoom), identificeerde **Hoofdstuk 3** specifieke en kwetsbare kinasedoelen in

EGFRi en mTORi-resistente TNBC cellen. Farmacologische remming van deze doelen onderdrukte de proliferatie van TNBC cellen in verschillende resistente scenario's sterk, en dit benadrukte het potentieel van het aanpakken van deze kinase kwetsbaarheden om deze moeilijk te behandelen ziekte te bestrijden. Bovendien werd een kinoombrede siRNA-screening uitgevoerd in EGFRi-resistente TNBC cellen in combinatie met lapatinib behandeling. Deze combinatie screen onderzocht de synthetisch letale interacties van genen met EGFR-gerichte remming. De resultaten hebben aangetoond dat een Src-familie lid FYN TNBC resistentie veroorzaakte tegen EGFR-kinase gerichte remming door het negatief te reguleren van de EGFR / PI3K / AKT-signaleringsroute. Het aangrijpen van FYN bevrijdde de activiteit van onderliggende PI3K- en AKT-signaleringsroutes, wat verklaart waarom deze gecombineerde aangrijpingsstrategie geneesmiddel resistentie tegen EGFR / PI3K / AKT-signaling terugdraait in kankercellen met verhoogde EGFR-expressie, zoals TNBC.

In **Hoofdstuk 4** werd een high-throughput screening uitgevoerd op een grote set van kinase remmers over ~20 TNBC cellijnen die representatief zijn voor zes belangrijke TNBC subtypen. Het onderzoek toonde een zwakke correlatie aan van moleculaire subtypen van TNBC en hun proliferatieve reacties op verschillende kinase remmers. Deze studie onderzocht welke geneesmiddelcombinaties deze resistentie tegen mTOR-remmers kunnen overwinnen. De aangrijpingspunten van de geïdentificeerde synergetische kinase remmers werden voorspeld door op cheminformatica-gebaseerd onderzoek en werden verder functioneel gevalideerd door siRNA-gemedieerde gensuppressie. De AEE788 + rapamycin combinatie die in dit hoofdstuk werd geïdentificeerd, vertegenwoordigt een nieuwe therapeutische strategie om TNBC te bestrijden. De verschillende aangrijpingspunten van AEE788 zijn onthuld en verklaren de synergetische interactie met rapamycin en andere soortgelijke mTOR-remmers (rapalogen). De combinatie, door zich te richten op meerdere kinasen, ondersteunt niet alleen geremde MAPK-activiteit, maar onderdrukt ook effectief mTOR-signaling, waardoor synergetische antiproliferatieve effecten in TNBC worden opgewekt. Bovendien zijn de bevindingen complementair aan het momenteel gepubliceerde spectrum van aangrijpingspunten van het kinase-medicijn AEE788. **Hoofdstuk 4** onthulde de synergetische effecten van de multi-kinase gerichte remmer AEE788 op de behandeling van rapalogen in TNBC's. Cheminformatica-geleide voorspelling van de aangrijpingspunten en experimentele validatie hiervan toonden verder de polyfarmacologische mechanismen aan die aan de synergie ten grondslag liggen.

Men denkt dat genetische veranderingen evolutionair geselecteerd worden tijdens de initiatie, ontwikkeling en progressie van kanker. Meer dan 80% van de TNBC tumoren vertoont een TP53-mutatie, wat een belangrijke reden is voor het veroorzaken van genetische instabiliteit in deze ziekte. Inzichtelijke analyse van genomische sequenties

(“sequencing”) bij (triple negatieve) borstkanker met behulp van bio-informatica, kan daarom mogelijk nieuwe therapeutische aangrijpingspunten identificeren. **Hoofdstuk 5** heeft gebruik gemaakt van het robuuste ADMIRE-algoritme om het aantal genetische kopieën en genexpressieprofielen in een reeks triple-negatieve tumoren te analyseren. Uit deze analyse kwamen 148 kandidaat genen, die mogelijk TNBC celgroei en proliferatie aansturen. Een siRNA-screening van deze genen heeft, naast bekende EGFR- en MYC-oncogenen, het belang van nieuwe aandrijvende (“driver”) genen verder gevalideerd, waaronder ASAP1, die ook een hoge amplificatiefrequentie en genexpressie in TNBC-cohorten vertoonden. Van belang is dat een hoog niveau van ASAP1-expressie correleert met een slechte prognose bij patiënten met TNBC. Een TempO-Seq-gebaseerde kwantitatieve analyse van RNA moleculen (“RNA sequencing”) liet zien dat het nieuwe TNBC driver-gen ASAP1 verschillende cytokine- en apoptose-siginaalcomponenten reguleert die significant geassocieerd zijn met TNBC prognose. Dit ondersteunt verder de potentie van ASAP1 als een therapeutisch doelwit voor deze agressieve ziekte.

Samenvattend heeft het in dit proefschrift gepresenteerde werk belangrijke kinase-verslavingen van resistente TNBC cellen blootgelegd, belangrijke regulatoren geïdentificeerd die resistentie tegen kinase remmers verlenen, en nieuwe driver-genen en combinatorische aangrijpingsstrategieën ontdekt om resistentie tegen geneesmiddelen te ondermijnen. Deze studies bieden nieuwe inzichten in de moleculaire basis die ten grondslag ligt aan de reacties op klinische kinase-geneesmiddelen van TNBC tumoren en bieden potentiële therapeutische aangrijpingsstrategieën aan voor deze slecht behandelbare vorm van borstkanker.

List of publications

1. **He J**, McLaughlin RP, van der Noord V, Foekens JA, Martens JWM, van Westen G, Zhang Y, van de Water B. Multi-targeted kinase inhibition alleviates mTOR inhibitor resistance in triple-negative breast cancer. *Breast Cancer Res Treat.* **2019** Aug 6. doi: 10.1007/s10549-019-05380-z.
2. **He J**, Wink S, de Bont H, Le Dévédec SE, Zhang Y, van de Water B. FRET biosensor-based kinase inhibitor screen for ERK and AKT activity reveals differential kinase dependencies for proliferation in TNBC cells. *Biochem Pharmacol.* **2019** Sep 16. doi: 10.1016/j.bcp.2019.113640.
3. **He J**, McLaughlin RP, Zhang Y, van de Water B. A kinome screen for lapatinib drug resistance identifies FYN as a suppressor of EGFR/PI3K/AKT signaling axis dependency in triple-negative breast cancer. *Submitted.*
4. **He J**, McLaughlin RP, van der Beek L, Canisius S, Wessels L, Martens JWM, Foekens JA, Zhang Y, van de Water B. Integrative analysis of genomic amplification-dependent expression and loss-of-function screen identifies ASAP1 as a driver gene in triple-negative breast cancer progression. *Submitted.*
5. McLaughlin RP, **He J**, van der Noord VE, Redel J, Foekens JA, Martens JWM, Smid M, Zhang Y, van de Water B. A kinase inhibitor screen identifies a dual cdc7/CDK9 inhibitor to sensitize triple-negative breast cancer to EGFR-targeted therapy. *Breast Cancer Res.* **2019** Jul 1;21(1):77.
6. Zhang Y, Wester L, **He J**, Geiger T, Moerkens M, Siddappa R, Helmijr JA, Timmermans MM, Look MP, van Deurzen CHM, Martens JWM, Pont C, de Graauw M, Danen EHJ, Berns EMJJ, Meerman JHN, Jansen MPH, van de Water B. IGF1R signaling drives antiestrogen resistance through PAK2/PIX activation in luminal breast cancer. *Oncogene.* **2018** Apr;37(14):1869-1884.
7. McLaughlin RP, **He J**, Karuntu J, van der Noord VE, Martens JWM, Foekens JA, Wang S, Zhang Y, van de Water B. Targeting the P-TEFb complex through CDK9 inhibition to combat triple-negative breast cancer. *In Preparation.*
8. McLaughlin RP, **He J**, Karuntu J, van der Noord VE, Martens JWM, Foekens JA, Wang S, Zhang Y, van de Water B. The synergistic effect of combined P-TEFb and EGFR inhibition on triple-negative breast cancer. *In Preparation.*
9. Liu W, Zhang J, Yao X, Jiang C, **He J**, Ni P, Liu J, Chen Q, Li Q, Zang X, Yao L, Liu Y, Wang M, Shen P, Wang G, Zhou F. Shenmai injection enhances the cytotoxicity of chemotherapeutic drugs against colorectal cancers via improving their subcellular distribution. *Acta Pharmacol Sin.* **2017** Feb;38(2):264-276.
10. Zhang J, Sun Y, Wang Y, Lu M, **He J**, Liu J, Chen Q, Zhang X, Zhou F, Wang G, Sun X. Non-antibiotic agent ginsenoside 20(S)-Rh2 enhanced the antibacterial effects of ciprofloxacin in vitro and in vivo as a potential NorA inhibitor. *Eur. J. Pharmacol.* **2014** Oct 5; 740:277-84.
11. Wang J, Zhu X, Peng Y, Zha W, Feng D, Zhu Y, Wan P, Qi H, **He J**, Zhou J, Sun J. Liquid chromatography/tandem mass spectrometry method for quantification of trans-stilbene glycoside in rat plasma and its pharmacokinetic application. *Biomed Chromatogr.* **2012** Nov; 26(11):1371-6.

Curriculum vitae

Jichao He was born in Zhoukou, China, on the 7th of September 1988. He studied Pharmaceutical Preparation at China Pharmaceutical University from 2007 to 2011. After obtaining his Bachelor's degree, Jichao continued with his Master study on the pharmacokinetic mechanisms of herb-drug interaction in the management of colorectal cancer, supervised by Prof. Dr. Guangji Wang. In 2014, he was awarded a scholarship under the State Scholarship Fund through a rigid academia evaluation process in China, and eventually granted the opportunity to pursue his doctoral degree at Leiden University in the Netherlands. He conducted his PhD project *Uncovering vulnerabilities in triple-negative breast cancer* under the supervision of Prof. Dr. Bob van de Water, funded by the European Research Council.

Acknowledgements

Doing a PhD is not as easy as one can expect. While completing my doctoral dissertation, I would like to express my sincere gratitude to people who have helped and supported me both physically and emotionally in the past five years.

It is a great opportunity for me to be supervised by Bob van de Water. I am so grateful for your time and efforts spent on me. Your trust and strong support always helped me regain confidence, even during the hardest period. Greatest thanks to Yinghui my co-supervisor for your endless help and patience. You are my most important guide in exploring the world of cancer biology.

I would also like to thank Sylvia for opening me the door to FRET imaging, as well as many valuable discussions and advices. I owe my gratitude to Hans, Ine and Chantal for unreserved technical support and kind explanations of Dutch culture during dinner and outdoor activities. To Steven W for the professional assistance in R. Special thanks to Ronan and Vera for our hard-working and teamwork. Esmee, I very much enjoyed the different kinds of meetings we joined together. Bas, thank you for your continuously quick response to my emails which are always helpful. And of course, we had lots of fun during the soccer tournament. Thank you Luc for the joyful conversations and invitations. Great thanks go to Britt, Melissa, Anne, Annelien, Linda and Johannes for organizing a list of social events including soccer and beach volleyball. I would like to extend my appreciation to Lynn, Marije, Huan and all other TOX members for your help and accompanying during my PhD study.

I would also like to thank my former roommates Gang, Feng and Gangqi, and my friends Yangan, Shuai, Xue, Feng J, Yao, Sijia, Guangsheng, Rongfang, Ningning, Wenxuan, Yiran, Weiwen, Lanpeng, Qiang, Hao, Qing and Tian, etc.

Lastly, I would like to thank my beloved parents and sisters for your endless love and tolerance.

Jichao He

October 31, 2019